Measurement of Residual Stresses in Type-304 Stainless Steel Piping Butt Weldments

EPRI

EPRI NP-1413
Project 449-1
Phase Report
June 1980

Keywords:
Residual Stress
Stress Corrosion
Piping
Welds
Measurements
Stainless Steel

Prepared by
Argonne National Laboratory
Argonne, Illinois

ELECTRIC POWER RESEARCH INSTITUTE

Measurement of Residual Stresses in Type-304 Stainless Steel Piping Butt Weldments

NP-1413
Research Project 449-1

Phase Report, June 1980

Prepared by

ARGONNE NATIONAL LABORATORY
Materials Science Division
9700 South Cass Avenue
Argonne, Illinois 60439

Principal Investigators
W. J. Shack
W. A. Ellingson
L. E. Pahis

Prepared for

Electric Power Research Institute
3412 Hillview Avenue
Palo Alto, California 94304

EPRI Project Manager
R. E. Smith

Reliability, Availability and Economics Program
Nuclear Power Division

ORDERING INFORMATION

Requests for copies of this report should be directed to Research Reports Center (RRC), Box 50490, Palo Alto, CA 94303, (415) 965-4081. There is no charge for reports requested by EPRI member utilities and affiliates, contributing nonmembers, U.S. utility associations, U.S. government agencies (federal, state, and local), media, and foreign organizations with which EPRI has an information exchange agreement. On request, RRC will send a catalog of EPRI reports.

NOTICE

This report was prepared by the organization(s) named below as an account of work sponsored by the Electric Power Research Institute, Inc. (EPRI). Neither EPRI, members of EPRI, the organization(s) named below, nor any person acting on their behalf: (a) makes any warranty or representation, express or implied, with respect to the accuracy, completeness, or usefulness of the information contained in this report, or that the use of any information, apparatus, method, or process disclosed in this report may not infringe privately owned rights; or (b) assumes any liabilities with respect to the use of, or for damages resulting from the use of, any information, apparatus, method, or process disclosed in this report.

Prepared by
Argonne National Laboratory
Argonne, Illinois

EPRI PERSPECTIVE

PROJECT DESCRIPTION

Intergranular stress corrosion cracking (IGSCC) of type-304 stainless steel piping has been a continuing problem for boiling water reactors (BWRs) since the mid-1960s. A major factor contributing to the occurrence of such cracking is the magnitude and distribution of residual stresses adjacent to the girth welds and resulting from the welding processes. This phase report on Research Project (RP) 449 presents measured values of residual stresses (both on the inside surfaces and through the wall thickness) for three pipe sizes representative of the recirculation system of BWRs. The effects of prewelding surface treatments are also examined.

The information presented should be of direct value to individuals investigating BWR pipe cracking and to those concerned with developing and applying measures to mitigate the problem. These results are closely related to EPRI publication NP-944, "Studies on AISI Type-304 Stainless Steel Piping Weldments for Use in BWR Applications," and to other projects underway. These include:

- RP701: "Near-Term BWR Piping Remedies"
- RP1174: "Analytical Predictions of Residual Stresses in Stainless Steel Pipe Welds"
- RP1394: "The Development of Residual Stress Improvement Techniques"
- RP1576: "Evaluation of Heat Sink Welding."

PROJECT OBJECTIVE

A knowledge of the total stress state associated with a given BWR pipe weld is essential in order to understand the relative influence of each parameter contributing to IGSCC. The objective of this project was to measure residual

stresses associated with typical weldments of type-304 stainless steel piping in BWRs. The influence of pipe size was to be evaluated for both surface and through-wall thickness residual stress distributions. Several welds removed from field service were to be studied in addition to the effects of various preweld surface treatments.

PROJECT RESULTS

The project objective was achieved by using combined X-ray diffraction and strain gage techniques to measure residual stresses on three 4-inch-diameter mockup weldments, a 10-inch-diameter weld that was removed from service, and a 26-inch-diameter lab weld that was fabricated to specifications typical of field procedures. Key results indicate significant differences in the distributions of through-wall residual stresses as a function of pipe size. The large, 26-inch-diameter pipe possesses a strongly compressive residual stress field at a depth of about 15 percent into the pipe wall thickness from the inside surface. In addition, preweld surface preparation appears to be a relatively insignificant contributor to the total residual stress problem in the weld heat-affected zone.

R. E. Smith, Project Manager
Reliability, Availability and Economics Program
Nuclear Power Division

ABSTRACT

Residual stresses have been shown to be a major factor contributing to intergranular stress corrosion cracking of weldments in austenitic stainless steel. Residual stresses developed during welding are measured for three pipe sizes including 4-, 10-, and 26-inch-diameter, schedule-80, type-304 stainless steel. Significant differences are found in both magnitude and distribution as a function of pipe size. Effects of preweld surface treatments are also evaluated.

Blank Page

TABLE OF CONTENTS

Blank Page

LIST OF FIGURES

LIST OF FIGURES (CONTD.)

LIST OF FIGURES (CONTD.)

LIST OF FIGURES (CONTD.)

LIST OF TABLES

EXECUTIVE SUMMARY

Beginning in 1974, a number of cracks have been found in the austenitic stainless steel piping systems of several Boiling Water Reactors (BWRs). Failure analyses at Argonne National Laboratory and elsewhere have shown that the cracks have developed through intergranular stress-corrosion cracking (ISCC). Austenitic stainless steels become susceptible to ISCC in the presence of microstructural changes, commonly called sensitization, and high stresses. Although the piping systems were designed in conformance with all applicable codes, no allowance was made for the residual stresses due to welding.

This report describes residual-stress measurements on Type 304 stainless steel Schedule-80 4-, 10-, and 26-in. pipe weldments. Some of these weldments are from autopsy pipes, i.e., pipes that have seen actual field service. Others are mock-ups that have been fabricated following standard nuclear-industry welding practices, but which have not been in actual reactor service. The strain measurements have used both strain-gauge and x-ray diffraction techniques. Measurements have been made on the inner surface; these stress levels presumably control the initiation of ISCC. Complete through-the-thickness stress profiles have also been obtained; the throughwall distribution controls the growth of a crack once it has initiated.

Both azimuthal and axial variations of the residual-stress distributions have been considered, although the primary concern has been the measurement of the peak tensile axial stresses in the region 2-3 mm from the weld fusion line on the inner surface where the peak sensitization levels generally occur. For the three 4-in. mock-up weldments examined, these peak stress levels were 273 (38), 326 (46), and 367 (51) MPa (ksi). The 10-in. autopsy weldment has a peak stress leak of 430 (60) MPa (ksi). For the 26-in. weldment the peak stress was 193 (28) MPa (ksi).

The mock-up weldments were prepared with different preweld surface treatments (light grinding, heavy grinding, etc.) to determine the effect of these

surface treatments on the inner surface. X-ray diffraction measurements on the inner surface show that in the heavily sensitized region 2-3 mm from the weld fusion line the effects of the preweld surface treatments have largely been erased by the thermomechanical treatment that occurred during welding. Thus the large tensile stresses on the inner surface are due to the welding process itself and not the preweld surface treatment.

Of the weldments examined, the 26-in. weldment had the lowest peak stress on the inner surface. However, the 10-in. weldment had the highest peak stress, and thus no clear trend in the variation of the peak residual-stress level on the inner surface with pipe size is evident. On the other hand, there appear to be significant differences in the distributions of throughwall residual stress in the 4- and 10-in. weldments and the 26-in. weldment. At least at certain azimuthal positions, not only are there large tensile stresses on the inner surface of the 4- and 10-in. weldments, but also the throughwall residual stresses remain tensile through a large part ($\sim$50-75%) of the wall thickness. This is not true for the 26-in. weldment. Although there may be significant residual tensile stresses on the inner surface, the residual stresses become strongly compressive at a depth >15% of the wall thickness.

THE MEASUREMENT OF RESIDUAL STRESSES IN TYPE 304 STAINLESS STEEL PIPING BUTT WELDMENTS

by

W. J. Shack, W. A. Ellingson, and L. Pahis

Materials Science Division
ARGONNE NATIONAL LABORATORY
Argonne, Illinois 60439

1. INTRODUCTION

Between September 13, 1974, and January 28, 1975, 15 cracks were discovered in the heat-affected zones (HAZs) of welds in the 4-in. recirculation bypass lines of several Boiling Water Reactors (BWRs) manufactured by the General Electric Company (GE). In addition, cracks were discovered in a 10-in. core-spray line at the Dresden-2 BWR on February 10, 1975.[1] These incidents caused widespread concern, and GE, the Nuclear Regulatory Commission (NRC), and the Electric Power Research Institute (EPRI) initiated extensive investigations of the pipe-cracking problem.

Most of the cracks, at the time of discovery, had not propagated completely through the wall of the pipe. Those that had penetrated the wall and were leaking had not propagated around the circumference of the pipe; thus, no pipe separations have occurred. The failures are believed to have developed through intergranular stress-corrosion cracking (ISCC). Austenitic stainless steels become susceptible to ISCC in the presence of microstructural changes, commonly called sensitization, and high (near yield) stresses. Both conditions can result simultaneously from welding. Preweld surface treatment and water chemistry may also contribute to the cracking problem.

To develop a more complete understanding of the ISCC problem in BWR piping systems, EPRI has supported a program at Argonne National Laboratory to provide information that will help to determine (1) the causes of cracking, (2) the locations at which future cracks will most probably occur, and (3) the corrective options available to prevent cracking.

The work is divided into four tasks: (1) determination of the residual-stress distributions associated with Type 304 stainless steel pipe weldments; (2) development of a quantitative measure of the sensitization associated with the HAZ; (3) determination of the relationship (if any) between residual stress, sensitization, and the susceptibility to ISCC; and (4) determination of the reliability of current volumetric inspection methods for detecting ISCC.

2. TASK OBJECTIVES

The objectives of the residual stress analysis task are to determine the residual stresses in Type 304 stainless steel 4- and 10-in. Schedule-80 pipe weldments that result from both the actual welding operation and the weld preparation and to examine the possibility of shake-down effects during service.

3. SCOPE OF THE REPORT

Residual-stress measurements on Type 304 stainless steel Schedule-80 4- and 10-in. pipe weldments are reported. Some of the weldments are from autopsy pipes,* which have seen actual field service. The other weldments are mock-ups** fabricated especially for testing purposes. Both bulk residual stresses obtained by strain-gauge measurements and surface residual stresses obtained by X-ray diffraction measurements are reported. The emphasis is on the measurement of residual stresses on the inner surface of the weldments where initiation of ISCC occurs; however, data are also reported for residual stress levels on the outer surface of the weldments and complete through-the-thickness stress profiles. The report also describes the experimental and analytical techniques used to obtain the residual-stress field mapping.

---

*An autopsy weldment has been in actual reactor service.

**Mock-up weldments are fabricated in the laboratory following standard nuclear-industry welding practice, but they have not been in reactor service.

4. EXPERIMENTAL PROCEDURE AND RESULTS

4.1 Test Matrix and Welding Details

The test matrix for the ANL residual-stress program is shown in Table 4.1.1. The test program for 4-in. weldments includes two autopsy weldments (one from the Dresden-3 BWR and one from the Monticello BWR) and three mock-up weldments (identified as W27A, W27B, and W27C). The mock-up weldments were provided to ANL by the General Electric Company, Nuclear Energy Division. The weld procedure and weld heat input followed the welding technique specified in Procedure Specification IA-MA-88 for Gas Tungsten Arc Welding and Shielded Metal Arc Welding of Corrosion-Resisting Steel Pipe, Fittings, Values and Flanges in Group P No. 8 as qualified by the Phillips, Getschow Co. The welds are seven pass 2G welds, with the first pass using a consumable Grinnel insert. The basic geometry of the weld preparation is shown in Fig. 4.1.1. A typical weld cross section is shown in Fig. 4.1.2. Details of the weld heat input for each mock-up weld are given in Appendix B.

No temperature measurements were made during the fabrication of the mock-up weldments. However, in connection with studies by GE on BWR pipe cracking, additional weldments were fabricated under nominally identical conditions, and during the fabrication of these weldments, the temperatures on the inner and outer surfaces were measured. Since the temperature distributions of the weldments analyzed in the present program are probably similar, the results of the GE study are summarized in Appendix B.

4.2 Outline of Experimental Procedures

4.2.1 Strain-gauge Residual-stress Measurement Procedures

Bulk residual stresses in 4- and 10-in. seamless Schedule-80 Type 304 stainless steel pipe weldments have been measured. The bulk residual stresses were measured using strain-relief techniques, where the strain relief was measured

Table 4.1.1

Residual-stress Test Matrix for Type 304 Stainless Steel Pipe Weldments

Weld Preparation	Pipe Diameter, in.	Fabricator	Weld Position	Strain-gauge Residual-stress Measurement	Weld Identification
Lightly Ground (63 rms Finish)/Heavily Ground (125 rms Finish)	4	General Electric	2G	ID 2 axial positions 4 azimuthal	W27B
Lightly Machined (63 rms Finish)/ Heavily Machined (125 rms Finish)	4	General Electric	2G	ID 2 axial positions, 4 azimuthal locations OD 1 axial, 4 azimuthal	W27C
Standard Machined (125 rms Finish)/ Standard Grinding (125 rms Finish)	4	General Electric	2G	Six axial positions across weld at every 45° around weld	W27A
Standard Grinding, Both Sides	4	Field Weld from Dresden-2	2G	Same as W27A but one side of weld only (three axial positions)	Either PD21/1DIA or PD23/PD10A
Standard Machining, Both Sides	4	Field Weld from Monticello	2G	Same as W27A but one side of weld only (three axial positions)	Unspecified
Standard Machining, Both Sides	10	Field Weld from Dresden-2	2G--to be verified	Three axial positions normal to weld at every 45° around weld	

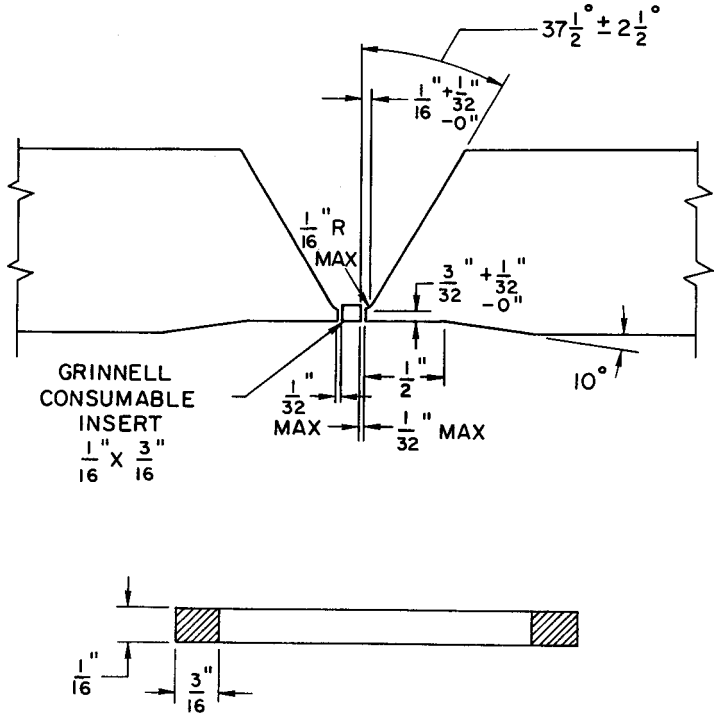

Fig. 4.1.1. Weld-Prep Geometry. To convert dimensions to mm multiply by 25.4.

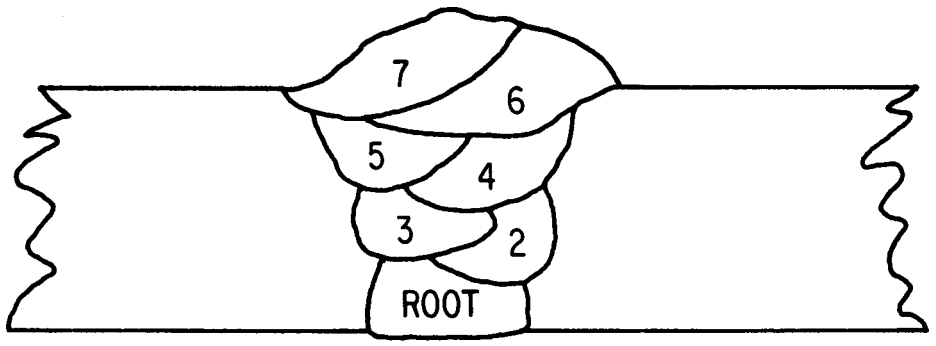

Fig. 4.1.2. Cross Section of Seven-pass 2G Butt Weld.

by electrical-resistance strain gauges. Measurements on the weld metal utilized Micro Measurements EA-09-030YB-120 rosette gauges, which are 120° rosette gauges with 120-Ω resistance and an active length of 0.76 mm (0.03 in.). The remainder of the measurements were made with Micro Measurements EA-09-062UR-120 rosette gauges, which are 45° rosette gauges with 120-Ω resistance and an active length of 1.57 mm (0.062 in.).

The placement of the gauges on each weldment is described in detail in later sections, since surface roughness dictated minor variations for each weldment. The general pattern, however, can be described as follows. Rosettes were placed every 45° on both the inner and outer surfaces of the weldments, as shown schematically in Fig. 4.2.1.1. At each azimuthal position, seven gauges were distributed axially over a distance ∿17 mm on either side of the weld, as shown schematically in Fig. 4.2.1.2.

The following sections describe the placement of the strain gauges on the inner surfaces in terms of distance from the weld fusion line. This is convenient experimentally, since the location of the weld fusion line is fairly precise and readily identifiable. However, the results are plotted in terms of distance to the weld centerline. This distance is the sum of the distance to the weld fusion line plus half the average width (∿5 mm) of the weld bead on the inner surface of the weld. The average widths of the weldments studied are listed in Table 4.2.1.1.

The adhesive used for mounting the gauges was Micro Measurements M-Bond 200, which is a cyanoacrylate resin (similar to Eastman 910) that cures completely at room temperature. The lead wires were 30-gauge Teflon-coated, silver-plated, stranded copper wire, kept short to reduce line resistance. Hence, three-wire connections were not needed. After the gauges and lead wires were attached, they were protected by applications of Micro Measurements M-Coat A and M-Coat B.

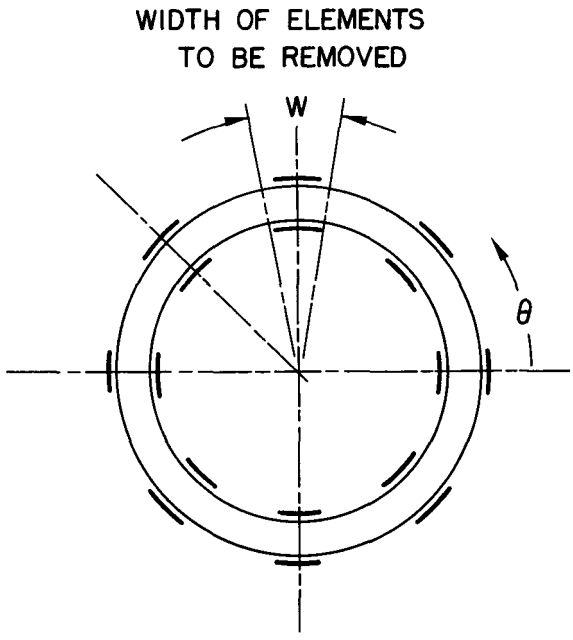

Fig. 4.2.1.1. Cross Section of Pipe Showing Azimuthal Strain-gauge Locations.

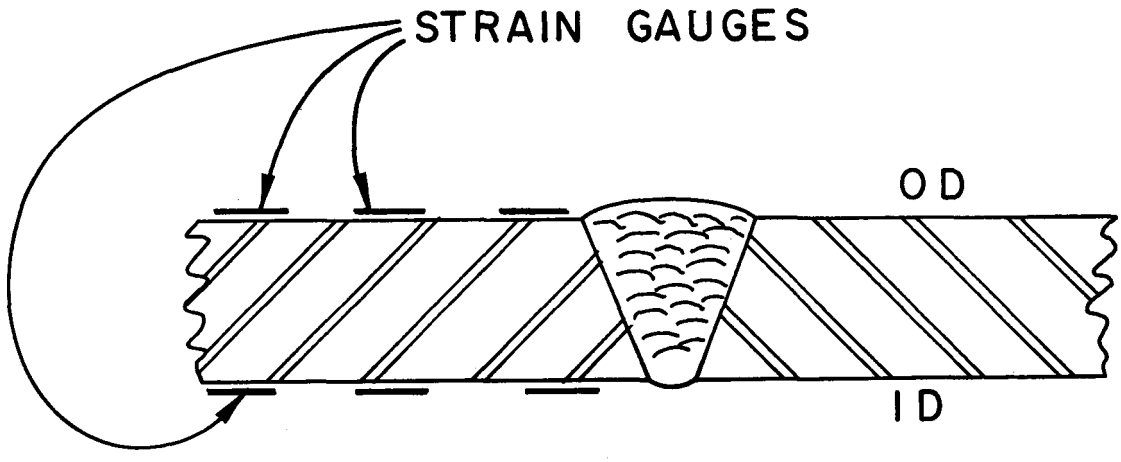

Fig. 4.2.1.2. Cross Section of Typical Weld Showing Axial Strain-Gauge Positions at a Given Azimuthal Position.

TABLE 4.2.1.1

Average Width of Weldment on Inner Surface

Weldment	Average Width of Weldment on Inner Surface (mm)
W27A	4.0
W27B	5.6
W27C	4.8
Monticello	4.8
10-in. Dresden 2	4.8

The instrumented weldments were sectioned using electric-discharge-machining (EDM) methods. Full-wall-thickness specimens 15 mm wide and ∿200 mm long were cut using a 1.5-mm-diam wire electrode. This machining technique is time-consuming and expensive. However, some preliminary studies of the stresses induced by mechanical sawing were done using completely stress-relieved segments of Type 304 stainless steel 4-in. pipe, and although the sawing was done quite carefully, surprisingly large stresses were induced [140 MPa (20 ksi)]. It was concluded that high reliability would require EDM techniques.

The strain relief that occurred during sectioning was measured using a half-bridge configuration and a BLH 1200 digital-readout strain indicator. These strains were then used to calculate preliminary estimates of the residual stresses.

The residual stresses in the weldment are due primarily to the thermo-mechanical deformations occurring during the welding process and the pre- and postweld surface treatments. The stresses due to the surface treatments are significant only in a shallow surface layer, typically 0.25 mm (10 mils) thick. Their contribution to the net force and bending moment acting on a section through the pipe wall is very small. Strain-gauge techniques measure changes in strain due to the relief of the force and moment acting on the section after it is parted out. The stress redistribution that occurs is indicated schematically in Fig. 4.2.1.3. The initial residual-stress distribution is shown schematically in Fig. 4.2.1.3(a). There is a smoothly varying distribution through the wall of the pipe, and a sharp spike, which represents the surface stresses produced by surface treatment. The unloading that occurs during the parting-out process is illustrated in Fig. 4.2.1.3(b).

Although the initial stress redistribution may be highly nonlinear, the elastic unloading produces a linear redistribution, since the specimen is basically a beam. The change in stress detected by strain-gauge measurements $\Delta\sigma_1$ is

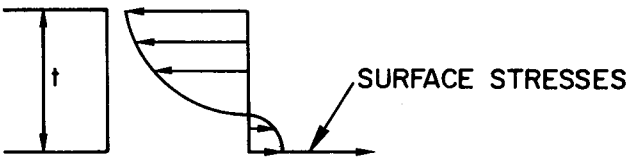

(a) Residual Stress Distribution Through the Thickness for Thick-walled Pipe Weldment

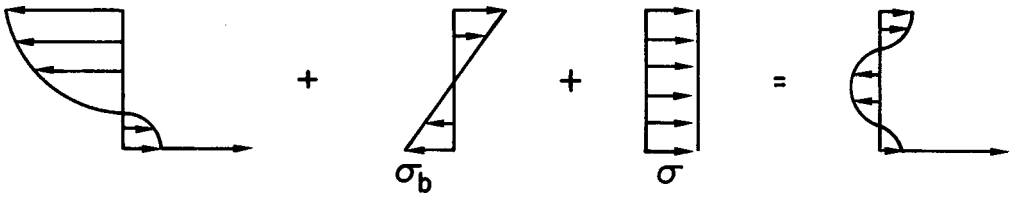

(b) Stress Redistribution as a Specimen is Parted Out from the Weldment

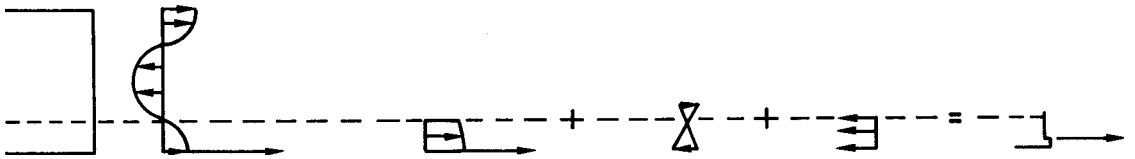

(c) Stress Redistribution as a Thin "Strip" is Cut from the Full Wall Thickness Specimen

Fig. 4.2.1.3. Schematic of Residual-stress Redistribution During Stress-relief Operations.

$$\Delta\sigma_1 = \sigma_R - \sigma_L \ ,$$

where σ_R denotes the actual residual stress and σ_L denotes the contribution from the linear distribution relieved during the parting-out process. Because of the nonlinearity of the initial stress distribution, $\Delta\sigma_1$ is not equal to the actual stress at the inner surface. The stress changes corresponding to $\Delta\sigma_1$, i.e., data obtained from full-thickness specimens, are identified in later discussion and figures as "bar data."

A rough estimate of the possible contribution of the surface-treatment induced stresses to this stress change can be obtained as follows. Assume that the surface stresses are equal to 300 MPa (∿45 ksi) over a depth of 0.1 mm (∿4 mil) and then they vanish. This stress distribution gives rise to a net force F and moment M per unit width acting on a section through the thickness:

$$F = 3 \times 10^{-2} \text{ MPa/m}$$

$$M = 1.2 \times 10^{-4} \text{ MPa} \cdot \text{m/m}$$

The change in stress at the inner surface when this force and moment are relieved can be estimated from simple beam theory:

$$\Delta\sigma = F/t + 6M/t^2 \ , \qquad (4.2.1.1)$$

where t is the wall thickness. For a 4-in. pipe, t = 8.6 mm and

$$\Delta\sigma \lesssim 13 \text{ MPa } (\sim 2 \text{ ksi}) \ .$$

This is probably an upper bound for the contribution of the surface-treatment-induced stresses to the stress changes detected by the strain gauges during the

parting out of the specimen, since our assumed surface-stress distribution overestimates the net resultant force associated with the throughwall distribution of the surface stresses (for actual distributions, see Fig. 4.4.3.). The estimate indicates that the surface stresses have little effect on the bar data.

Because the stresses are not completely relieved by parting out the specimen, the full-wall-thickness specimen was cut again using a 1.5-mm-diam wire electrode to produce a final 1.5-mm-thick specimen. The stress redistribution that occurs is shown schematically in Fig. 4.2.1.3(c). This section is sufficiently thin that all the stresses except those in a surface layer are relieved. We can again estimate the contribution of the assumed surface-stress distribution on the stress change $\Delta\sigma_2$ detected by strain gauges mounted on the inner surface using simple beam theory. The net force and moment due to the assumed surface-stress distribution acting on a section through the thickness (1.5 mm) of the specimen are

$$F = 3 \times 10^{-2} \text{ MPa/m}$$

$$M = 2.3 \times 10^{-5} \text{ MPa} \cdot \text{m/m} .$$

The change in stress is calculated from Eq. 4.2.1.1 with t = 1.5 mm:

$$\Delta\sigma \simeq 80 \text{ MPa } (\sim 12 \text{ ksi}) .$$

Note, however, that a significant portion of the surface stress has not been relieved, so that

$$\sigma = \Delta\sigma_1 + \Delta\sigma_2$$

is still only an approximation of the actual stress at the inner surface. The

stress changes $\sigma = \Delta\sigma_1 + \Delta\sigma_2$ (i.e., data obtained from the 1.5-mm-thick specimens) are identified in later discussion and figures as "strip" data.

Detailed measurements of the residual-stress distributions (see Section 4.5) indicate that, except for the rapidly varying surface stresses, the distribution of residual stress through the thickness of the 4-in. weldments is reasonably linear in most cases. For a linear distribution the "bulk" residual stress as measured by strain gauges on the inner and outer surfaces of full-wall-thickness specimens gives a good measure of the stress available to drive the crack. The "bulk" stress on the inner surface obtained from the strip specimens is a better measure of the actual stress at the inner surface, although there may still be significant surface stresses not relieved. The difference in the "bulk" residual-stress values obtained from the "bar" and "strip" specimens is due to the nonlinearlity of the residual-stress distribution and the relief of the surface stresses. The rough estimate obtained here indicates that a significant portion of any observed stress changes between the bar and strip specimens from 4-in. weldments may be attributed to the stresses induced by surface treatments. The thick 26-in. weldment has a significant nonlinear residual-stress distribution remaining after the specimen is parted out, and hence the meaningfulness of "bulk" residual stresses obtained from full-thickness specimens is difficult to interpret.

The calculation of the residual stresses from the measured strains was done using isotropic, plane-stress, stress-strain relations

$$\sigma_x = \frac{E}{1 - \nu^2} (\varepsilon_x + \nu\varepsilon_y) \qquad (4.2.1.2)$$

and

$$\sigma_y = \frac{E}{1 - \nu^2} (\varepsilon_y + \nu\varepsilon_x) \ . \qquad (4.2.1.3)$$

The values of Young's modulus E and Poisson's ratio ν used in the calculations are

$$E = 2 \times 10^5 \text{ MPa } (28 \times 10^6 \text{ psi})$$

and

$$\nu = 0.3 \ .$$

A systematic assessment of the errors involved in the bulk residual-stress measurements is difficult to make; however, it is worthwhile to consider some of the major possible sources of error in at least a qualitative manner. The strain-gauge measurements are well understood. The gauge factor for each individual element of each rosette is guaranteed to $\pm$0.5%. The time required to make the measurements, i.e., the time between strain readings before and after sectioning the pipe, is relatively short (<4 weeks); thus gauge drift is not a major problem, since the measured drift rate is $\sim$0.5 $\mu\varepsilon$/day.

The use of two-dimensional, isotropic, elasticity analysis with "Handbook" values of Young's modulus and Poisson's ratio for the calculation of stress values from the measured strain values is a source of error, since these values could vary in the HAZ by $\pm$5%. However, the error introduced by these assumptions will be relatively consistent for all measurements. Hence, although it may affect the actual magnitudes of the calculated residual stresses, it will have little effect on the form of the residual-stress distribution.

The largest source of a nonconsistent error in the strain measurements is in the axial placement of the gauges. Because of the steep axial gradients of residual stress, small errors in the axial position could lead to relatively large errors in the measured stresses and introduce a spurious azimuthal variation

in the stresses. In most instances, gauges were laid at fixed distances from the weld fusion line. The actual distance of the gauges in the critical region close to the weld fusion line is accurate to within ±0.25 mm; the error introduced by this uncertainty depends on the steepness of the axial gradient of the stress. Examination of the data for the 4- and 10-in. pipes suggests that this gradient is always <70 MPa/mm (250 ksi/in.), even close to the weld. Thus the variation in the azimuthal distribution of stress attributable to errors in the axial placement of the gauges is less than ±18 MPa (±2.5 ksi). At gauge positions greater than 4 mm from the weld fusion line, the axial placement of the gauges is much less critical, since the stress gradients are much smaller.

As our earlier discussion pointed out, the largest uncertainty is in the actual interpretation of the bar and strip data. Neither gives an estimate of the actual stress at the surface; however, they are both reasonable measures of the stress available to begin propagation of the crack once it has actually initiated.

The procedure outlined here is adequate for determining the bulk residual stresses at the inner and outer surfaces of the pipe weldments. However, to predict crack propagation through the wall, we must know the complete through-the-thickness distribution of stress. To obtain this information, a full-thickness specimen was cut from a weldment and successive thin [0.4 mm (15-mil)] layers were removed from the inner surface. To ensure the removal of a uniform thickness of material, a special EDM apparatus was built. The specimen was mounted on a movable stage, and a rotating circular electrode was used to prevent excessive wear of the electrode and the development of a "flat spot." Figures 4.2.1.4 and 4.2.1.5 are photographs of the apparatus, and Fig. 4.2.1.6 shows schematically the relative position of the specimen and the electrode. After each layer was removed, strain gauges mounted on the outer surface were read, and the strain relief due to the removal of each layer was recorded.

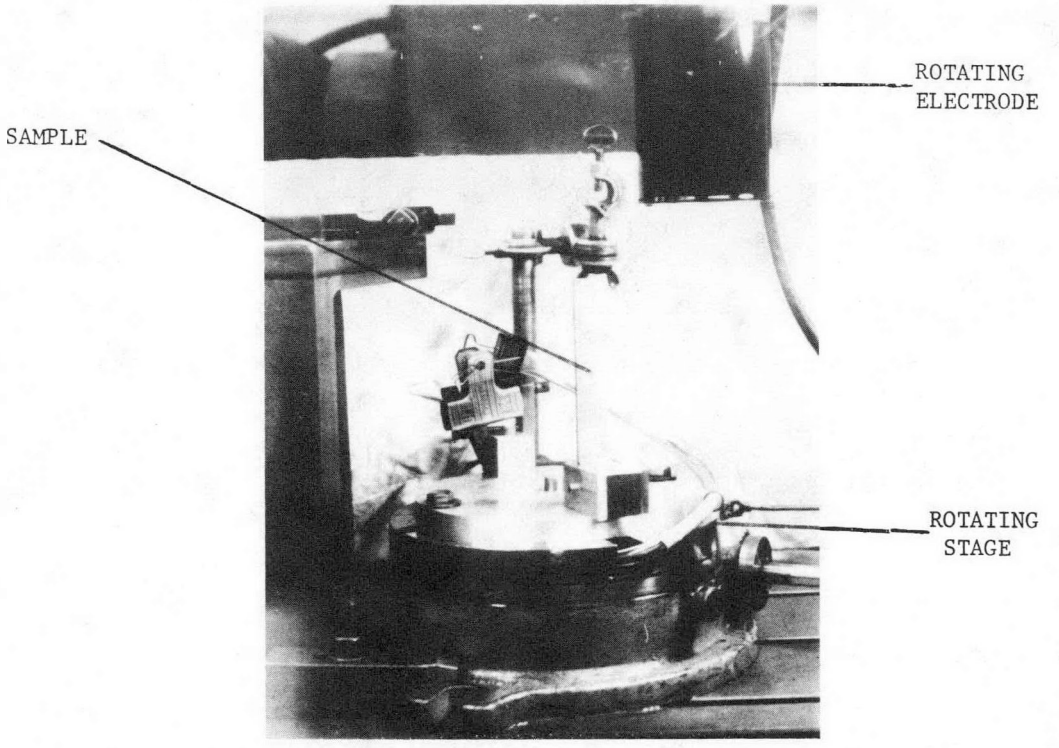

Fig. 4.2.1.4. Close-up of Circular Rotating Electrode and the Specimen.

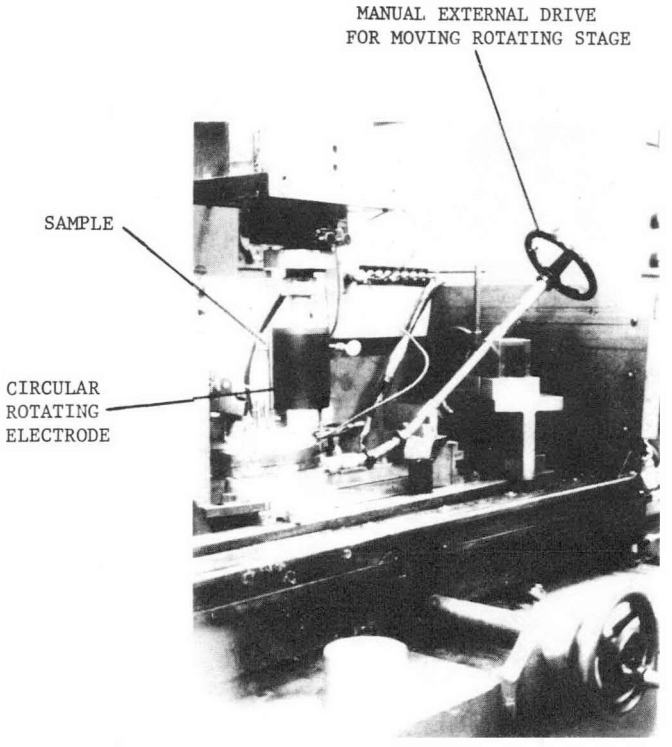

Fig. 4.2.1.5. View of EDM Apparatus Showing Mechanism Used to Rotate the Sample into the Electrode.

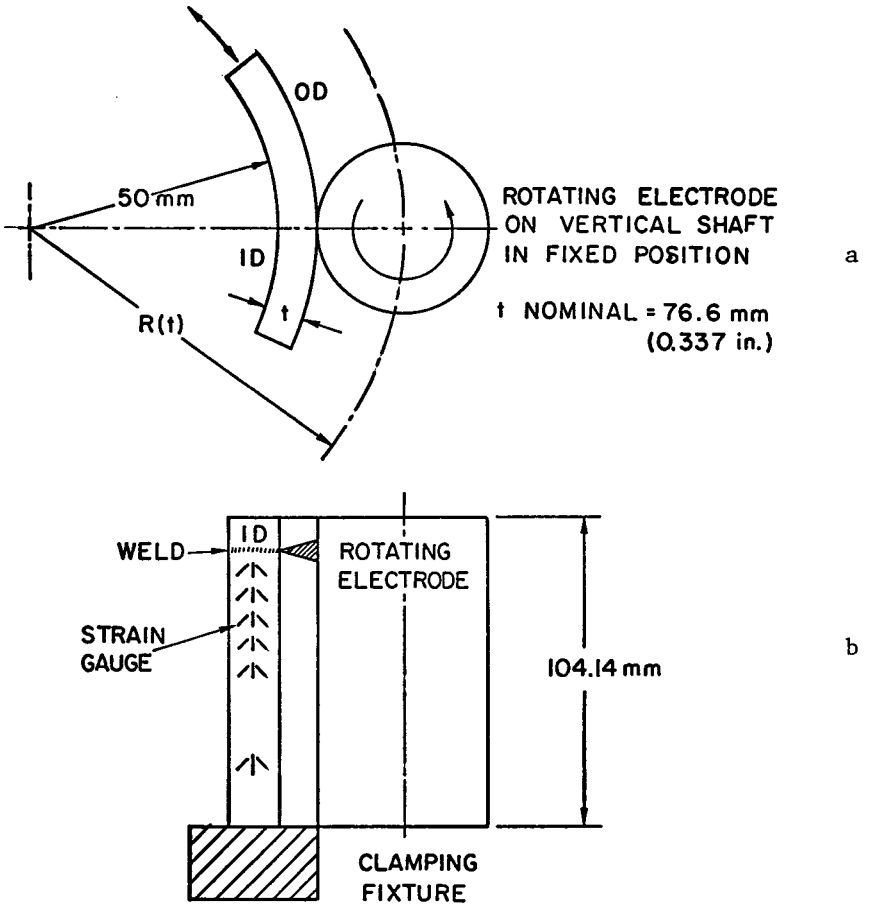

Fig. 4.2.1.6. Schematic Diagram Showing Electrode in Position Relative to Sample. (a) Plan view showing sample and rotating electrode relative position and (b) front view showing axial location of rotating electrode relative to sample weld.

Since the removal of each layer produces a redistribution of stress in the rest of the specimen, the measured strain relief cannot be used to directly calculate the residual-stress distribution in the undisturbed weldment. However, an analysis that accounts for the redistribution of stress was developed and is presented in Appendix A. This analysis shows that if the strains at the inner surface (denoted ε_{xL} and ε_{yL}) are known as a function of the remaining thickness (h), then the throughwall distribution of stress in the undisturbed specimen is given by

$$\sigma_x(z) = \frac{Ez}{2(1 - \nu^2)} \left(\frac{d\varepsilon_{xL}}{dh} + \nu \frac{d\varepsilon_{yL}}{dh} \right) \Bigg|_{h=z} + \frac{E}{1 - \nu^2} \int_z^{h_o} 1 - 3 \frac{z}{h} \left(\frac{d\varepsilon_{xL}}{dh} + m \frac{d\varepsilon_{yL}}{dh} \right) dh \qquad (4.2.1.4)$$

and

$$\sigma_y(z) = \frac{E_z}{2(1 - \nu^2)} \left(\frac{d\varepsilon_{yL}}{dh} + \nu \frac{d\varepsilon_{xL}}{dh} \right) \Bigg|_{h=z} + \frac{E}{1 - \nu^2} \int_z^{h_o} 1 - 3 \frac{z}{h} \left(\frac{d\varepsilon_{yL}}{dh} + \nu \frac{d\varepsilon_{xL}}{dh} \right) dh \; . \qquad (4.2.1.5)$$

The assumptions and limitations of this analysis are discussed in Appendix A. In the analysis of the experimental data, simple numerical approximations to the derivative and integral terms were used. The adequacy of the numerical procedures can be checked using the self-equilibrating nature of the stress distribution.

It is impractical to remove layers thicker than 0.6 mm (25 mils) by this EDM technique. Thus use of this technique to analyze the throughwall residual stresses in the 26-in. weldment, which is ∿33 mm thick, becomes prohibitively expensive, and an alternative technique was used. Strain gauges were laid on the inner and outer surfaces of the specimen as shown schematically in Fig. 4.2.1.7(a). The specimen was then cut into two equal thickness parts by EDM with a 0.7-mm-diam wire electrode. The axial stress changes on the inner and outer surfaces (denoted σ_x^i and σ_x^o, respectively) can be measured directly.

Since no net force or moment is acting on the section,

$$F_{x_1} + F_{x_2} = 0 ,$$

$$M_{x_1} + M_{x_2} + \frac{h}{2} F_{x_1} - \frac{h}{2} F_{x_2} = 0 , \qquad (4.2.1.6)$$

$$F_{y_1} + F_{y_2} = 0 ,$$

and

$$M_{y_1} + M_{y_2} + \frac{h}{2} F_{y_1} - \frac{h}{2} F_{y_2} = 0 , \qquad (4.2.1.7)$$

where F_{x_1}, F_{x_2}, M_{x_1}, M_{x_2}, etc., are the net forces and moments in the x- and y-coordinate directions associated with the two halves of the specimen, as shown schematically in Fig. 4.2.1.7(b). In accordance with the usual assumptions of thin-plate theory (see, e.g., Ref. 2), the distribution of strains across the thickness can be expressed in terms of the resultant forces and moments:

$$\varepsilon_x = \frac{y}{D} (M_x - \nu M_y) + \frac{1}{Eh} (F_x - \nu F_y)$$

and

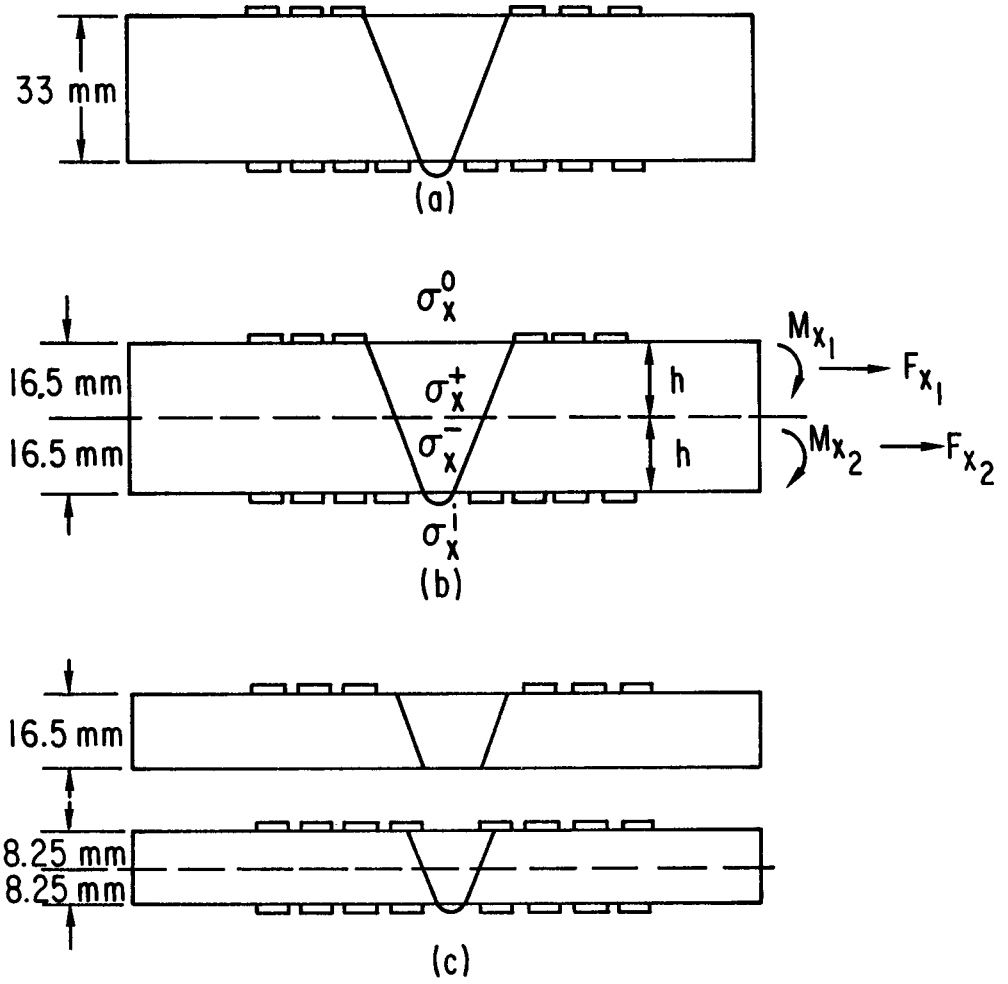

Fig. 4.2.1.7. Slicing Technique for 26-in. Pipe Segment: (a) Strain-gauge Locations, (b) EDM Wire Cut Dividing Specimen into Two Equal-thickness Parts, and (c) Strain-gauge Locations after the First Division.

$$\varepsilon_y = \frac{y}{D}(M_y - \nu M_x) + \frac{1}{Eh}(F_y - \nu F_x) , \qquad (4.2.1.8)$$

where y is measured from the midpoint of the section and

$$D = \frac{Eh^3}{12(1 - \nu^2)} \qquad (4.2.1.9)$$

The stresses can be computed from Eqs. 4.2.1.2 and 4.2.1.3. Combining Eqs. 4.2.1.6-9 and Eqs. 4.2.1.2-3, we find, after some algebra, expressions for the stress changes at the midsection (denoted σ_x^+ and σ_x^-) in terms of the stress changes on the inner and outer surfaces:

$$\sigma_x^+ = -(1 + \beta)\sigma_x^o + \beta\sigma_x^i$$

and

$$\sigma_x^- = \beta\sigma_x^o - (1 + \beta)\sigma_x^i \qquad (4.2.1.10)$$

where

$$\beta = \frac{1}{(2 - 3\nu^2)} . \qquad (4.2.1.11)$$

This estimate of the throughwall stress can be refined by instrumenting the two halves and repeating the procedure as indicated in Fig. 4.2.1.7(c).

Equation 4.2.1.10 shows that the stresses are discontinuous at the interfaces unless the stress is linearly distributed across the thickness. To obtain a smooth curve the values at each interface are averaged to obtain the final estimate of the stress.

4.2.2 X-ray Residual-stress Measurement Procedures

The strains measured by the strain gauges are average strains. The averaging occurs over an area on the order of the active area of the strain-gauge rosette [1.6 x 3 mm (0.1 x 0.12 in.)] and may "smear" the steep axial gradients of residual stress. Also, since the strains in a shallow surface layer cannot be completely relieved, strain-gauge techniques are not reliable as a method of determining stress profiles near the surface. To supplement the strain-gauge measurements, X-ray diffraction techniques have been used to profile the stresses in thin [0.08-mm (3-mil)] surface layers.

The X-ray diffraction residual-stress measurements were made using the two-angle technique. The specific technique was similar to that recommended by the Society of Automotive Engineers (SAE) publication Residual Stress Measurement by X-ray Diffraction, SAE J784a. However, it differed from the common SAE technique in three respects. First, the diffraction peak used for stress measurement was located using a five-point parabolic regression procedure rather than the more common three-point algebraic procedure. Second, the intensities measured at each of the five points were corrected for background intensity. Third, a method was used in which the sample was oscillated $\pm 0.5°$ about the mean ψ angle setting during measurement. This was done in an attempt to average over a large number of grains. This modification has provided a more linear dependence of the lattice spacing upon $\sin^2 \psi$ than can be obtained using the stationary-sample technique. Overall, these modifications improve the repeatability of the stress measurements. Details of the technique and diffractometer fixturing are as follows:

Diffraction Peak: (220)

Radiation: CrK_α

Incident-beam Divergency: 3.0°

Detection Slit: 0.5°

Filter: 0.018-mm Vanadium Foil

Counts per Point: 20,000

ψ Rotation: 0.0-45.0°

Beam Size: 3.3 x 7.1 mm (0.13 x 0.28 in.)

The apparent residual stress in an annealed powdered nickel zero stress standard was measured before and after the residual-stress measurements to determine the error due to instrument misalignment and sample positioning. These sources produce a systematic error of approximately $\pm$14 MPa ($\pm$2 ksi). Material was removed for subsurface measurement by electropolishing in a sulfuric-phosphoric-chromic acid solution to minimize the alteration of subsurface stresses by layer removal. Metcut Research Associates carried out the X-ray diffraction measurements under a subcontract from ANL.

4.3 Bulk Residual-stress Distributions

4.3.1 Stress Distributions in 4-in. Weldments

4.3.1.1 Weldment W27A

Weldment W27A is a mock-up fabricated from pipes from Heats 2P1486 and 454659 of Type 304 stainless steel. One side of the weldment was given a standard machining preparation (125 rms finish); the other was machined and then ground (125 rms finish). More detailed information on the weld preparation and the welding procedure for weldment W27A appears in Appendix B.

Strain gauges were mounted every 45° around the circumference of the weldment on the inner surface and every 90° on the outer surface. The azimuthal distribution and a typical axial distribution are shown schematically in Fig. 4.3.1.1. In the plots of residual stress, the actual data points are indicated by the symbols □ and ○ for axial and hoop stresses, respectively. Smooth curves were then drawn between the data points using cubic spline interpolation. Detailed information on strain-gauge placement appears in Table 4.3.1.1.

Strain-relief measurements were made on 12-mm-wide by 125-mm-long specimens of full wall thickness. These data can be compared with the strains obtained

TABLE 4.3.1.1

Strain-Gauge Locations for Weldment W27A

AZIMUTH	ROSETTE POSITION						
	3	2	1	4	5	6	7
	Inner Surfaces (Axial Distance from Weld-fusion Line, mm)						
0	18.2	7.9	2.4	on weld	2.4	7.9	15.1
45	18.2	7.9	2.4	-	2.4	7.9	21.4
90	18.2	7.9	2.4	on weld	2.4	7.9	15.1
135	18.2	7.9	2.4	-	2.4	7.9	15.1
180	18.2	7.9	2.4	on weld	2.4	7.9	15.1
225	18.2	7.9	2.4	-	2.4	7.9	15.1
270	18.2	7.9	2.4	on weld	2.4	7.9	15.1
315	18.2	7.9	2.4	-	2.4	7.9	15.1
	Outer Surface (Axial Distance from Weld Centerline, mm)						
45	23.0	17.9	10.3	-	-	-	-
135	26.2	19.8	13.5	-	13.5	19.8	26.2
225	23.0	17.9	10.3	-	13.5	19.8	26.2
312	23.0	17.9	10.3	-	-	-	-

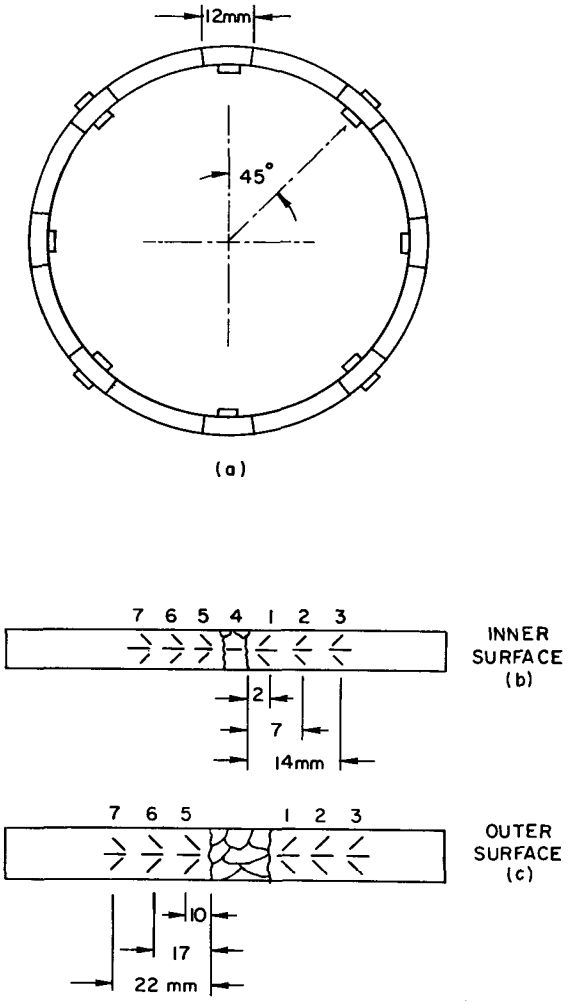

Fig. 4.3.1.1. Schematic Diagram of Azimuthal and Axial Distributions of Strain Gauges on Weldment W27A.

after the full-thickness bar specimens have been sliced to produce a final "strip" specimen 1.5 mm thick.

Figure 4.3.1.2 presents the azimuthal distribution of bulk residual stress on the inner surface for Heat 2P1486 at gauge positions 1-3 (2.4, 7.9, and 18.2 mm from the edge of the weld fusion line, respectively). The solid lines indicate data obtained from the thin (1.5-mm) strip specimens, and the dashed lines indicate data obtained from the full-thickness (8.6-mm) bar specimens. Figure 4.3.1.3 presents the same information at gauge positions 5-7. The material on this half of the weldment is fabricated from Heat 454659. Figure 4.3.1.4 shows azimuthal distribution of the residual stress on the weld.

The stresses at most gauge positions show a doubly periodic oscillation, and to accurately map the residual welding stresses, gauges must be placed at least every 45°. However, the peak-to-peak variations at each gauge position are modest compared with the magnitude of the peak stress at each position. Since the yield strength at the service temperature of 280°C (540°F) is 160 MPa (22 ksi), Figs. 4.3.1.2 and 4.3.1.3 show that, at gauge positions 1 and 5, 2.4 mm from the weld fusion line, significant portions of the inner surface are stressed beyond the nominal yield.

Axial stress distributions normal to the weld at 45, 90, 180, and 270° are presented in Fig. 4.3.1.5. They conform to the expected bell-shape distribution.[3-5] The results of the bulk residual-stress measurements are summarized in Table 4.3.1.2, which shows the average stresses, peak stresses, and peak-to-peak variations at each gauge position.

4.3.1.2 Weldment W27B

Weldment W27B is a mock-up fabricated by the General Electric Company from Type 304 stainless steel (Heat 7772). The two sides of the weldment were given different inner surface preparations. One side was lightly ground to a 63 rms finish, and the other was heavily ground to a 125 rms finish. More detailed

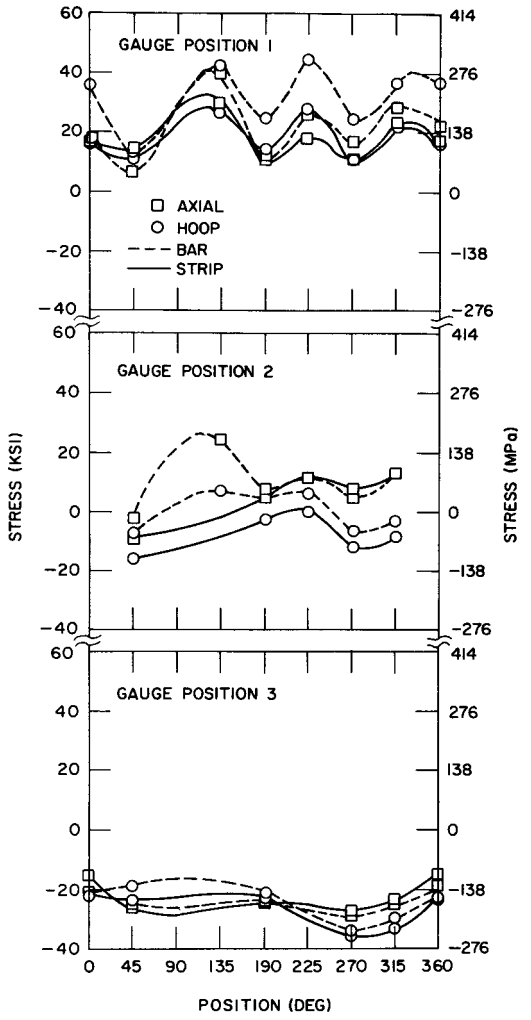

Fig. 4.3.1.2 Azimuthal Distribution of Axial and Hoop Stresses on Inner Surface at Gauge Positions 1-3 for Weldment W27A.

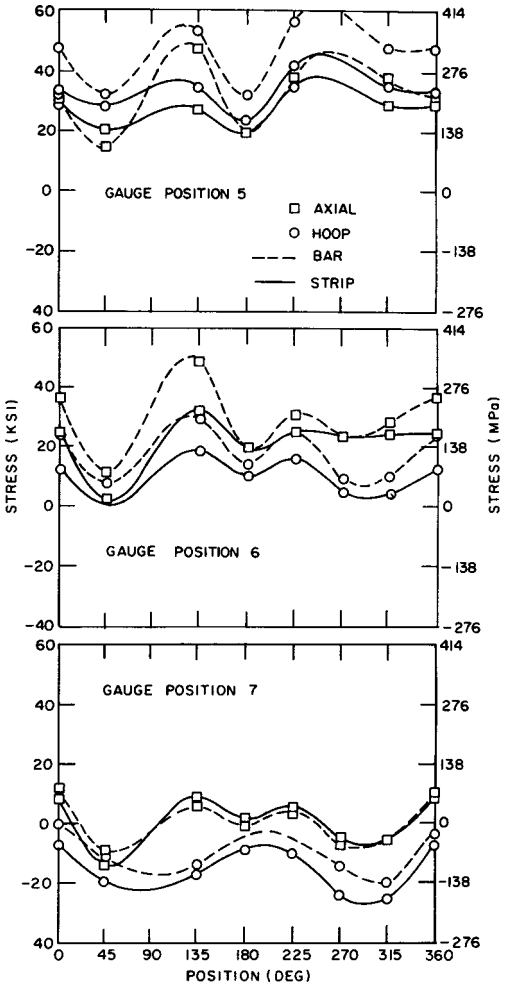

Fig. 4.3.1.3. Azimuthal Distribution of Axial and Hoop Stresses on Inner Surface at Gauge Positions 5-7 for Weldment W27A.

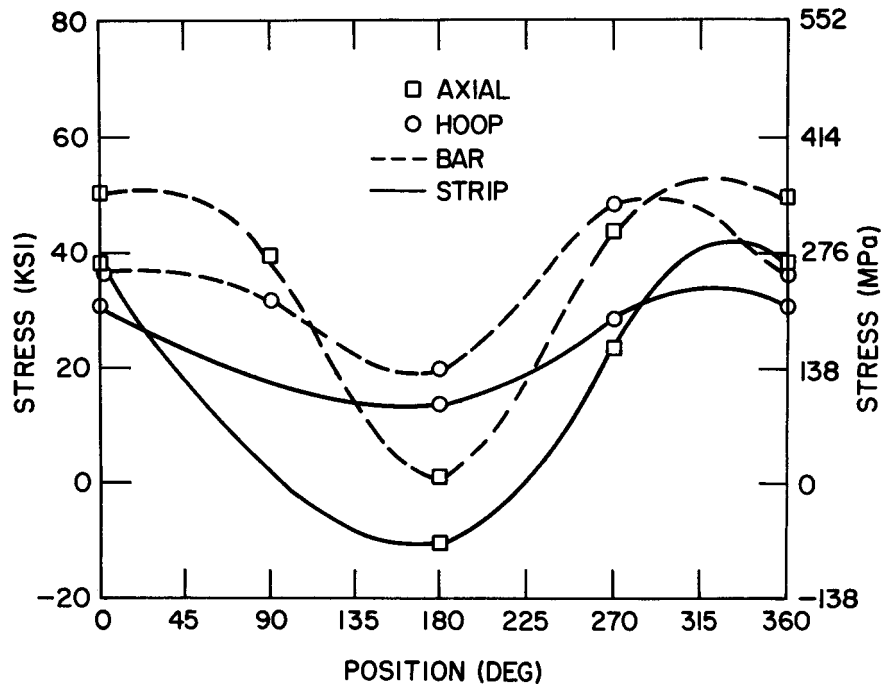

Fig. 4.3.1.4. Azimuthal Distribution of Axial and Hoop Stresses on Inner Surface at Gauge Position 4 on the Weld for Weldment W27A.

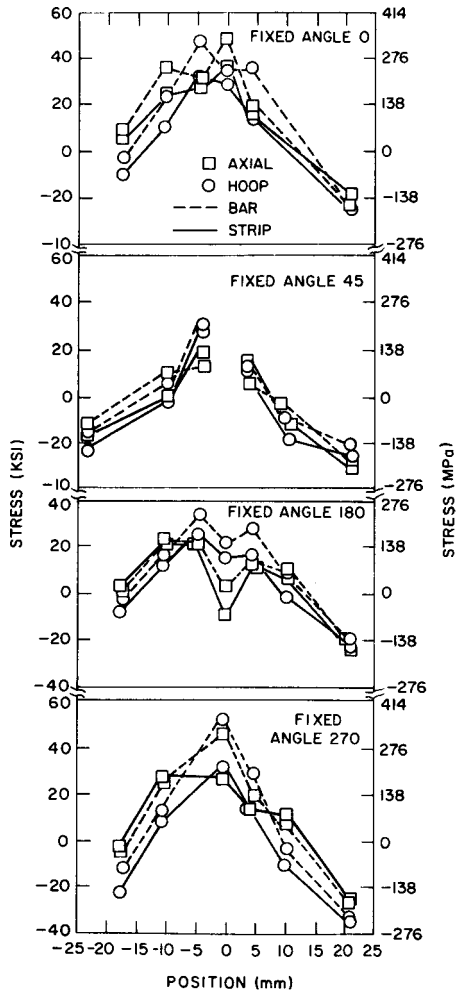

Fig. 4.3.1.5. Axial Variation of Hoop and Axial Stresses on Inner Surface Across the Weld for Weldment W27A.

TABLE 4.3.1.2

Bulk-Residual-Stress Summary on Inner Surface for Weldment W27A

	ROSETTE POSITION						
	3	2	1	4	5	6	7
Average Axial Stress	-164	93	136	236	193	157	0 MPa
	- 23	13	19	33	27	22	0 ksi
Average Hoop Stress	-164	21	143	242	250	71	-79 MPa
	- 23	3	20	34	35	10	-11 ksi
Peak Axial Stress	-107	96	170	273	249	234	64 MPa
	- 15	13	24	38	35	33	9 ksi
Peak Hoop Stress	-151	0	202	219	296	137	-51 MPa
	- 21	0	28	31	41	19	- 7 ksi
Axial Peak-to-Peak Variation	87	159	89	347	112	218	164 MPa
	12	22	13	48	16	31	23 ksi
Hoop Peak-to-Peak Variation	105	118	122	122	130	132	127 MPa
	15	16	17	17	18	18	18 ksi

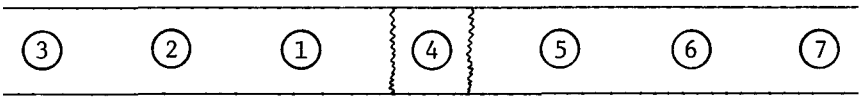

information on the weld preparation and welding procedure is given in Appendix B.

Strain gauges were laid every 45° around the circumference of the pipe on both the inner and outer surfaces. On the inner surface, four gauges were laid at the 0, 90, 180, and 270° azimuthal positions. At these positions, one gauge was laid directly on the weld bead (position 3), two others (positions 1 and 4) were laid in the land on each side of the weld 2.4 mm from the weld fusion line, and an additional gauge (position 2) was laid on one side of the weld 13.5 mm from the weld fusion line. At the 45, 135, 225, and 315° positions, two gauges were laid, one directly on the weld (position 3), and the other in the weld land (position 1), 2.4 mm from the weld fusion line. On the outer surface, two gauges were laid every 45°, one directly on the weld centerline (position 3), and the other 8.7 mm from the weld centerline (position 1). The placement of the gauges is summarized in Table 4.3.1.3.

The azimuthal distribution of axial and hoop stress is shown in Figs. 4.3.1.6 and 4.3.1.7. The peak stresses far exceed the yield stress of 160 MPa (22 ksi) at the service temperature of 280°C (540°F). Not only do the peak stress values exceed the yield stress, but, as Fig. 4.3.1.6 shows, the stresses exceed yield for large portions of the inner surface at gauge positions 1 and 4. The peak-to-peak variations for this weldment are the largest in the group of weldments studied.

The results of the bulk residual-stress measurements are summarized in Table 4.3.1.4, which shows the average stresses, peak stresses, and peak-to-peak variations at each gauge position.

4.3.1.3 Weldment W27C

Weldment W27C is a mock-up fabricated from Type 304 stainless steel. Both sides are from Heat 7772. The two sides of the weldment were given different surface preparations. One was lightly machined to a 63 rms finish; the other

TABLE 4.3.1.3

Strain-Gauge Locations for Weldment W27B

AZIMUTH	ROSETTE POSITION 2	1	3	4
	Inner Surface (Axial Distance from Weld-Fusion Line, mm)			
0	13.5	2.4	on weld	2.4
45	-	-	on weld	-
90	13.5	2.4	on weld	2.4
135	-	-	on weld	-
180	13.5	2.4	on weld	2.4
225	-	-	on weld	-
270	13.5	2.4	on weld	2.4
315	-	-	on weld	-
	Outer Surface (Axial Distance from Weld Centerline, mm)			
0	-	8.7	on weld	-
45	-	8.7	on weld	-
90	-	8.7	on weld	-
135	-	8.7	on weld	-
180	-	8.7	on weld	-
225	-	8.7	on weld	-
270	-	8.7	on weld	-
315	-	8.7	on weld	-

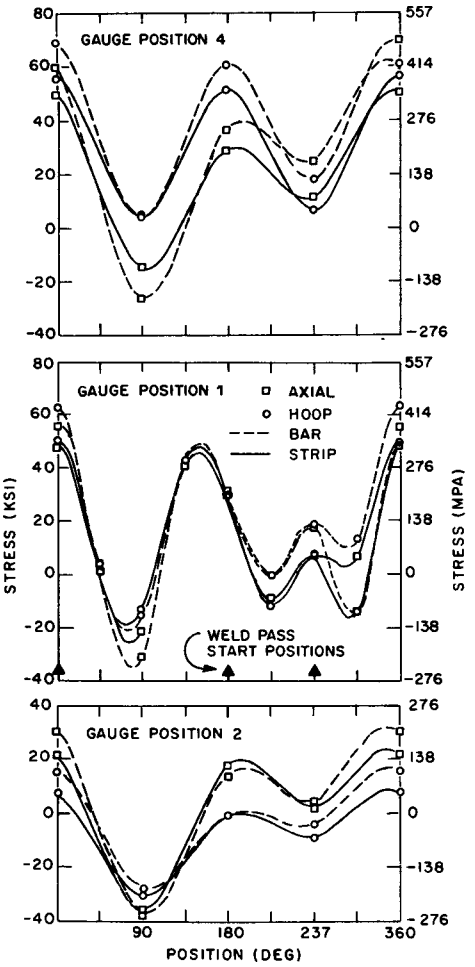

Fig. 4.3.1.6. Azimuthal Distribution of Axial and Hoop Stresses on Inner Surface at Gauge Positions 4, 1, and 2 for Weldment W27B.

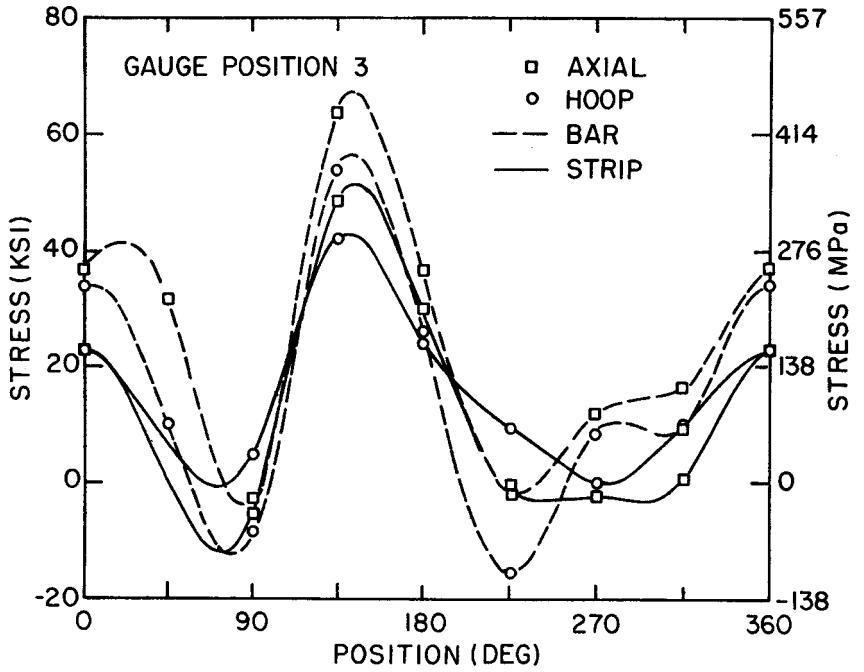

Fig. 4.3.1.7. Azimuthal Distribution of Axial and Hoop Stresses on Inner Surface at Gauge Position 3 on the Weld for Weldment W27B.

TABLE 4.3.1.4

Bulk-Residual-Stress Summary on Inner Surface for Weldment W27B

	ROSETTE POSITION				
	2	1	3	4	
Average Axial Stress	14	83	84	141	MPa
	2	12	12	20	ksi
Average Hoop Stress	-55	104	114	219	MPa
	- 8	15	16	30	ksi
Peak Axial Stress	159	352	347	367	MPa
	22	49	49	51	ksi
Peak Hoop Stress	59	364	301	413	MPa
	8	51	42	58	ksi
Axial Peak-to-Peak Variation	409	317	387	464	MPa
	57	44	55	65	ksi
Hoop Peak-to-Peak Variation	272	451	301	377	MPa
	38	63	42	53	ksi

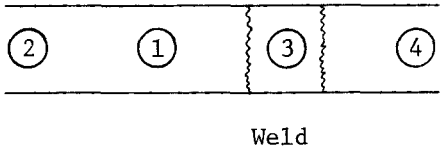

was heavily machined to a 125 rms finish. More detailed information on the weld preparation and welding procedure appears in Appendix B.

Strain gauges were laid every 90° around the circumference of the pipe on both the inner and outer surfaces. At each circumferential position, two gauges were laid on each side of the weld. On the inner surface, the gauges were laid 2.4 and 7.9 mm from the weld fusion line. On the outer surface, the spacing was more variable, due to the surface roughness; typically, the gauges were laid approximately 11 and 17 mm from the weld fusion line. Table 4.3.1.5 contains detailed information on strain-gauge placement.

Figure 4.3.1.8 presents the azimuthal distribution of bulk residual stress on the inner surface at gauge positions 1 and 2 (2.4 and 7.9 mm from the weld fusion line, respectively). The solid lines indicate data obtained from the thin (1.5-mm) strip specimens, and the dashed lines indicate data obtained from the full-thickness (8.6-mm) bar specimens. Figure 4.3.1.9 presents the same information for gauge positions 3 and 4 located on the other side of the weld.

The results of the bulk residual-stress measurements are summarized in Table 4.3.1.6, which shows the average stresses, peak stresses, and peak-to-peak variations at each guage position. The average axial stresses in the critical weld land region are ∿225 MPa (31 ksi), which is well above the nominal yield stress of 160 MPa (22 ksi) at the service temperature of 280°F (540°F).

The stresses at positions 1 and 3 close to the weld fusion line appear to be fairly symmetric. However, the stresses at gauge position 4 appear to be significantly higher than those at the corresponding position 2. The reason for this unexpected form of the distribution is not clear.

TABLE 4.3.1.5

Strain-Gauge Locations for Weldment W27C

AZIMUTH	ROSETTE POSITION 2	1	3	4
	Inner Surface (Axial Distance from Weld-Fusion Line, mm)			
0	7.9	2.4	2.4	7.9
90	7.9	2.4	2.4	7.9
180	7.9	2.4	2.4	7.9
270	7.9	2.4	2.4	7.9
	Outer Surface (Axial Distance from Weld Centerline, mm)			
0	19.8	13.5	11.1	17.5
90	17.5	11.1	10.3	16.7
180	15.9	9.5	10.3	15.9
270	18.2	11.9	7.9	12.7

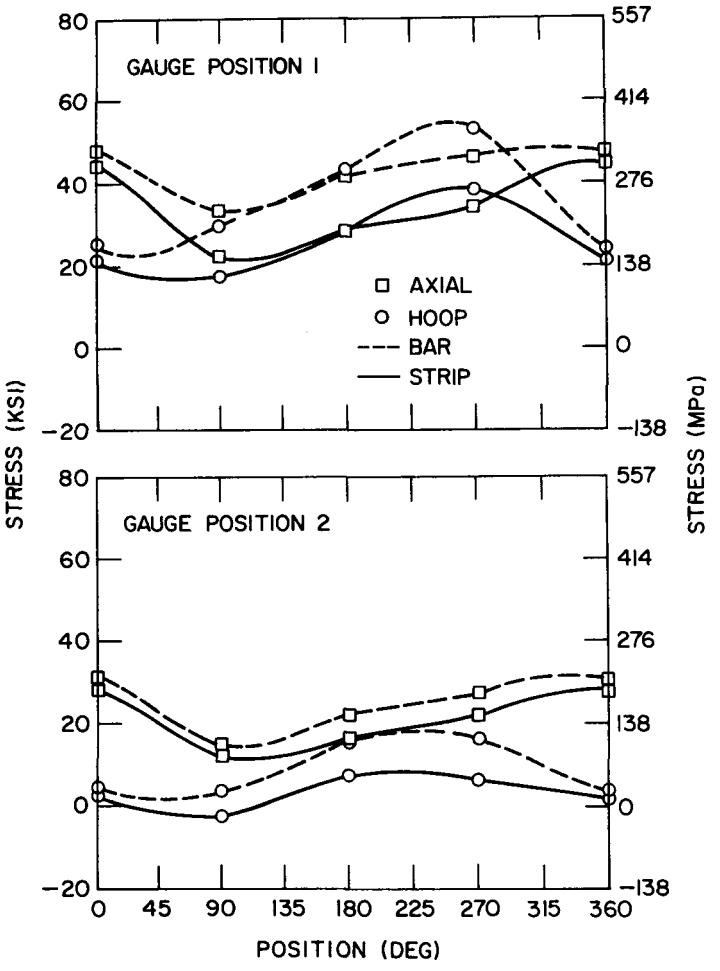

Fig. 4.3.1.8. Azimuthal Distribution of Axial and Hoop Stresses on Inner Surface at Gauge Positions 1 and 2 for Weldment W27C.

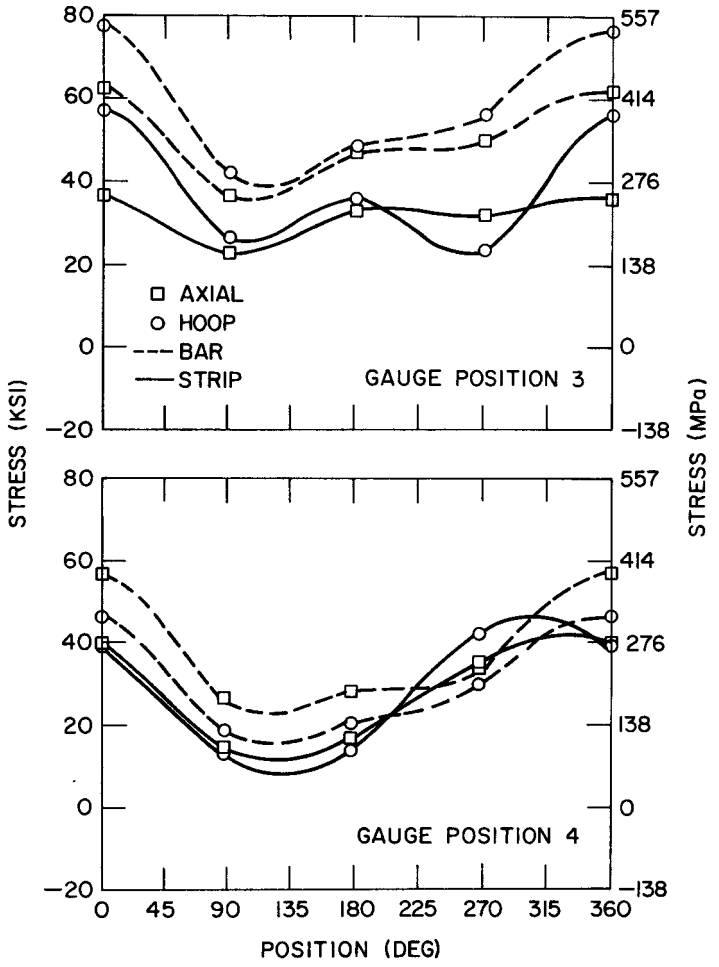

Fig. 4.3.1.9. Azimuthal Distribution of Axial and Hoop Stresses on Inner Surface at Gauge Positions 3 and 4 for Weldment W27C.

TABLE 4.3.1.6

Bulk-Residual-Stress Summary on Inner Surface for Weldment W27C

	ROSETTE POSITION			
	2	1	3	4
Average Axial Stress	140	229	220	234 MPa
	20	32	31	33 ksi
Average Hoop Stress	21	186	250	236 MPa
	3	26	35	33 ksi
Peak Axial Stress	199	315	256	326 MPa
	28	44	36	46 ksi
Peak Hoop Stress	52	270	401	346 MPa
	17	38	56	48 ksi
Axial Peak-to-Peak Variation	113	158	97	305 MPa
	16	22	14	25 ksi
Hoop Peak-to-Peak Variation	70	147	235	211 MPa
	10	21	33	29 ksi

Weld

Heavily Machined Lightly Machined

4.3.1.4 Autopsy Weldments from Monticello and Dresden-3 BWRs

In addition to the mock-up weldments, two autopsy weldments that have undergone actual reactor operating service have been examined. An objective of this portion of our work was to investigate the possibility that the high stresses associated with the weldments shakedown during service. Unfortunately, we could not obtain straight butt-welded pipe segments, and both autopsy weldments being analyzed consist of a 90° elbow butt welded to a straight pipe segment. However, both are 4-in. Type 304 stainless steel, Schedule 80, seamless piping. The constraint due to the elbow differs from the constraint due to a spool piece; hence, the form of the residual stress distribution differs for the two geometries. It was hoped there would be sufficient similarity to the straight-pipe weldments to study the possibility of shakedown.

The first autopsy weldment examined was from the Monticello BWR. On the inner surface of the weldment, strain rosettes were laid every 45°. One rosette was laid directly on the weld (gauge position 3); a second gauge was laid in the weld land 2.4 mm from the weld fusion line (gauge position 1); a third rosette was laid 13.5 mm from the weld fusion line (gauge position 2). At the 0, 90, 180, and 270° azimuthal positions, an additional gauge was laid in the weld land on the other side of the weld 2.4 mm from the weld fusion line (gauge position 4). Gauge positions 1 and 2 are on the straight-pipe section, and gauge position 4 is on the elbow side of the weld. Rosettes were also laid every 45° on the outside surface. One rosette was laid directly on the weld bead (gauge position 3), and additional rosettes were laid 10.3 (gauge position 1) and 16.7 mm (gauge position 2) from the center of the weld. The details of the strain-rosette placement are summarized in Table 4.3.1.7. The 4-in. weldment from the Dresden-3 BWR was instrumented in identical fashion.

The azimuthal distributions of hoop and axial strain for the Monticello weldment are shown in Fig. 4.3.1.10, and the results are summarized in Table

TABLE 4.3.1.7

Strain-Gauge Locations for Dresden 3 and Monticello
Autopsy Weldments

AZIMUTH	ROSETTE POSITION 2	1	3	4
	Inner Surface (Axial Distance from Weld-fusion Line, mm)			
0	13.5	2.4	on weld	2.4
45	13.5	2.4	on weld	-
90	13.5	2.4	on weld	2.4
135	13.5	2.4	on weld	-
180	13.5	2.4	on weld	2.4
225	13.5	2.4	on weld	-
270	13.5	2.4	on weld	2.4
315	13.5	2.4	on weld	-
	Outer Surface (Axial Distance from Weld Centerline, mm)			
0	16.7	10.3	on weld	-
90	16.7	10.3	on weld	-
180	16.7	10.3	on weld	-
270	16.7	10.3	on weld	-

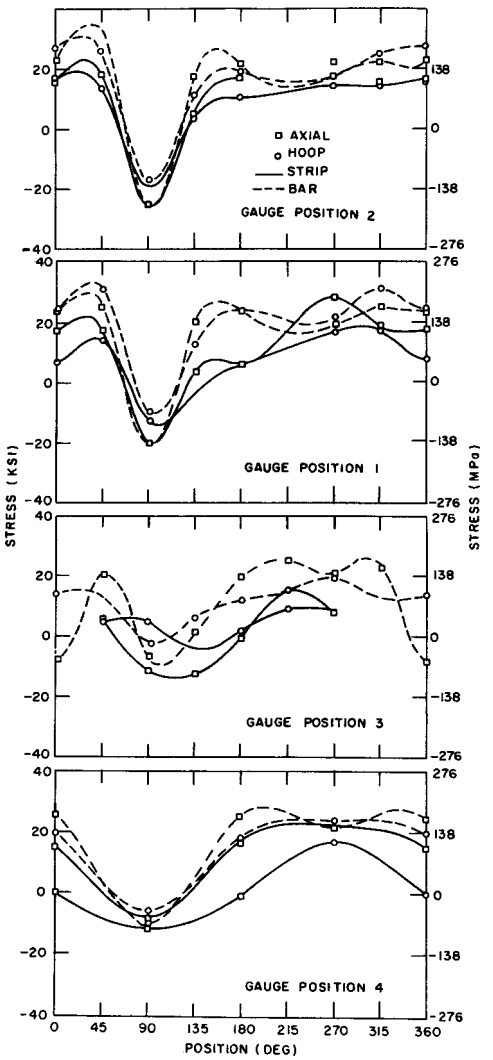

Fig. 4.3.1.10. Azimuthal Variation of Axial and Hoop Stresses on the Inner Surface for the Monticello Autopsy Weldment.

4.3.1.8. The values at gauge positions 1 and 4 slightly away from the weld fusion line are of most interest. The qualitative character of the stress distributions is similar to that of the other 4-in. weldments. The peak values are only slightly higher than the nominal yield stress, 160 MPa (22 ksi), at the service temperature of 280°C (540°C). The magnitude of the average axial stress is approximately half the average value for the mock-up weldments in the critical regions 2.5 mm from the weld fusion line. However, it is within the spread of values obtained for the mock-up weldments. The magnitude of the hoop stress is approximately one-third the average hoop stress for the mock-up weldments and is outside the spread of values obtained for the mock-up weldments.

Figure 4.3.1.11 shows the azimuthal distributions of hoop and axial stress for the Dresden-3 weldment, and Table 4.3.1.9 summarizes the results. The stresses are remarkably low compared with the mock-up weldments and the similar weldment from Monticello. The average axial stress is compressive at all gauge positions, and the absolute magnitude is relatively small. This suggests that the low stresses are not due to shakedown in service, since this would be expected to produce stresses (tensile or compressive) just below the yield stress at the service temperature. Thus, the relatively low stresses seen in the straight-pipe-to-elbow weldments are most likely due to the different restraint imposed by the elbow geometry. The two elbow welds may also have been stress-relieved; however, metallurgical examination, while not conclusive, suggests that this is not the case.

4.3.2 10-in. Dresden-2 Autopsy Weldment

The 10-in. autopsy pipe weldment examined is a seamless Type 304 stainless steel Schedule-80 field-welded piece from the Dresden-2 BWR. It was taken from the loop A emergency core-spray line just ahead of a check valve on the pump side.

Strain gauges were mounted every 45° around the circumference on the inside surface of the weldment. At the 0, 90, 180, and 270° positions, five gauges were mounted along the axial direction. One gauge was laid directly on the weld

TABLE 4.3.1.8

Bulk-Residual-Stress Summary on Inner Surface Monticello Weldment

	ROSETTE POSITION			
	2	1	3	4
Average Axial Stress	86	86	73[a]	103 MPa
	12	12	10	14 ksi
Average Hoop Stress	57	51	67[a]	81 MPa
	8	7	10	12 ksi
Peak Axial Stress	157	199	110	159 MPa
	22	28	15	22 ksi
Peak-to-Peak Axial Variation	339	344	199	219 MPa
	47	48	27	30 ksi
Peak-to-Peak Hoop Variation	256	210	95	205 MPa
	36	30	13	29 ksi

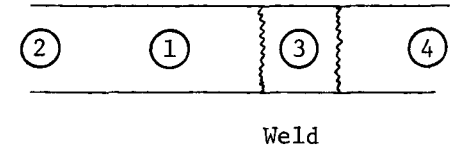

[a]In reading the "strip" specimens, we found these gauges to be open. The values here are estimates equal to 80% of the values obtained from "bar" specimens; this is consistent with the change from "bar" to "strip" specimens observed at other locations and for other 4-in. weldments.

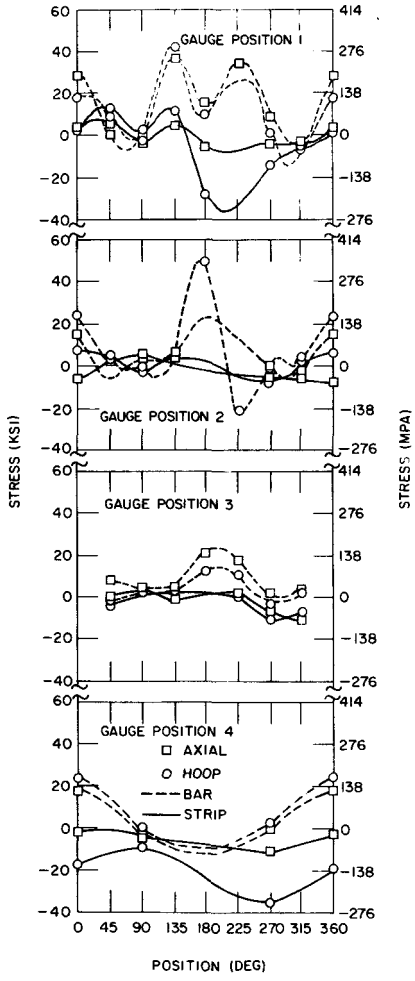

Fig. 4.3.1.11. Azimuthal Variation of Axial and Hoop Stresses on the Inner Surface for the Dresden 3 Autopsy Weldment.

TABLE 4.3.1.9

Bulk-Residual-Stress Summary on the Inner Surface for Dresden 3 Weldment

	ROSETTE POSITION				
	2	1	3	4	
Average Axial Stress	-20	-2	-16	-34	MPa
	-2	-0.3	-2.2	-4.3	ksi
Average Hoop Stress	12	-20	-18	-141	MPa
	1.7	-2.6	-2.7	-19.7	ksi
Peak Axial Stress	30	45	16	-10	MPa
	4	6	2	-1	ksi
Peak-to-Peak Axial Variation	51	84	90	60	MPa
	7	11	12	8	ksi
Peak-to-Peak Hoop Variation	92	284	88	182	MPa
	13	39	12	25	ksi

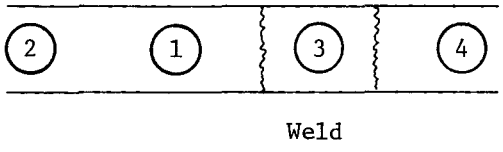

(position 3) and two additional gauges on each side of the weld. On one side, one was laid in the weld land 2.4 mm from the weld fusion line (position 1), and a second was laid 15.1 mm from the weld fusion line (position 2). On the other side of the weld, gauges were laid 2.4 and 18.2 mm from the weld fusion line, positions 4 and 5 respectively. At the 45, 135, 225, 315, 330, and 345° positions, one gauge was laid directly on the weld (position 1). On the outer surface, a gauge was placed every 45° on the weld centerline position 3). At the 0, 90, 180 and 270° positions, two additional gauges were mounted 13.5 and 19.8 mm from the weld centerline, positions 1 and 2, respectively. The gauges placed on the weld were Micro Measurements EA-09-030YB-120 gauges, rather than the MM CEA-09-062UR-120 gauges used for the bulk of the measurements. The placement of the strain gauges is summarized in Table 4.3.2.1.

Figure 4.3.2.1 presents the azimuthal distribution of bulk residual stress on the inner surface at gauge positions 1 and 2 (2 and 14 mm from the edge of the weld fusion line, respectively). The solid lines indicate data obtained from thin (1.5-mm) strip specimens, and the dashed lines indicate data obtained from the full-thickness (8.6-mm) bar specimens. Figure 4.3.2.2 presents the same information for gauge position 4 and 5.

Figure 4.3.2.3 shows the stresses on the weld (gauge position 3). Unlike the 4-in. weldments, large differences exist between the stress values obtained from the bar specimens and those from the strip specimens, at least for gauge positions close to the weld. For example, the axial stress at position 1 obtained from the strip specimen has a peak value of 360 MPa (50 ksi); the peak axial stress at position 1 obtained from the bar specimen is only 215 MPa (30 ksi). Similar changes occur at position 4 symmetrically located on the other side of the weld and at position 3 on the weld.

Two striking qualitative differences exist between the stress distributions shown in Figs. 4.3.2.1-3 and those typical of the 4-in. pipe weldments. First, although the hoop and axial stresses were virtually equal at points for all the

TABLE 4.3.2.1

Strain-Gauge Locations for the 10-in. Dresden 2 Weldment

AZIMUTH	ROSETTE NUMBER 2	1	3	4	5
	Inner Surface (Axial Distance of Strain Rosettes from the Weld-fusion Line, mm)				
0	15.1	2.4	on weld	2.4	18.2
45	-	2.4	on weld	-	-
90	15.1	2.4	on weld	2.4	18.2
135	-	2.4	on weld	-	-
180	15.1	2.4	on weld	2.4	18.2
225	-	2.4	on weld	-	-
270	15.1	2.4	on weld	2.4	18.2
315	-	2.4	on weld	-	-
330	-	2.4	on weld	-	-
345	-	2.4	on weld	-	-
	Outer Surface (Axial Distance of Strain Rosettes from the Weld Centerline, mm)				
0	19.8	13.5	on weld	-	-
45	-	-	on weld	-	-
90	19.8	13.5	on weld	-	-
135	-	-	on weld	-	-
180	19.8	13.5	on weld	-	-
225	-	-	on weld	-	-
270	19.8	13.5	on weld	-	-
315	-	-	on weld	-	-

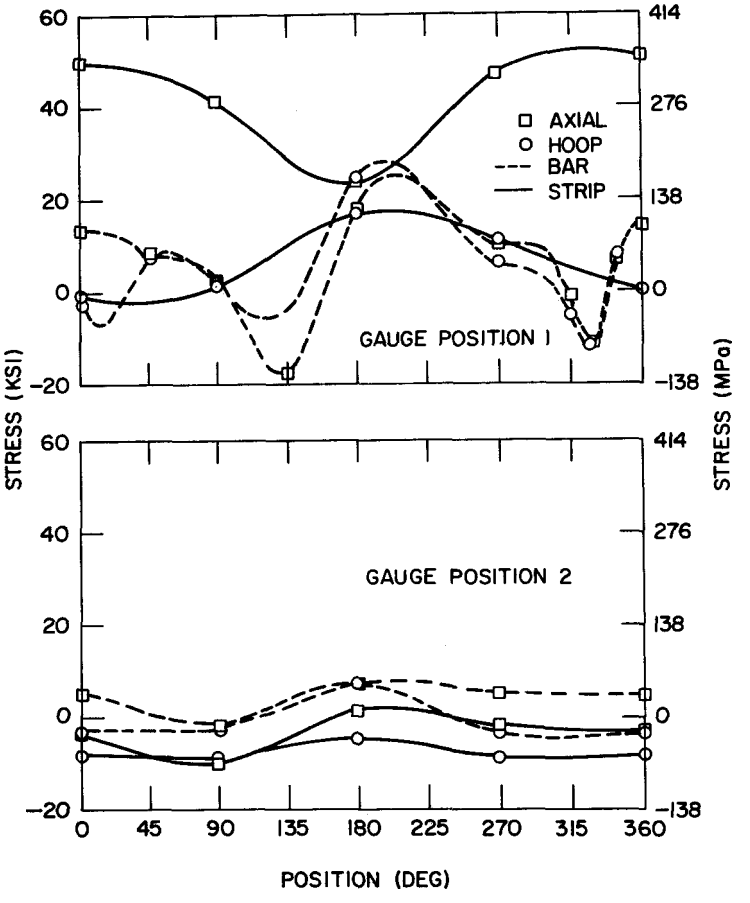

Fig. 4.3.2.1. Azimuthal Variation of Axial and Hoop Stresses on the Inner Surface at Gauge Positions 1 and 2 for the 10-in. Dresden 2 Weldment.

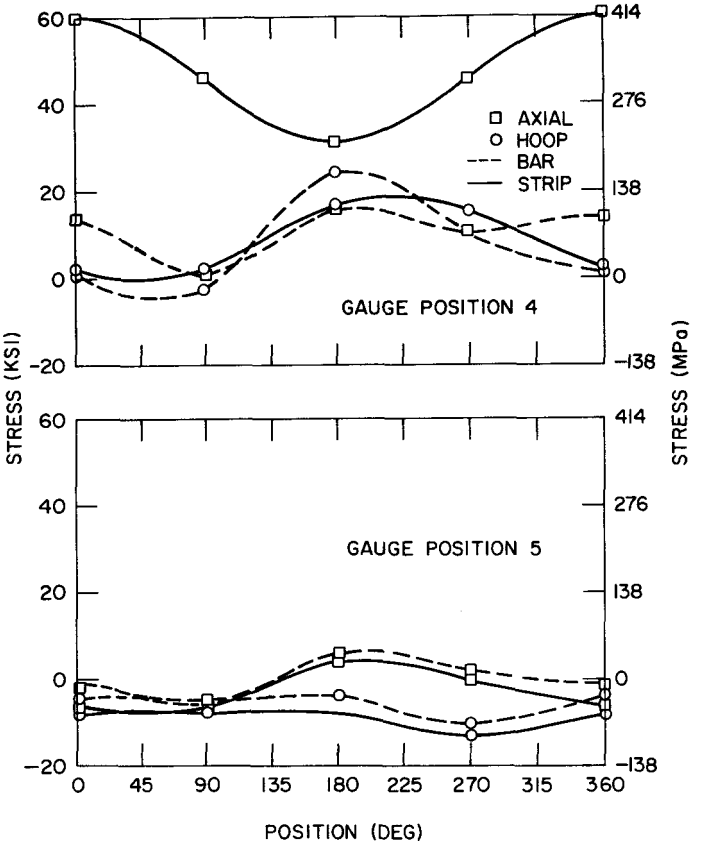

Fig. 4.3.2.2. Azimuthal Variation of Axial and Hoop Stresses on the Inner Surface at Gauge Positions 4 and 5 for the 10-in. Dresden 2 Weldment.

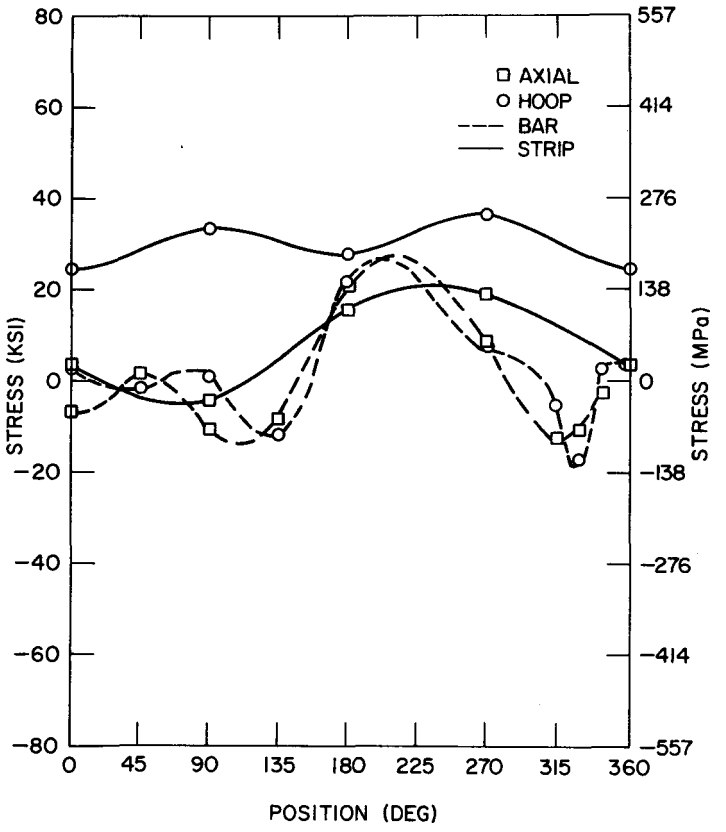

Fig. 4.3.2.3. Azimuthal Variation of Axial and Hoop Stresses on the Inner Surface on the Weld for the 10-in. Dresden 2 Weldment.

4-in. weldments examined, large differences in magnitude exist between the axial and hoop stresses for the 10-in. weldment, with the axial stress generally much larger than the hoop stress.

An additional difference is also observable in the axial distribution of stress at fixed azimuthal angles shown in Fig. 4.3.2.4. The hoop stresses follow the expected bell-shape distribution (see, e.g., Refs. 3-5), with the peak stresses occurring on the weld; however, the axial stresses follow a bimodal "rabbit-ear" distribution with the peak stresses occurring on either side of the weld. Similar results have been observed in other investigations,[6-8] and several explanations of the phenomenon have been proposed. Computer simulation of the welding process using an elastic-plastic finite-element model also predicts a bimodal distribution.[9]

The results of the bulk residual-stress measurements are summarized in Table 4.3.2.2, which shows the average stresses, peak stresses, and peak-to-peak variation at each gauge position. The results in Table 4.3.2.2 indicate that the stress distribution is symmetrical about the weld.

4.4 Surface Residual Stresses

To assess the importance of preweld surface treatment on the final postweld distribution of residual stress, X-ray diffraction techniques were used to measure surface residual stresses on specimens from each of the mock-up weldments W27A, W27B, and W27C. As shown in Table 4.2.1.1, the two halves of the weldment received different preweld surface treatments. Nine full-wall-thickness specimens ∿15 mm wide and ∿200 mm long were cut from these weldments using EDM techniques and sent to Metcut Research Associates for X-ray diffraction measurements. During the parting-out process, the thermomechanically induced welding stresses are almost completely relieved. Thus the surface stresses on the specimens are due solely to the surface treatment. Of course, to obtain the actual surface stresses on

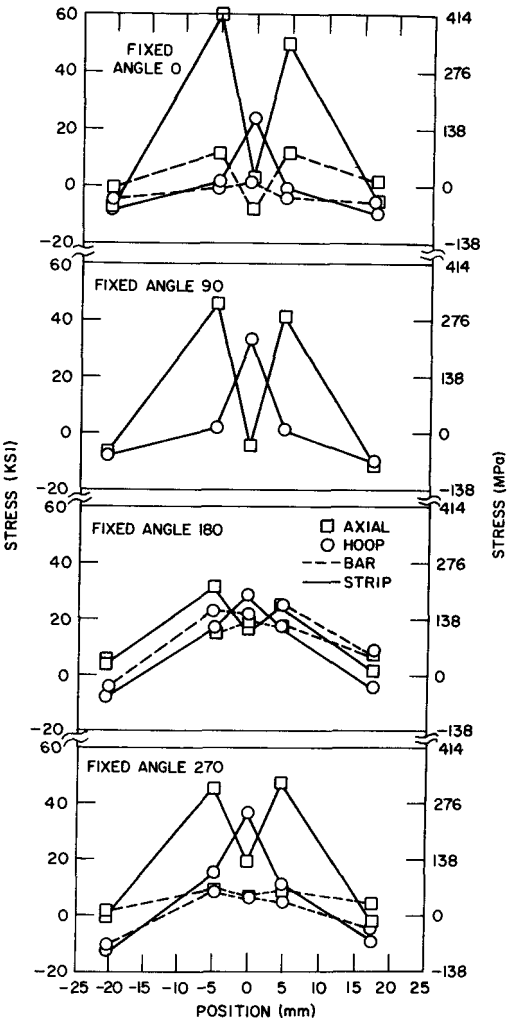

Fig. 4.3.2.4. Axial Variation of Hoop and Axial Stresses Across the Weld for the 10-in. Dresden 2 Weldment.

TABLE 4.3.2.2

Inner-Surface Bulk-Residual-Stress Summary for
The 10-in. Dresden 2 Weldment

	ROSETTE POSITION					
	2	1	3	4	5	
Average Axial Stress	-29	293	62	325	-16	MPa
	-4	41	9	45	-2	ksi
Average Hoop Stress	-57	54	220	62	-66	MPa
	-8	8	31	9	-9	ksi
Peak Axial Stress	7	361	138	430	28	MPa
	1	51	19	60	4	ksi
Peak Hoop Stress	36	121	261	117	-55	MPa
	-5	17	37	16	-8	ksi
Axial Peak-to-Peak Variation	82	190	167	209	77	MPa
	11	26	23	29	11	ksi
Hoop Peak-to-Peak Variation	30	121	86	102	38	MPa
	4	17	12	14	5	ksi

a weldment, the stresses relieved during the parting-out process must be added to the stresses due to the surface treatment.

The first piece examined was from weldment W27A. The stress-measurement points on this specimen were arranged in two rows with five measurement points in each row, as shown schematically in Fig. 4.4.1. This configuration was chosen to check the consistency of X-ray diffraction measurements in the metallurgically complex HAZ.

The results of the surface-stress measurements are shown in Fig. 4.4.2 (only axial stresses were measured). A reasonable consistency exists in the form of the distribution associated with the two rows of measurements, but a 180 MPa (25 ksi) difference exists in the actual magnitudes of the stresses. The overall state of stress associated with the machining-plus-grinding preparation is more tensile than that associated with the standard machining preparation, although the peak tensile stresses associated with each surface preparation are approximately equal.

Subsurface-strain measurements were made after electropolishing to remove surface layers. Figure 4.4.3 shows the variation of stress with depth 2.5 and 7.6 mm (0.1 and 0.3 in.), respectively, from the weld-fusion line. Note that, at a depth of 0.1 mm (0.003 in.), the stresses induced by the standard machining preparation have diminished considerably, but the effect of machining plus grinding seems to penetrate to a greater depth.

Less extensive measurements were made on eight additional specimens. The residual stresses were measured at six locations on each specimen as shown schematically in Fig. 4.4.4. There are three measurement sites on each side of the weld; they are located approximately 2.5, 5.1, and 7.6 mm (0.1, 0.2, and 0.3 in.) from the weld fusion line.

The results of the measurements on the specimens from the three-mock-up weldments are summarized in Figs. 4.4.5(a)-7(a). For a given weldment and a fixed axial distance from the weld there is some scatter between the data taken

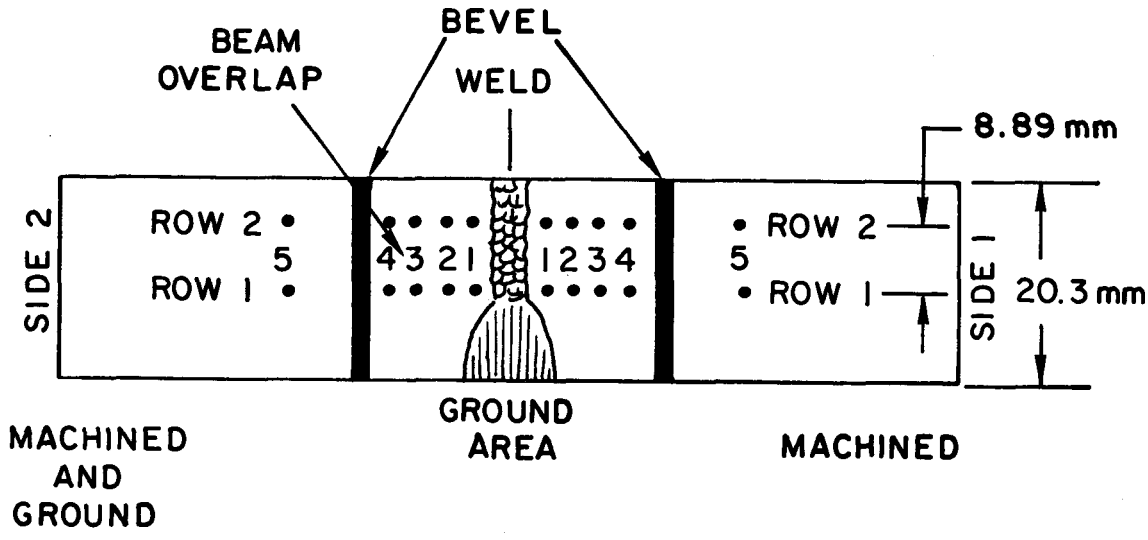

Fig. 4.4.1. X-ray Diffraction Residual-stress-measurement Locations on Weldment W27A.

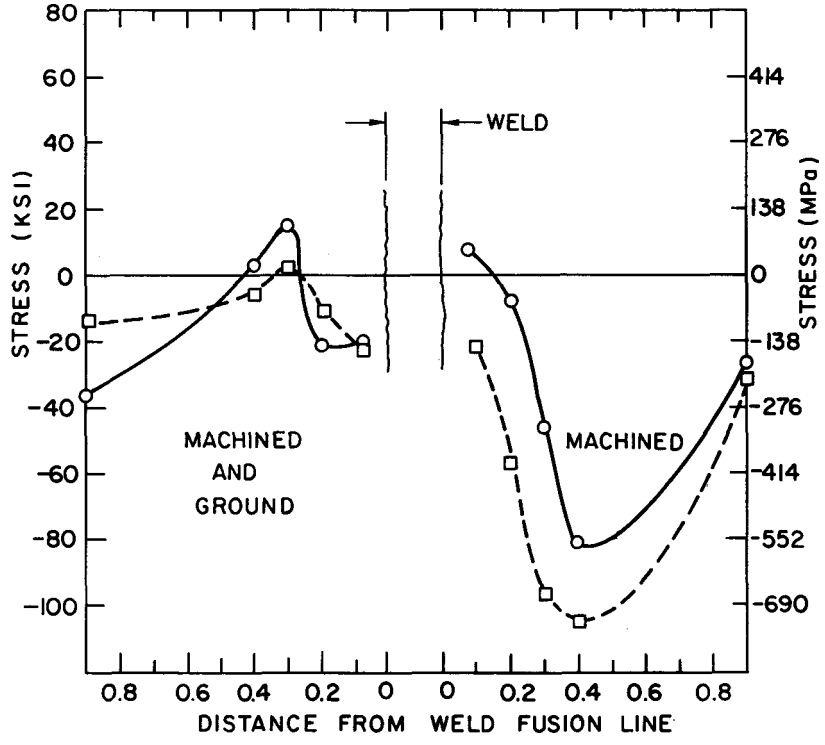

Fig. 4.4.2. Surface Stresses for Weldment W27A Determined by X-ray Diffraction Measurements.

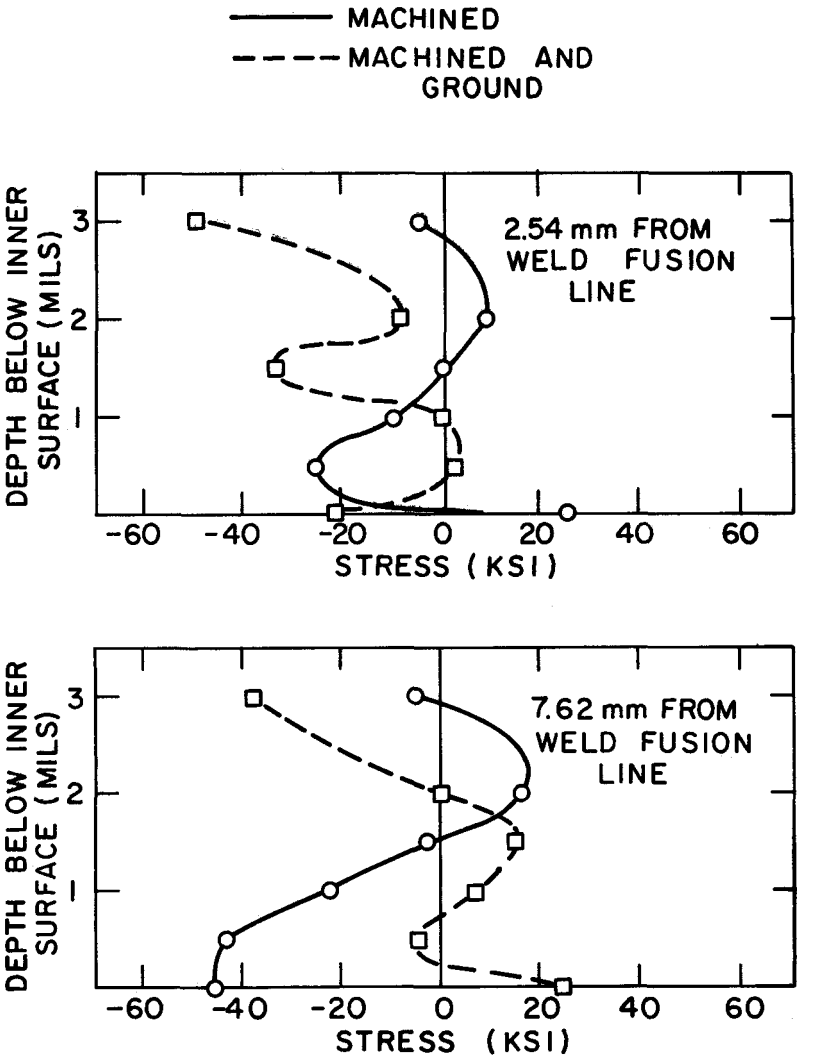

Fig. 4.4.3. Surface-stress Depth Profiles for Weldment W27A.

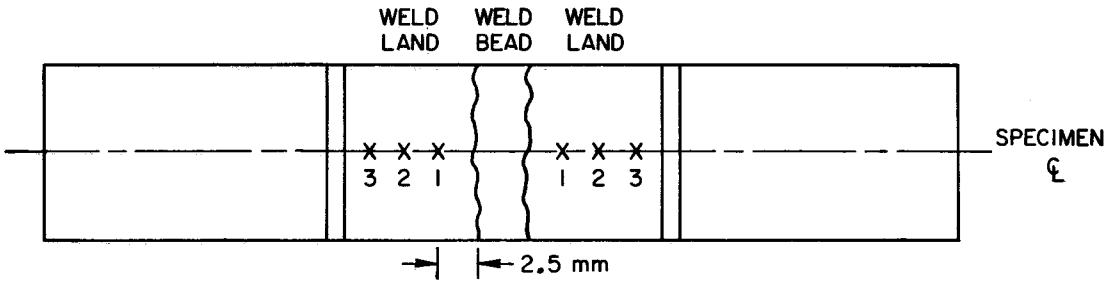

Fig. 4.4.4. Locations for X-ray Residual-stress Measurements on Specimens from Mock-up Pipe Weldments.

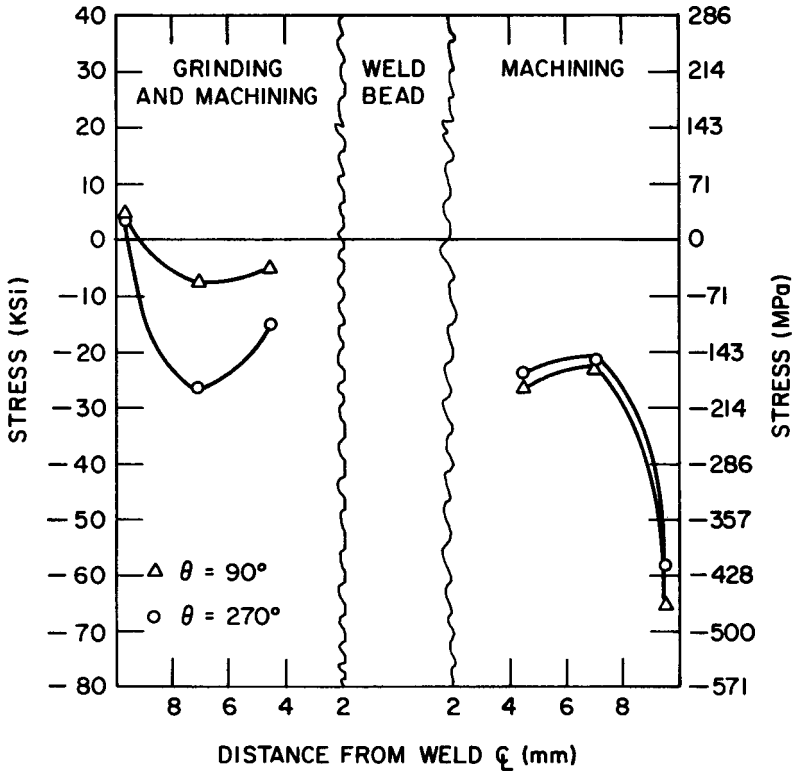

(a)

Fig. 4.4.5. (a) X-ray Surface Residual-stress Measurements for Mock-up Weldment W27A.

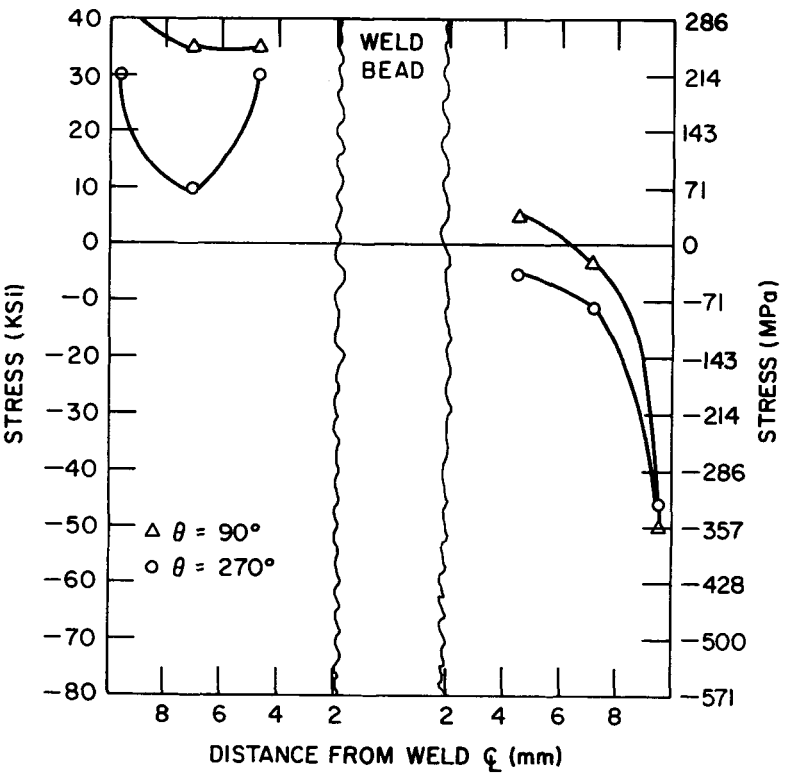

(b)

Fig. 4.4.5. (b) Total Surface Residual Stresses for Mock-up Weldment W27A.

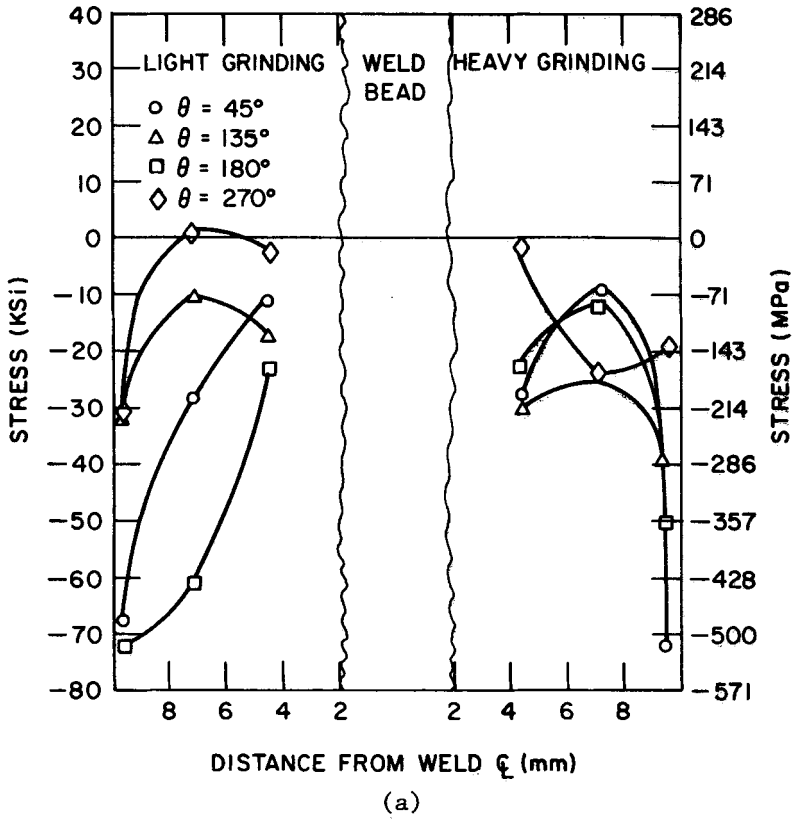

(a)

Fig. 4.4.6. (a) X-ray Surface Residual-stress Measurements for Mock-up Weldment W27B.

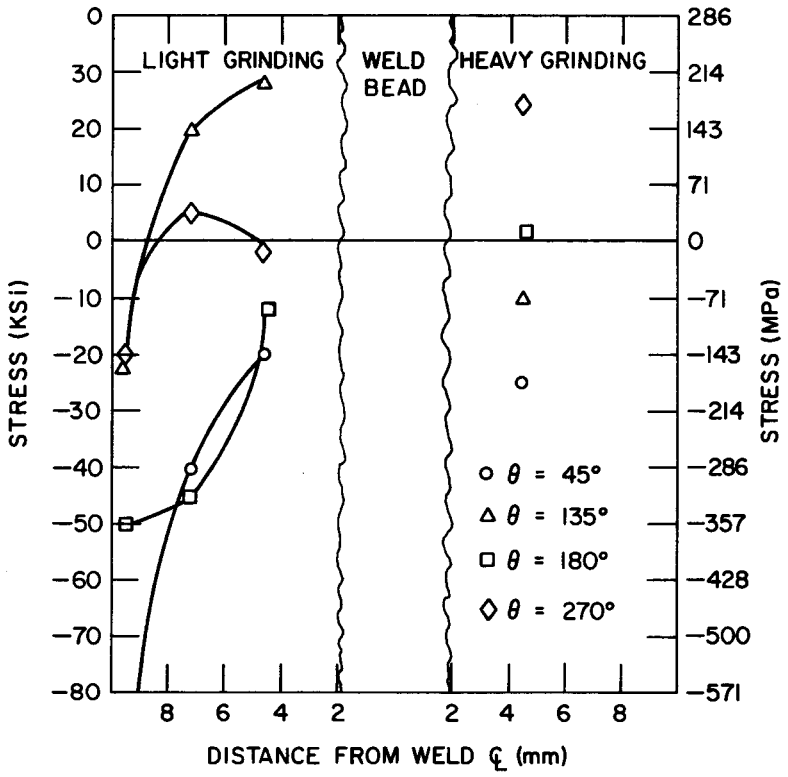

(b)

Fig. 4.4.6. (b) Total Surface Residual Stresses for Mock-up Weldment W27B.

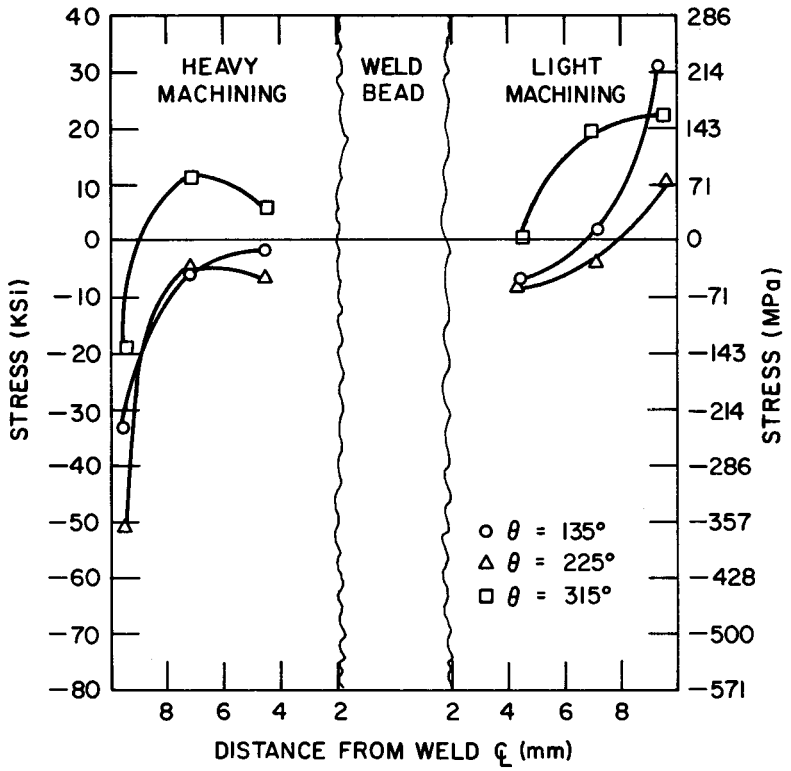

(a)

Fig. 4.4.7. (a) X-ray Surface Residual-stress Measurements for Mock-up Weldment W27C.

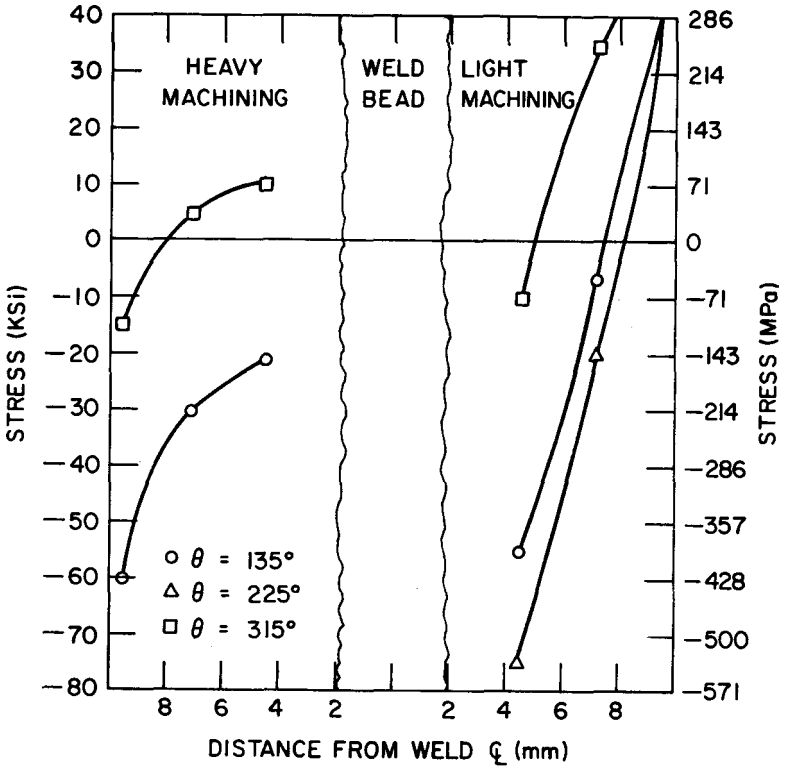

(b)

Fig. 4.4.7. (b) Total Surface Residual Stresses for Mock-up Weldment W27C.

at different azimuths. As the data at axial locations far from the weld-fusion lines indicate, the various preweld surface treatments induce very large residual stresses. At most of the measurement locations, these very large stresses are compressive; however, other studies have shown that these stresses can vary widely, with small regions exhibiting tensile stresses in the midst of relatively large regions exhibiting compressive stresses.

Near the weld-fusion line, the high surface residual stresses induced by the preweld treatments seem to be modestly compressive. However, to obtain the actual surface stresses on a weldment, the stresses relieved during the parting-out process, which are presumably due to the welding process, must be added to the stresses due to the surface treatment. The total stresses on the inner surfaces are shown in Figs. 4.4.5(b)-7(b). Butt weldments W27A [Fig. 4.4.5(b)] and W27B [Fig. 4.4.6(b)] show high tensile residual stresses, at least at certain azimuthal positions.

The results presented here suggest that, at least for regions close (<5 mm) to the weld-fusion line, the effect of the preweld surface treatment is not particularly important. The treatments do induce high residual surface stresses, but these are largely relieved during welding. Even if the preweld surface treatment produces a compressive residual stress, the shrinkage and thermo-mechanical history associated with the welding process can produce high tensile residual stresses on the inner surface of the weldments. Attempts to obtain favorable residual-stress states must involve changes in the welding process itself, not just in the preweld surface treatment.

4.5 Throughwall Residual Stresses

Because the "bulk" residual stresses are measures of the net force and moment acting across a cross section of the pipe, as discussed in Section 4.2.1, they may be good measures of the driving force available for crack propagation. However, since these weldments are relatively thick, there may be significant nonlinear self-equilibrating contributions to the throughwall stresses. These

self-equilibrating stresses may play an important role in the propagation of ISSC cracks that initiate on the inner surface.

To experimentally determine the throughwall distributions in 4-, 10-, and 26-in. weldments, the "layering" and "slicing" techniques outlined in Section 4.2.1 were used. The relatively thin 4- and 10-in. weldments were analyzed using the "layering" technique; the "slicing" technique was used to analyze the 26-in. weldment.

Both the layering and the slicing analysis are performed on specimens cut from the full weldment. (Nominal specimen dimensions for each pipe size are shown in Fig. 4.5.1.)

To obtain the throughwall stress distribution in the undisturbed weldment, the stresses relieved during the parting-out process must be added to the stresses obtained from the layering or slicing analyses. Since the specimen is "beam-like" in geometry, the parting-out stresses can be assumed to be linearly distributed across the thickness of the pipe. Because of this linearity, the parting-out stresses can be completely characterized by the stress changes on the inner and outer surfaces.

Specimens were cut from the 4-in. weldments W27A and W27B, and the 10-in. autopsy weldment from Dresden 2. Parting-out stresses for these specimens were obtained by interpolation from the axial and azimuthal distributions of residual stress on the inner and outer surfaces described in Sections 4.3.1.1 and 4.3.1.2.

To facilitate comparison with these results, we note that the azimuthal positions of the specimens from weldments W27B and W27A are $\theta = 202°$ and $\theta = 284°$. The two specimens from the Dresden 2 reactor are taken from the $\theta = 97°$ and $\theta = 128°$ azimuthal positions. (These specimens are denoted as D2A and D3A, respectively.)

In order to lay strain-gauge rosettes on the outer surfaces of the specimens from the 4- and 10-in. weldments, the outer weld crown was milled smooth. Since the regions of interest on the inner surface are usually described in terms of

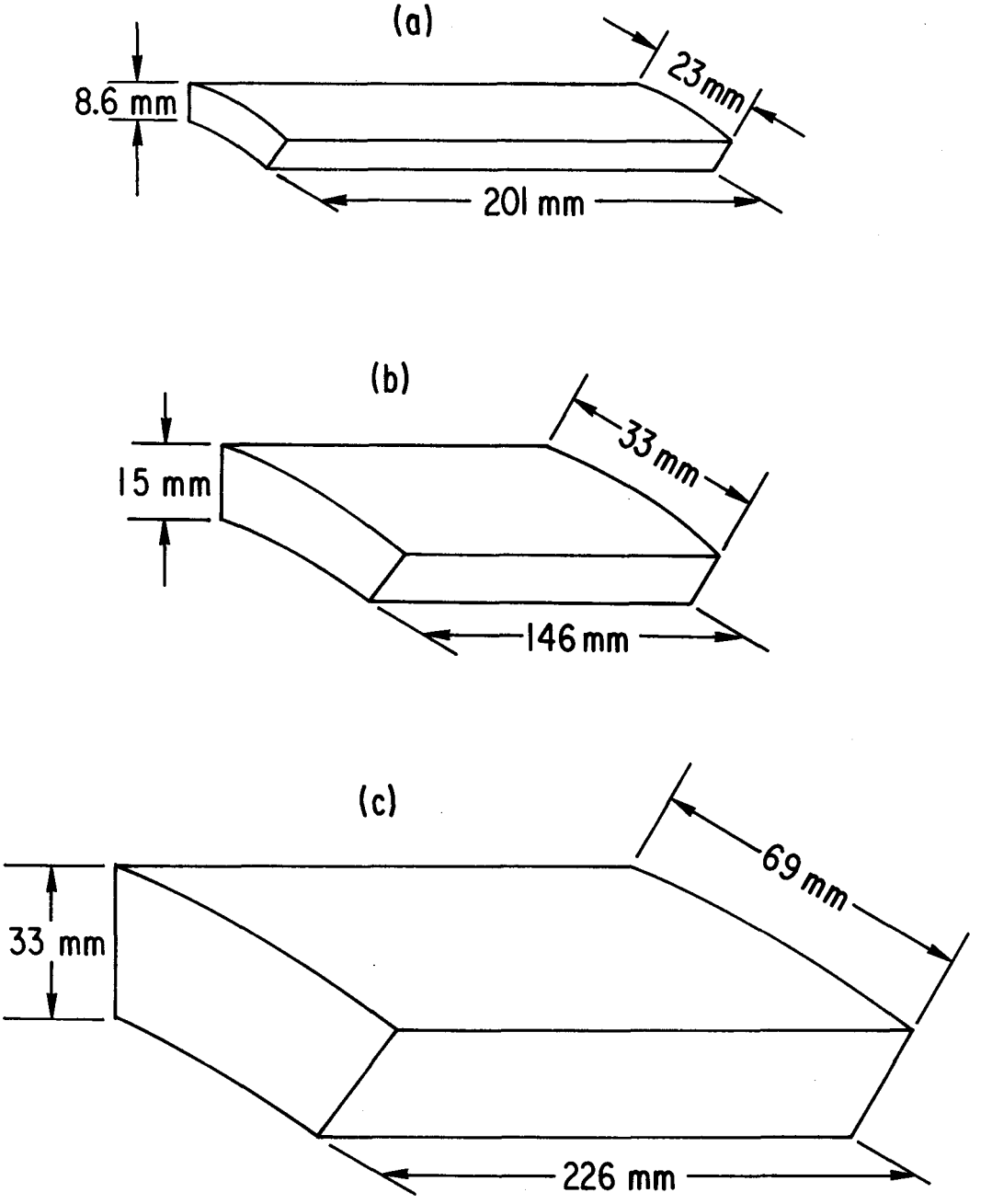

Fig. 4.5.1. Dimensions of Specimens from 4-, 10-, and 26-in. Weldments Used in Throughwall Residual-stress Studies.

distances from the weld fusion lines on the inner surfaces, the placement of the gauges in subsequent discussion will be referred to in terms of distances from the projections of the inner weld-fusion lines on the outer surface. Six rosettes were laid on the specimens from the 4-in. weldments, three on each side of the weld. The gauges were laid 3, 6, and 9 mm and 3, 6, and 12 mm from the projections of the inner weld-fusion line for the specimens from W27A and W27B, respectively. Figure 4.5.2 is a schematic showing the placement of the gauges and the numbering scheme used to identify the rosette locations. Seven rosettes were laid on the specimens from the 10-in. weldment; on one side, the rosettes were laid 3, 6, 12 and 18 mm from the projection of the inner weld-fusion line, on the other side, the rosettes were laid 3, 6, and 12 mm from the projection of the inner weld-fusion line. The placement and numbering scheme are shown schematically in Fig. 4.5.3.

The specimen from the 26-in. weldment was cut from a quadrant of a 26-in. weldment supplied by the General Electric Company. This weldment was fabricated of piping from two different heats of material, Heats 834264 and 17192. The two were welded together following standard nuclear-industry practice. A quadrant, which includes an ∿35° azimuthal portion of the circumference of the enture weldment, was cut from the weldment. X-ray and stress-relief measurements by G.E. indicated that only minor amounts of bulk stress relief occurred when the quadrant was cut from the complete weldment.

After the quadrant was received by ANL, additional strain-gauge rosettes were laid on the inner and outer surfaces at the 308, 319, and 330° azimuthal positions. Eight rosettes were laid on the inner surface, four on each side of the weld. Six rosettes were laid on the outer surface, three on each side of the weld. The placement of the gauges is shown schematically in Figs. 4.5.4(a) and (b). These gauges were laid as close as possible to the weld fusion lines. A specimen ∿69 mm wide and ∿226 m long, centered about the 319° azimuth, was cut from the quadrant by electric-discharge machining with a 0.7-mm-diam wire electrode.

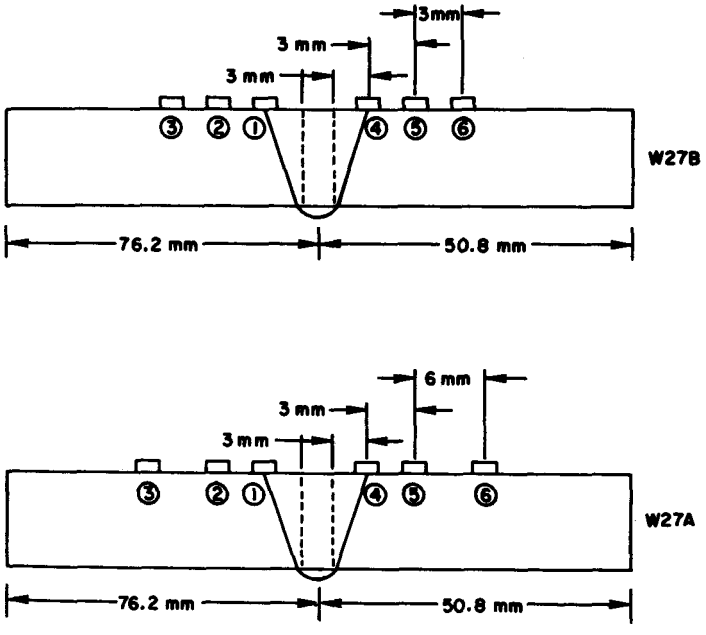

Fig. 4.5.2. Location of Strain-gauge Rosettes on Weldments W27B and W27A

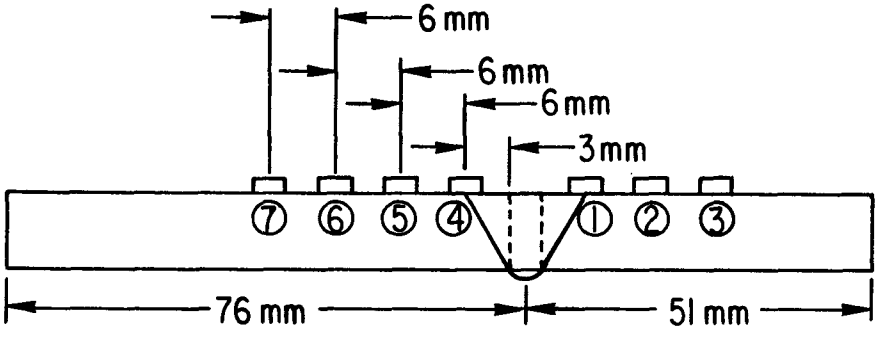

Fig. 4.5.3. Location of Strain-gauge Rosettes on the 10-in. Autopsy Weldment.

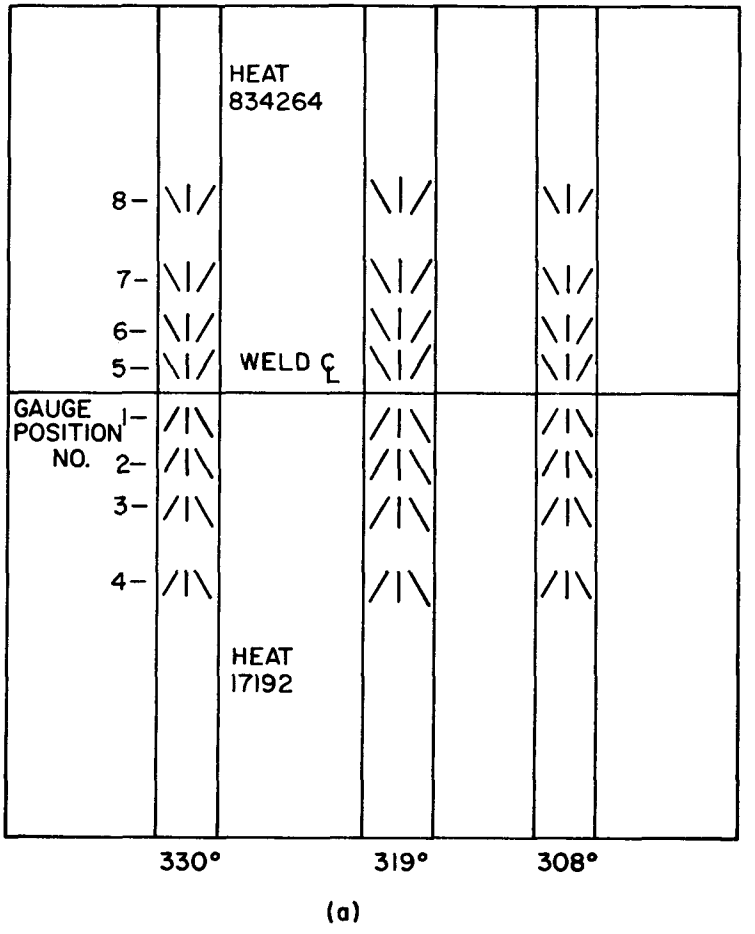

Fig. 4.5.4. (a) Location of Strain-gauge Rosettes on the Inner Surface of the 26-in. Weldment; (b) Axial Distribution of Strain-gauge Rosettes on the 26-in. Weldment (only the locations on one side of the weldment are shown).

The stress changes that occurred on the inner and outer surfaces during the parting-out process are shown in Figs. 4.5.5(a) and (b), respectively. Because of the weld crown, a gauge could not be laid on the outer surface corresponding to the innermost gauge on the inner surfaces [Fig. 4.5.4(b)]. However, the calculation of the net moment on a section requires both inner- and outer-surface measurements. Therefore values for the outer-surface stress change at axial positions 7.9 mm from the weld centerline were obtained by extrapolation from data obtained at other axial positions. The value chosen for this stress change is 21 MPa (3 ksi). Because of the linear variation in stress across the section, even a 40-MPa (6-ksi) error in the outer-surface value would yield only a 20-MPa (3-ksi) error at the half thickness and an even smaller error closer to the inner surface.

The throughwall distributions of residual stress in the specimens from the 4-in. weldments are shown in Figs. 4.5.6-11. The results for the specimen from weldment W27B exhibit the expected symmetry across the weld; the results for the specimen from weldment W27A exhibit somewhat less symmetry, but are similar. The total stresses in the actual weldment are obtained by adding the parting-out stresses, which are relieved when the specimen is cut from the weldment, to the stresses obtained by the layering analysis. Figures 4.5.12 and 4.5.13 show the throughwall distributions of the total residual stress at the $\theta = 202°$ azimuthal position for weldment W27B and at the $\theta = 248°$ azimuthal position for weldment W27A.

The throughwall distributions of residual stress in the specimens from the 10-in. Dresden 2 weldment are shown in Figs. 4.5.14-19 for the $\theta = 90°$ and 112° azimuthal positions. Only a relatively small fraction of the thickness was examined in this case. The stresses appear to vary sharply with depth, and the magnitudes of the nonlinear throughwall residual stresses appear to be somewhat larger than those at corresponding depths in the 4-in. weldments.

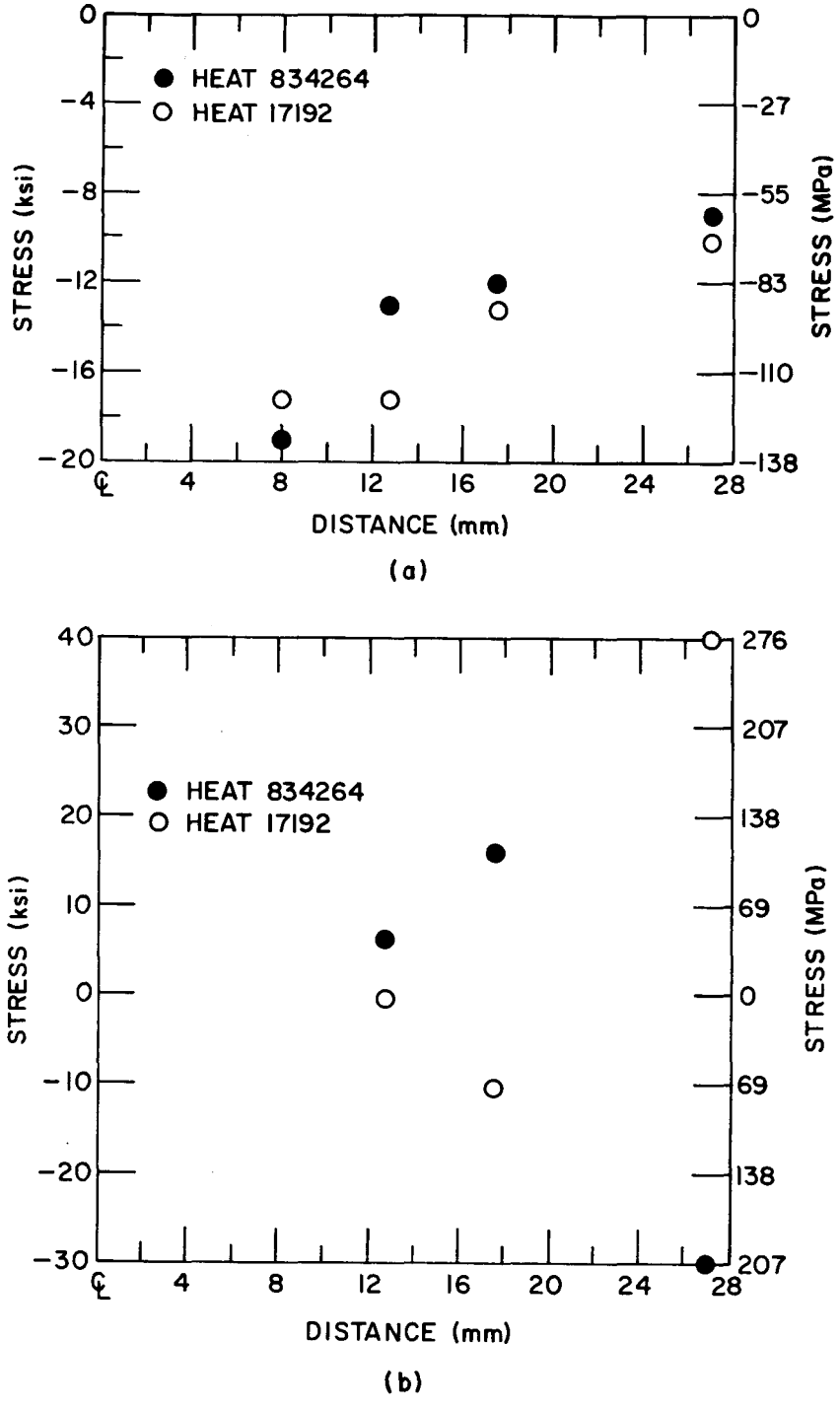

Fig. 4.5.5. Parting-out Stress Changes on the (a) Inner Surface; (b) Outer Surface.

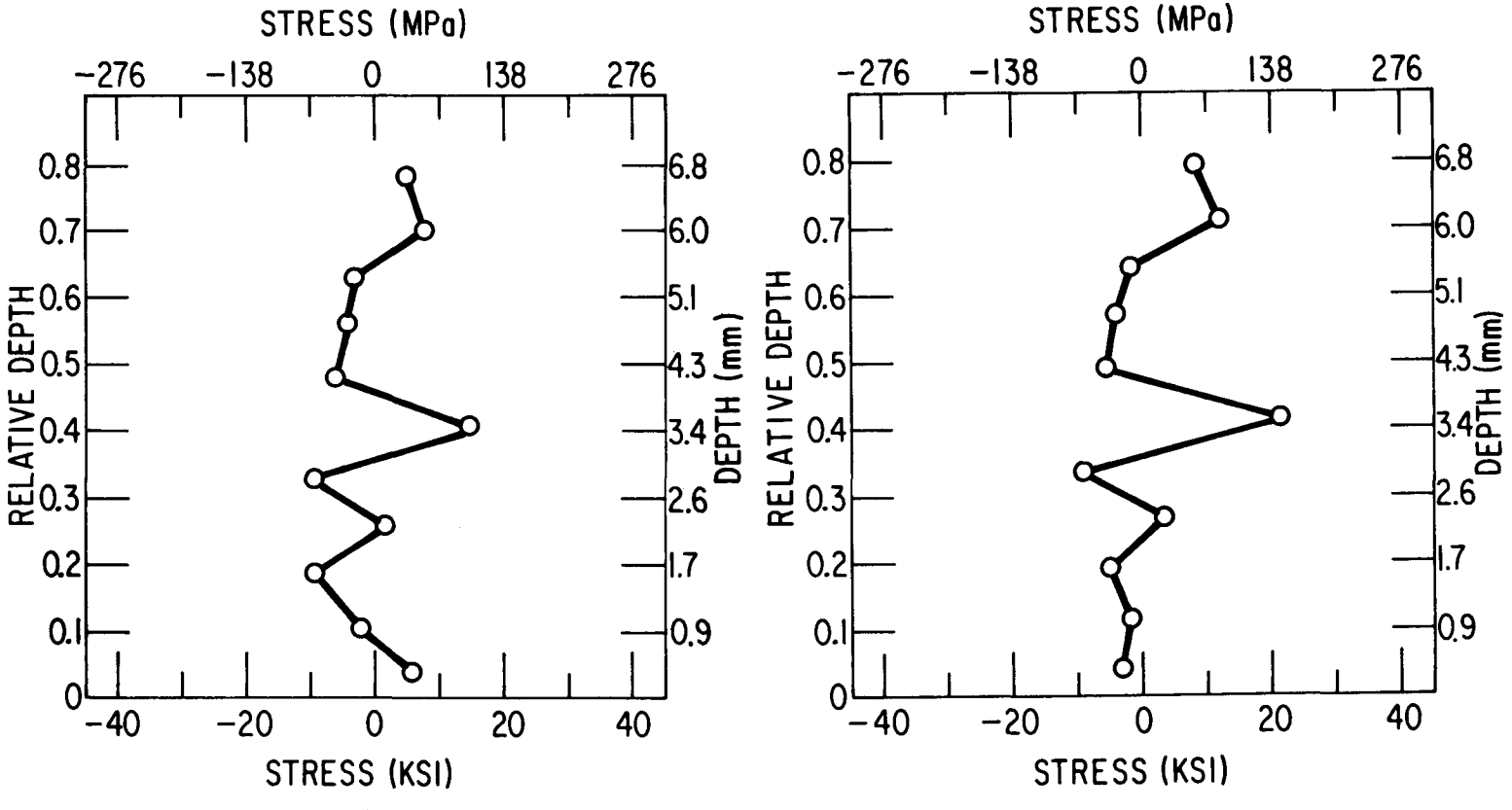

Fig. 4.5.6. Throughwall Distribution of Self-equilibrated Residual Stresses in 4-in. Weldment W27B (θ = 202°) ~6 mm on Either Side of the Weld Center Line.

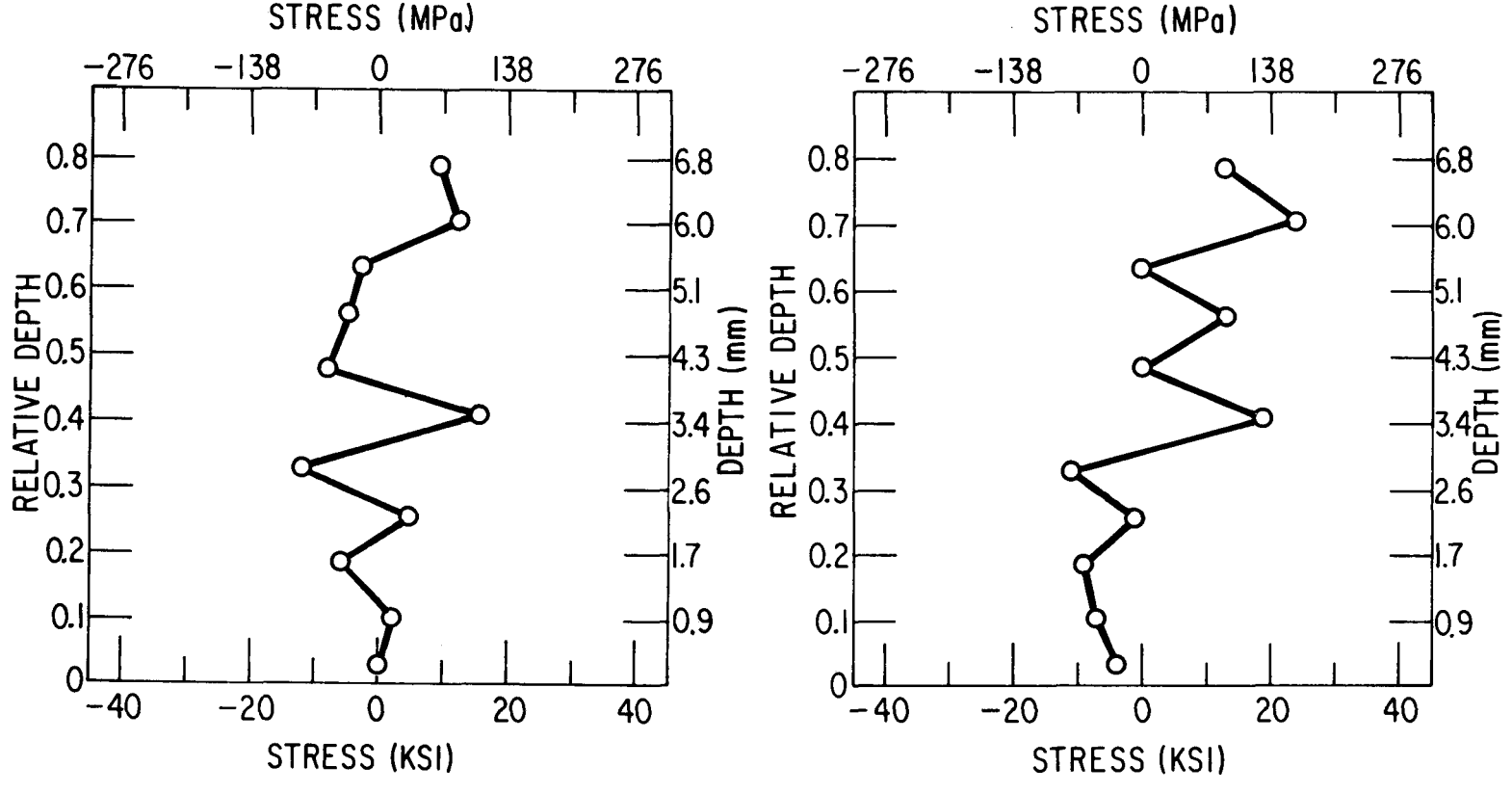

Fig. 4.5.7. Throughwall Distribution of Self-equilibrated Residual Stresses in 4-in. Weldment W27B (θ = 202°) ∿9 mm on Either Side of the Weld Center Line.

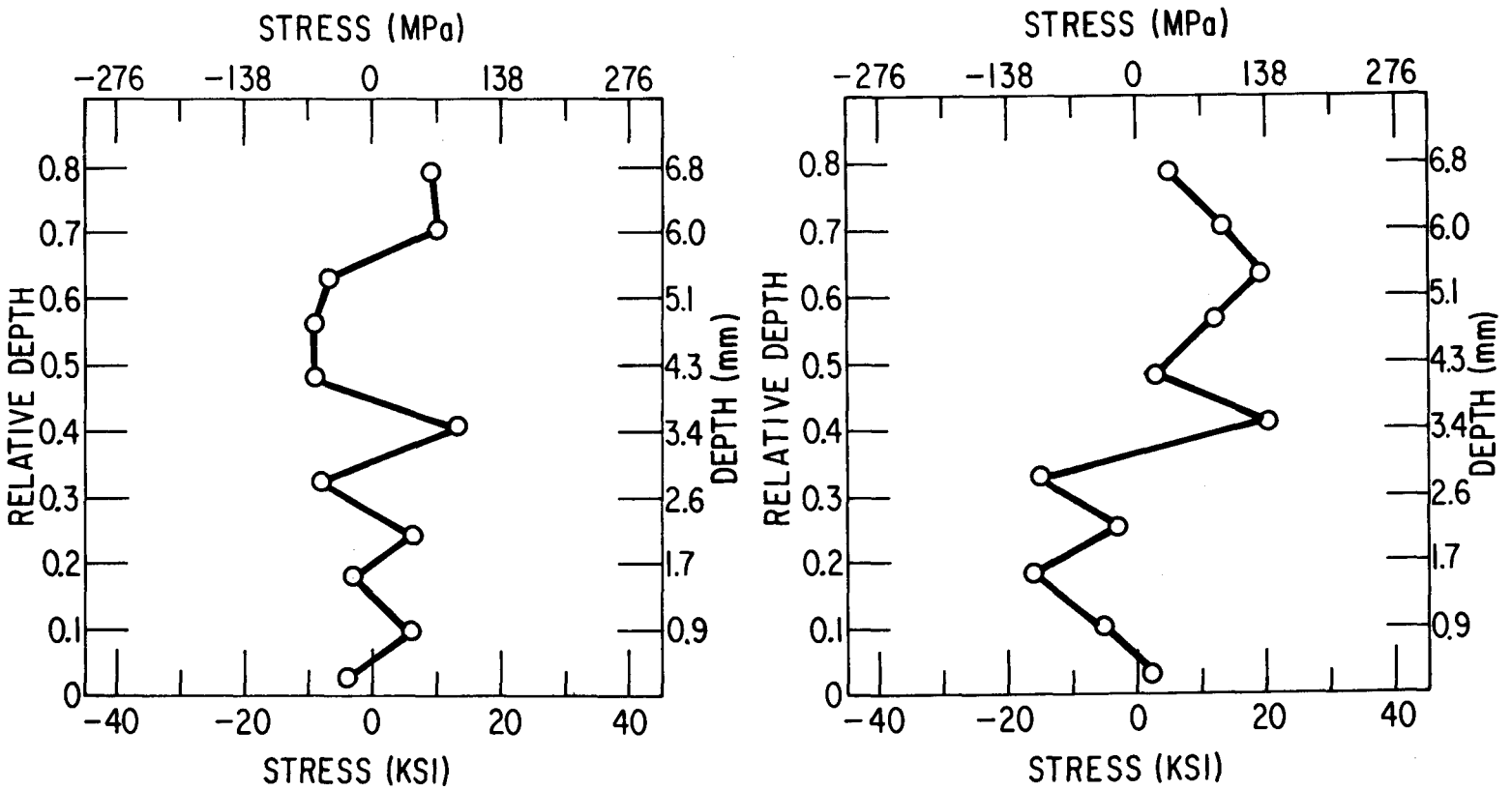

Fig. 4.5.8. Throughwall Distribution of Self-equilibrated Residual Stresses in 4-in. Weldment W27B (θ = 202°) ∿12 mm on Either Side of the Weld Center Line.

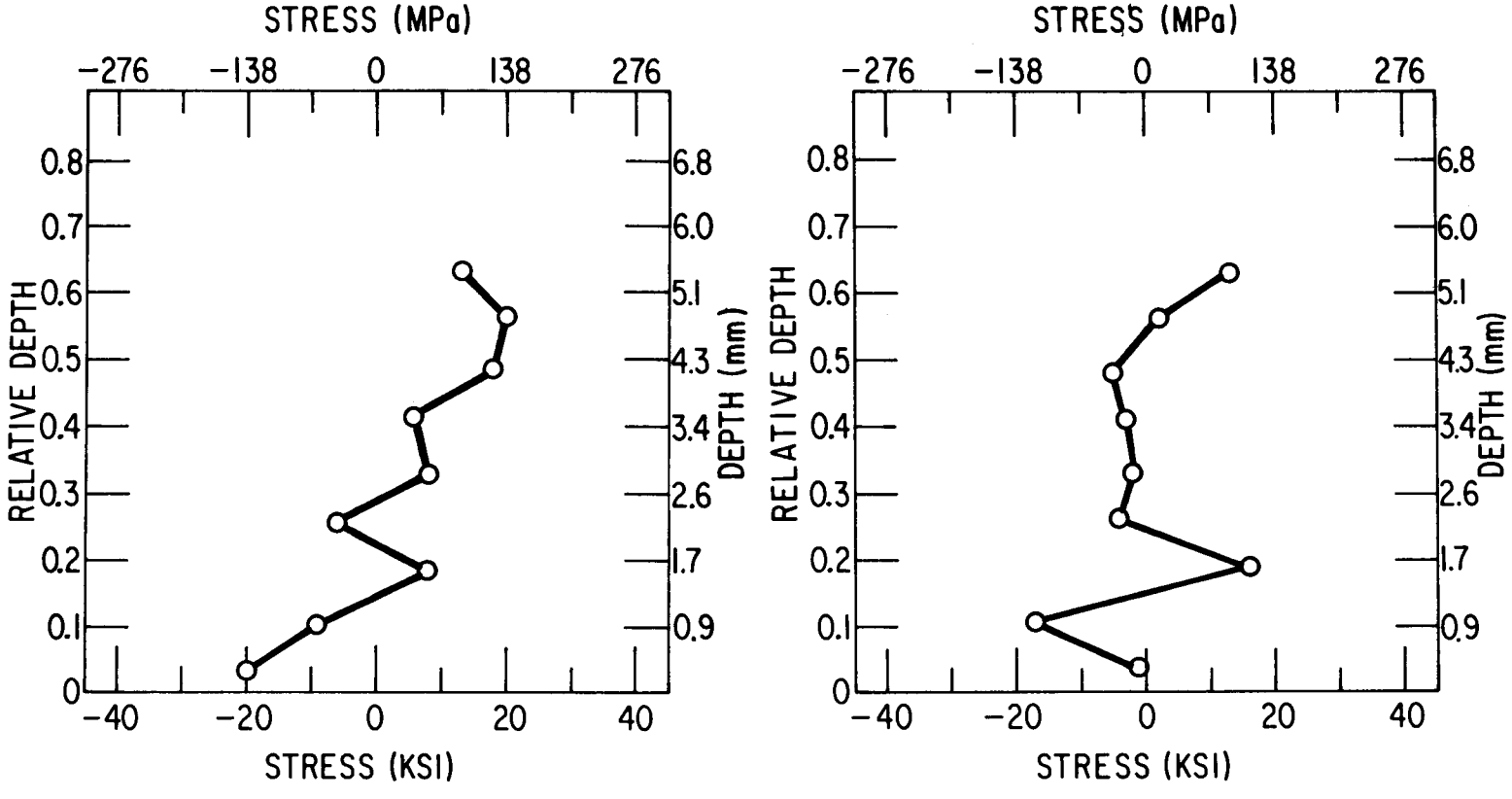

Fig. 4.5.9. Throughwall Distribution of Self-equilibrated Residual Stresses in 4-in. Weldment W27A (θ = 248°) ∿5 mm on Either Side of the Weld Center Line.

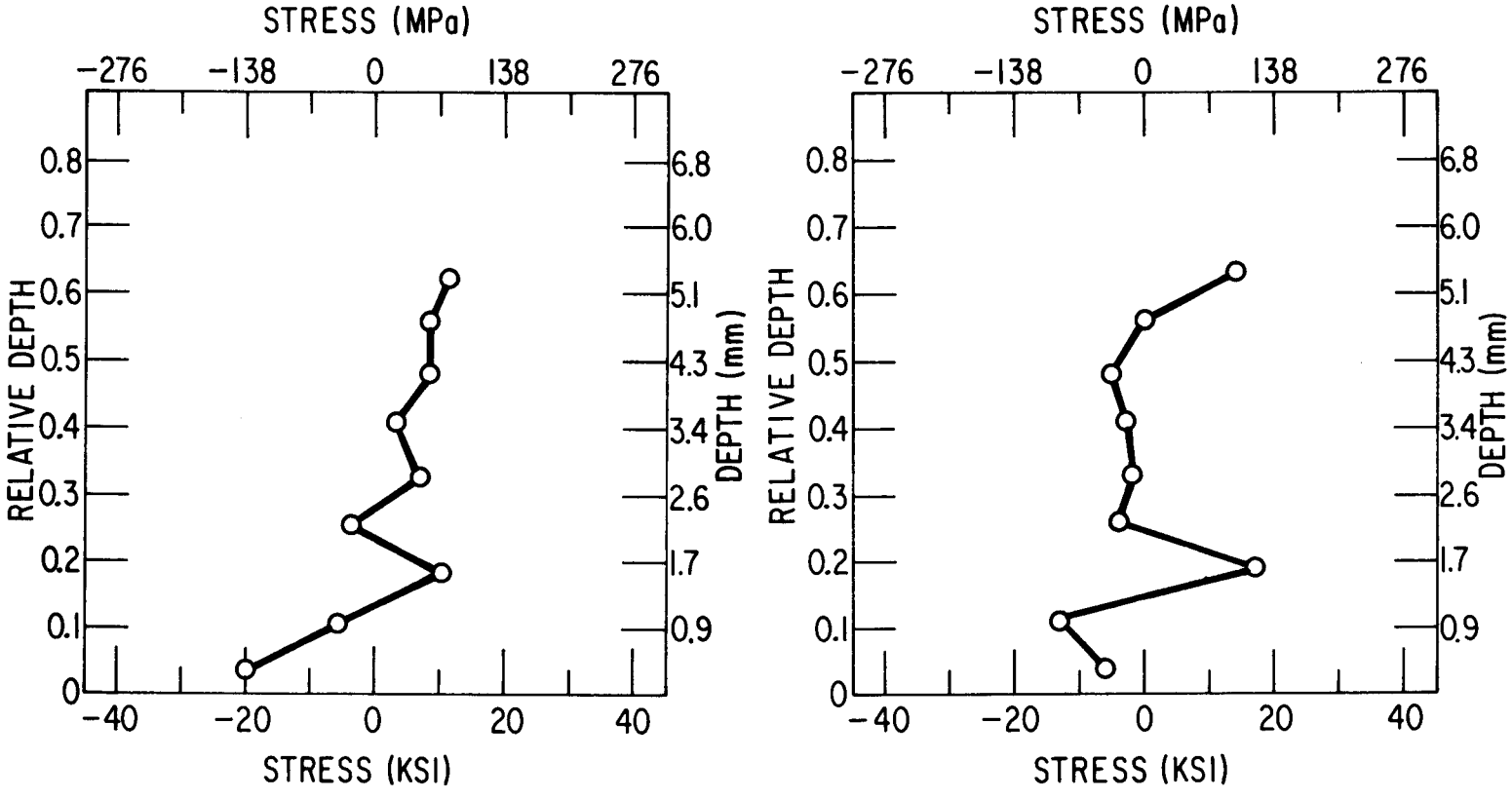

Fig. 4.5.10. Throughwall Distribution of Self-equilibrated Residual Stresses in 4-in. Weldment W27A (θ = 248°) ∿8 mm on Either Side of the Weld Center Line.

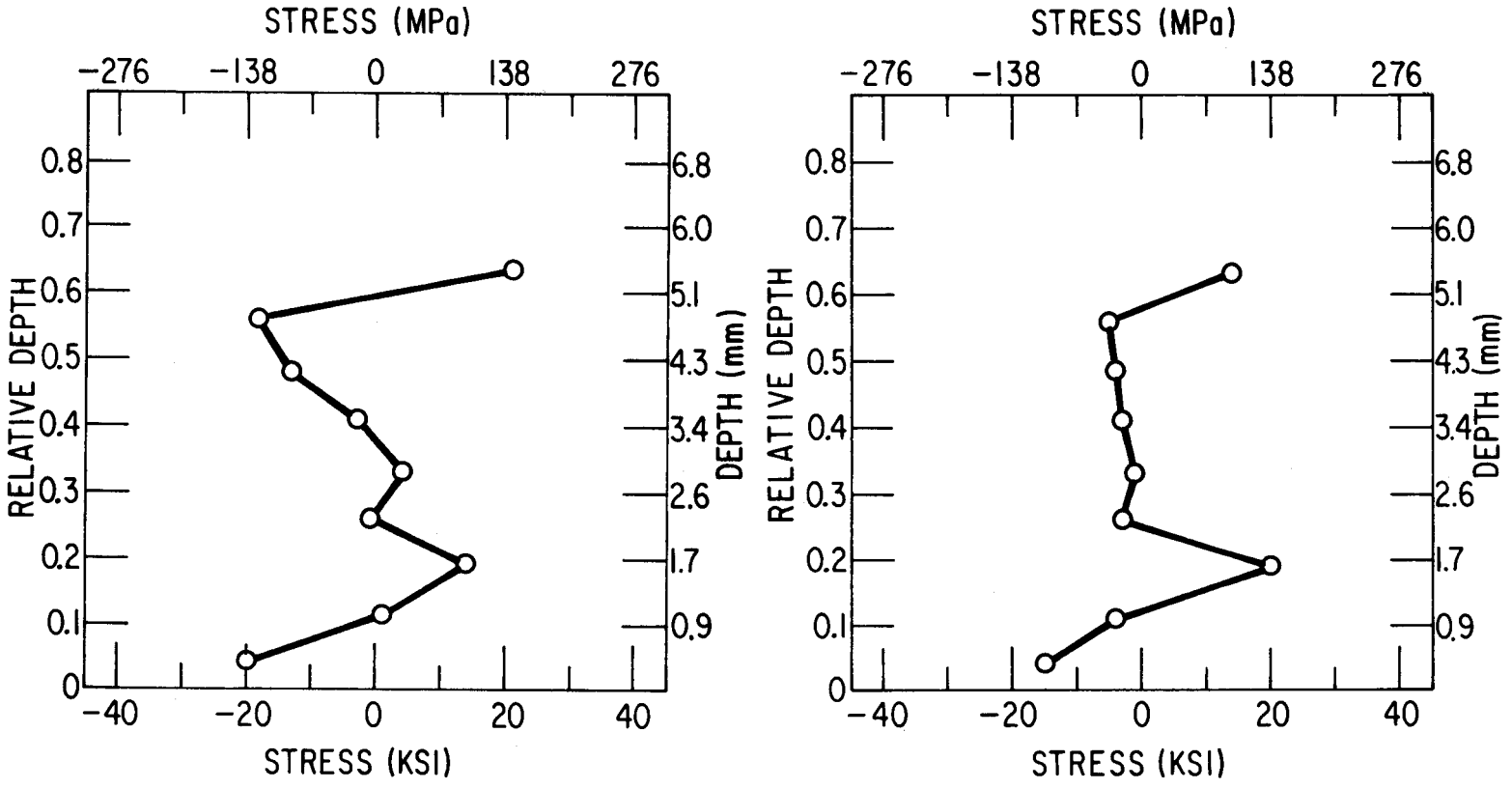

Fig. 4.5.11. Throughwall Distribution of Self-equilibrated Residual Stresses in 4-in. Weldment W27A (θ = 248°) ∿14 mm on Either Side of the Weld Center Line.

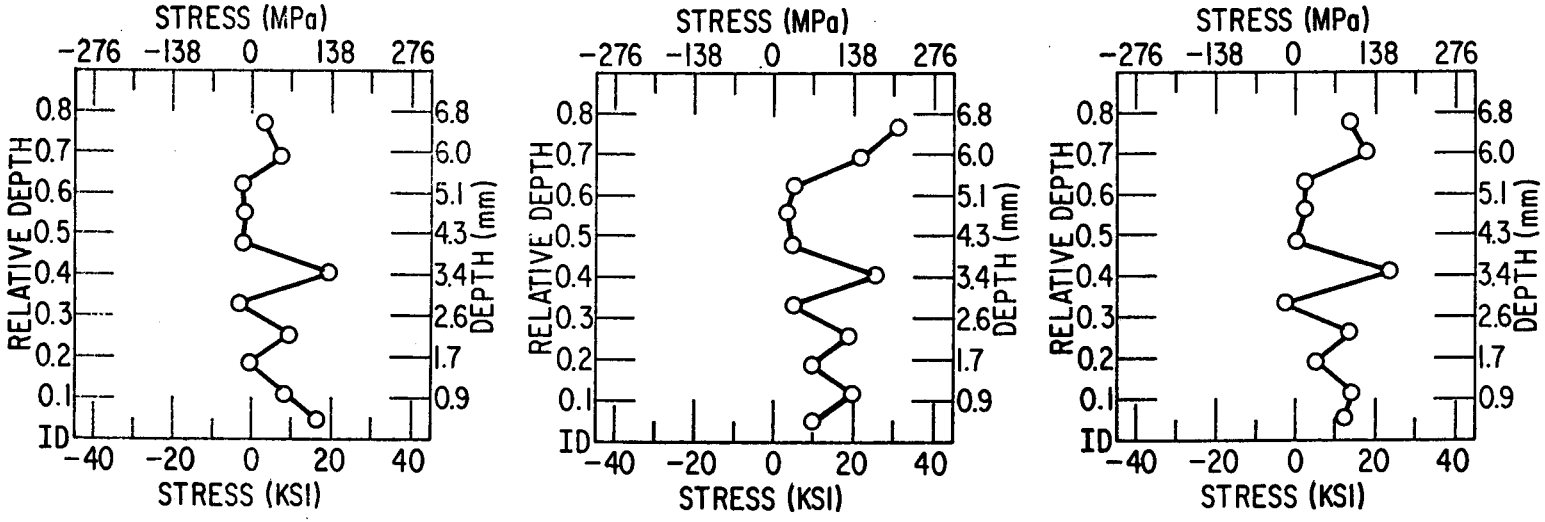

Fig. 4.5.12. Throughwall Distribution of Total Residual Stresses in 4-in. Weldment W27B (θ = 202°) (a) ∿6, (b) ∿9, and (c) ∿12 mm from the Weld Center Line.

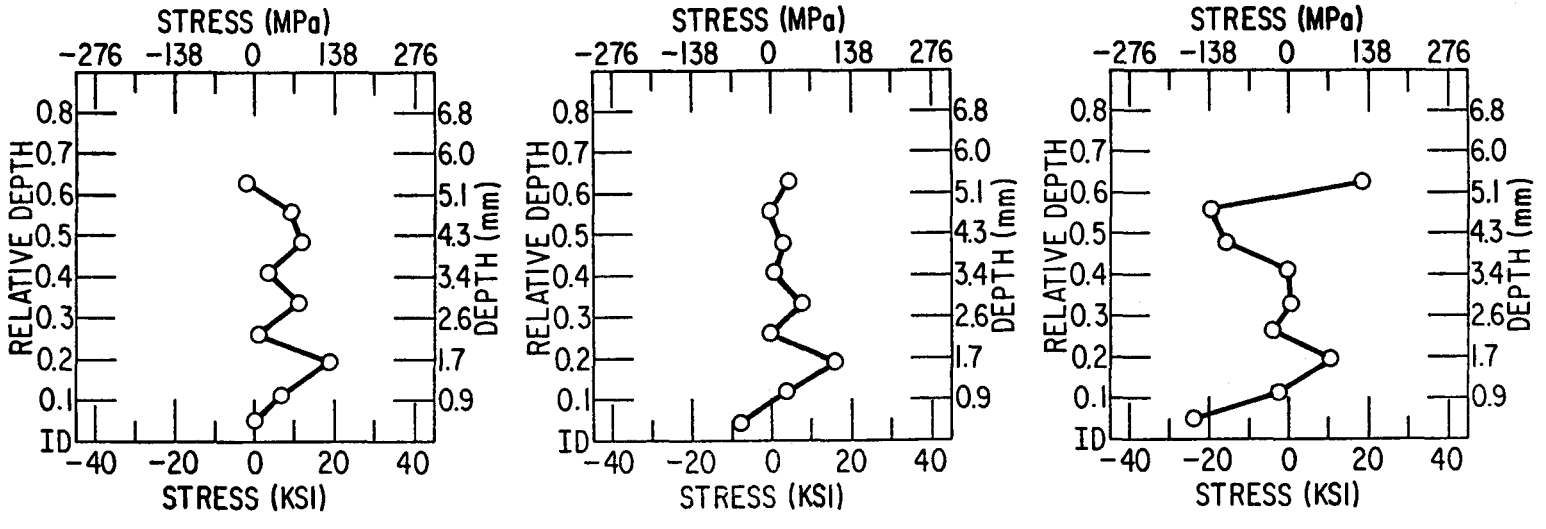

Fig. 4.5.13. Throughwall Distribution of Total Residual Stresses in 4-in. Weldment W27A (θ = 248°) (a) ∿5, (b) ∿8, and (c) ∿14 mm from the Weld Center Line.

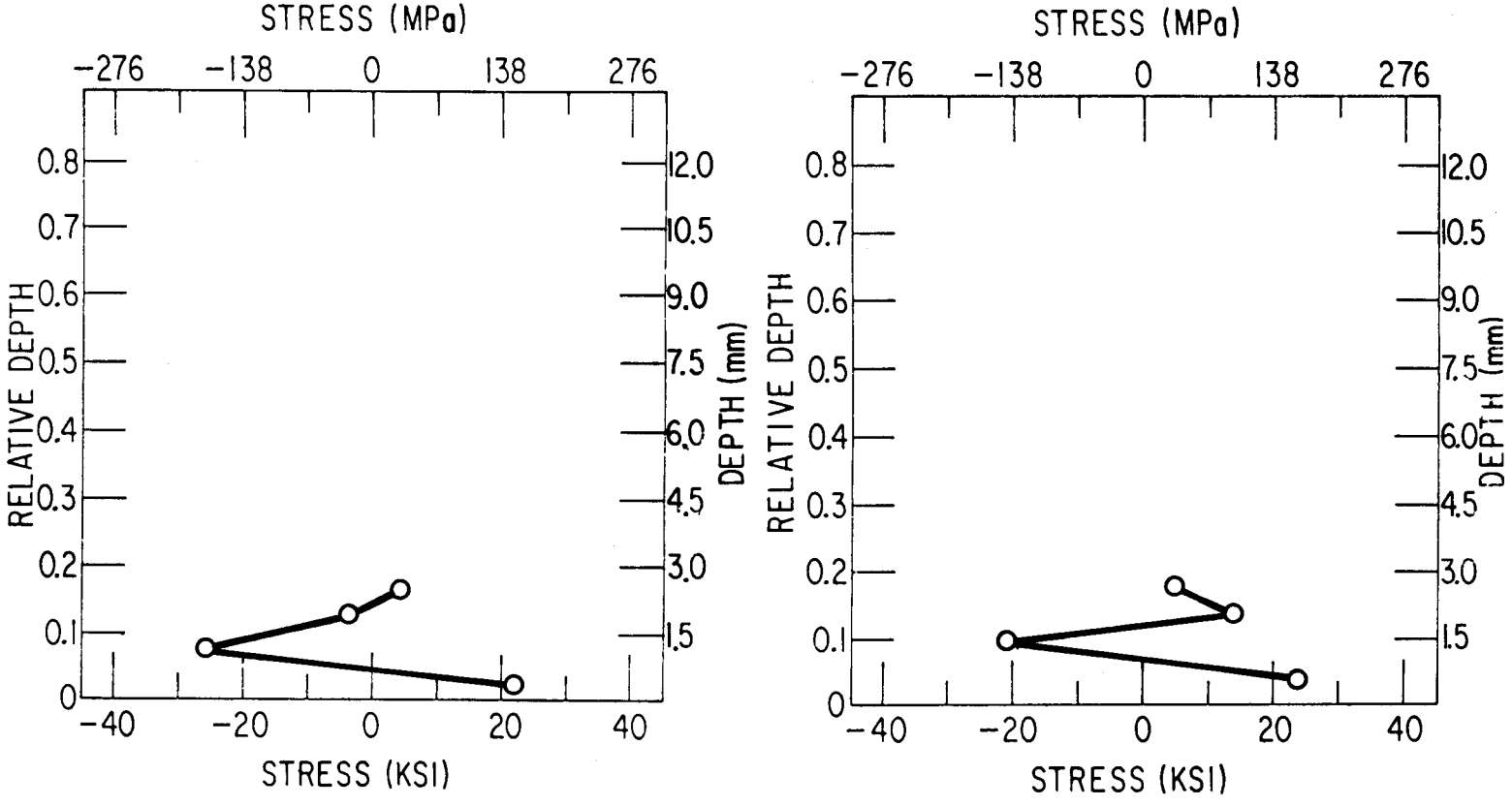

Fig. 4.5.14. Throughwall Distribution of Self-equilibrated Residual Stresses in the 10-in. Dresden 2 Weldment ($\theta = 90°$) ∿5 mm on Either Side of the Weld Center Line.

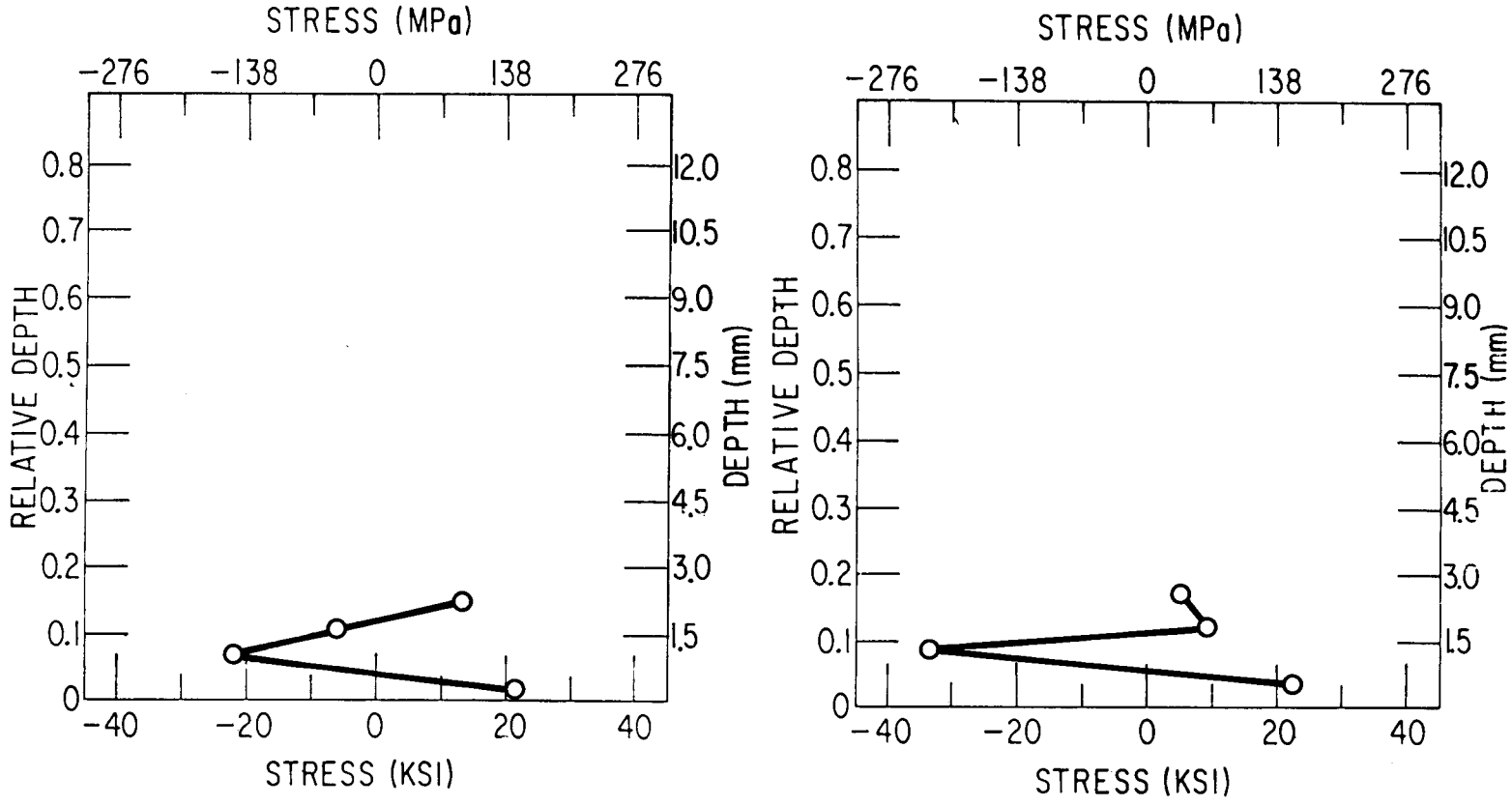

Fig. 4.5.15. Throughwall Distribution of Self-equilibrated Residual Stresses in the 10-in. Dresden 2 Weldment ($\theta = 90°$) ~11 mm on Either Side of the Weld Center Line.

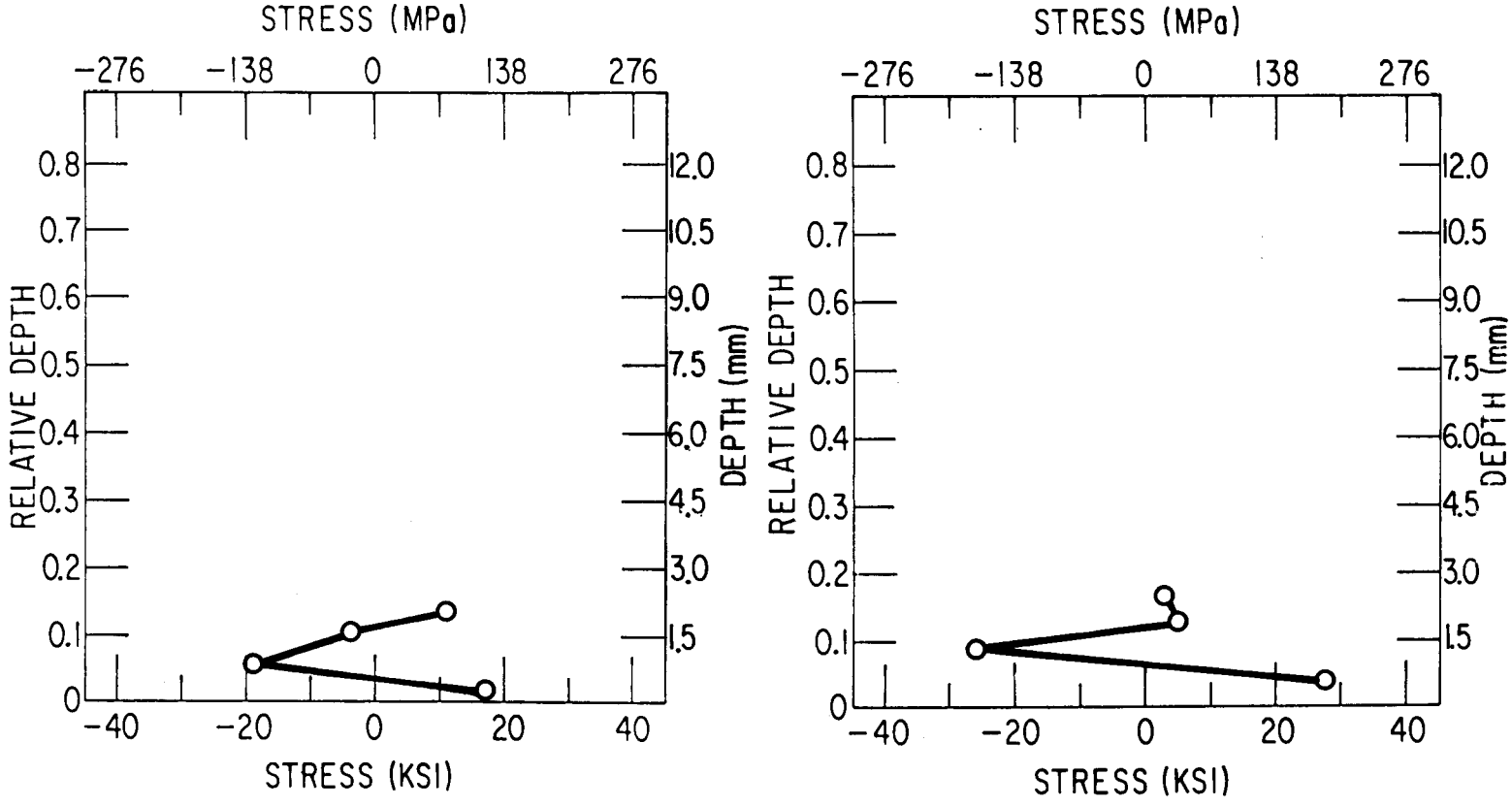

Fig. 4.5.16. Throughwall Distribution of Self-equilibrated Residual Stresses in the 10-in. Dresden 2 Weldment ($\theta = 90°$) ~17 mm on Either Side of the Weld Center Line.

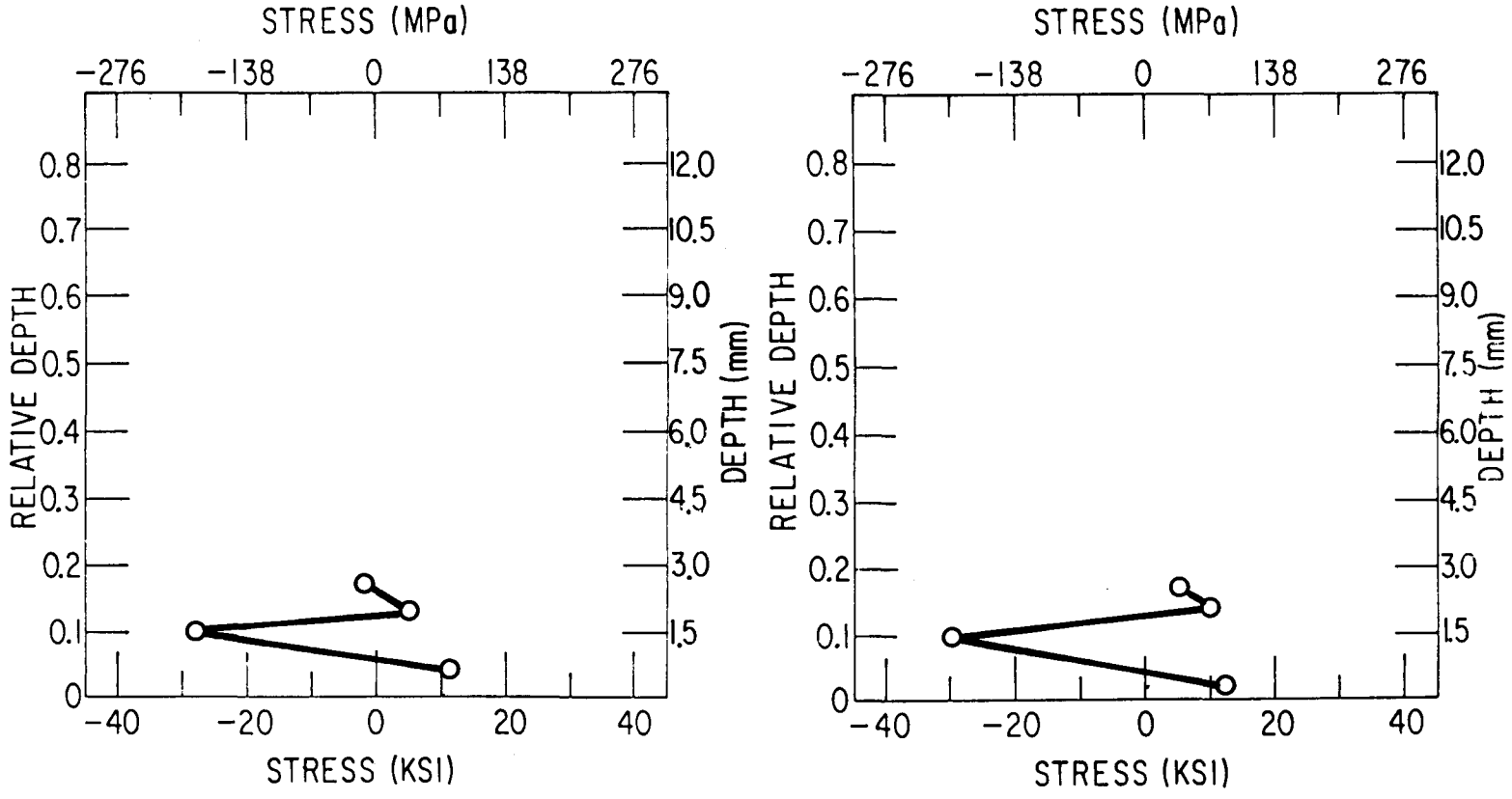

Fig. 4.5.17. Throughwall Distribution of Self-equilibrated Residual Stresses in the 10-in. Dresden 2 Weldment (θ = 112°) ~5 mm on Either Side of the Weld Center Line.

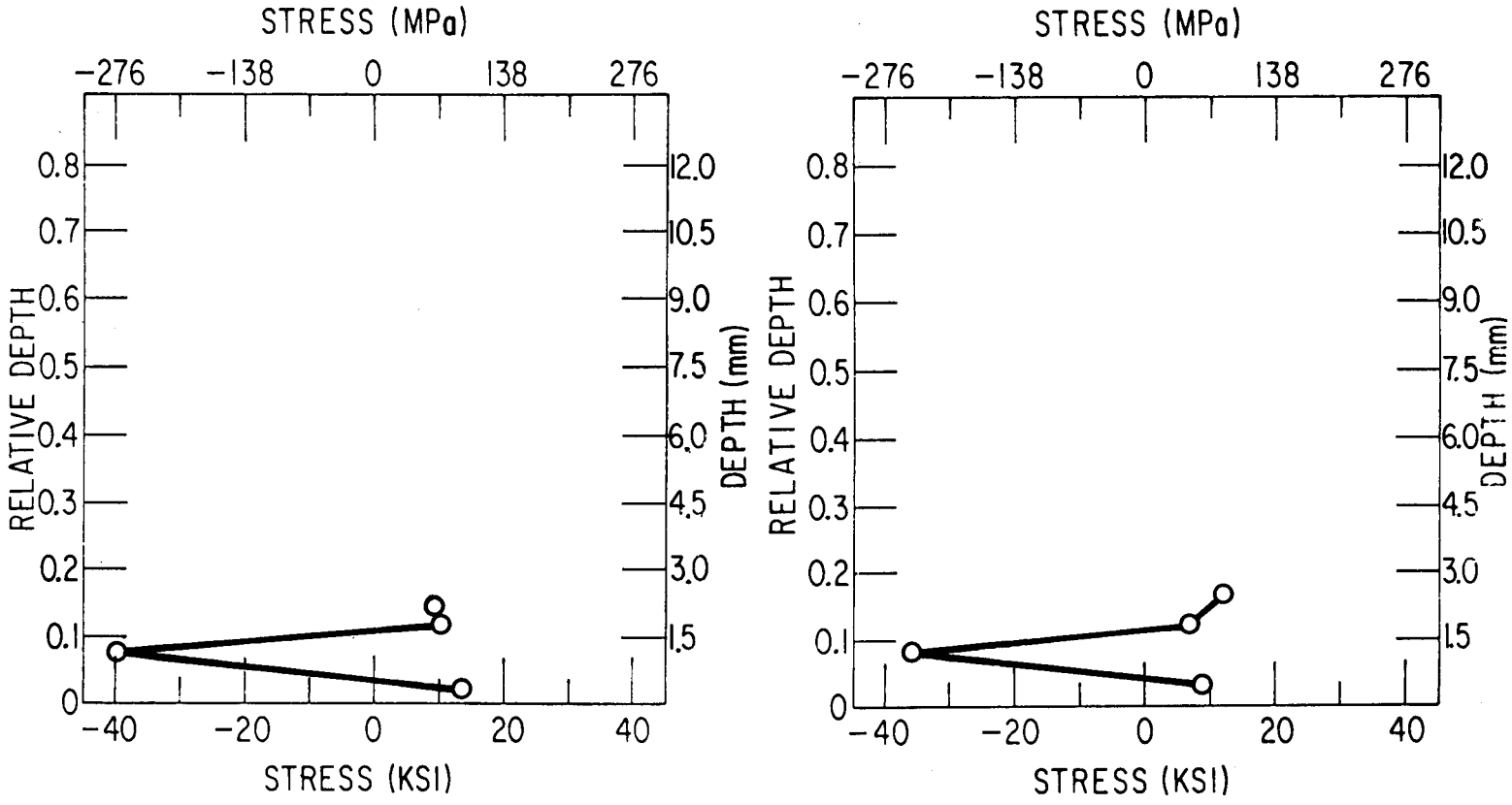

Fig. 4.5.18. Throughwall Distribution of Self-equilibrated Residual Stresses in the 10-in. Dresden 2 Weldment (θ = 112°) ∿11 mm on Either Side of the Weld Center Line.

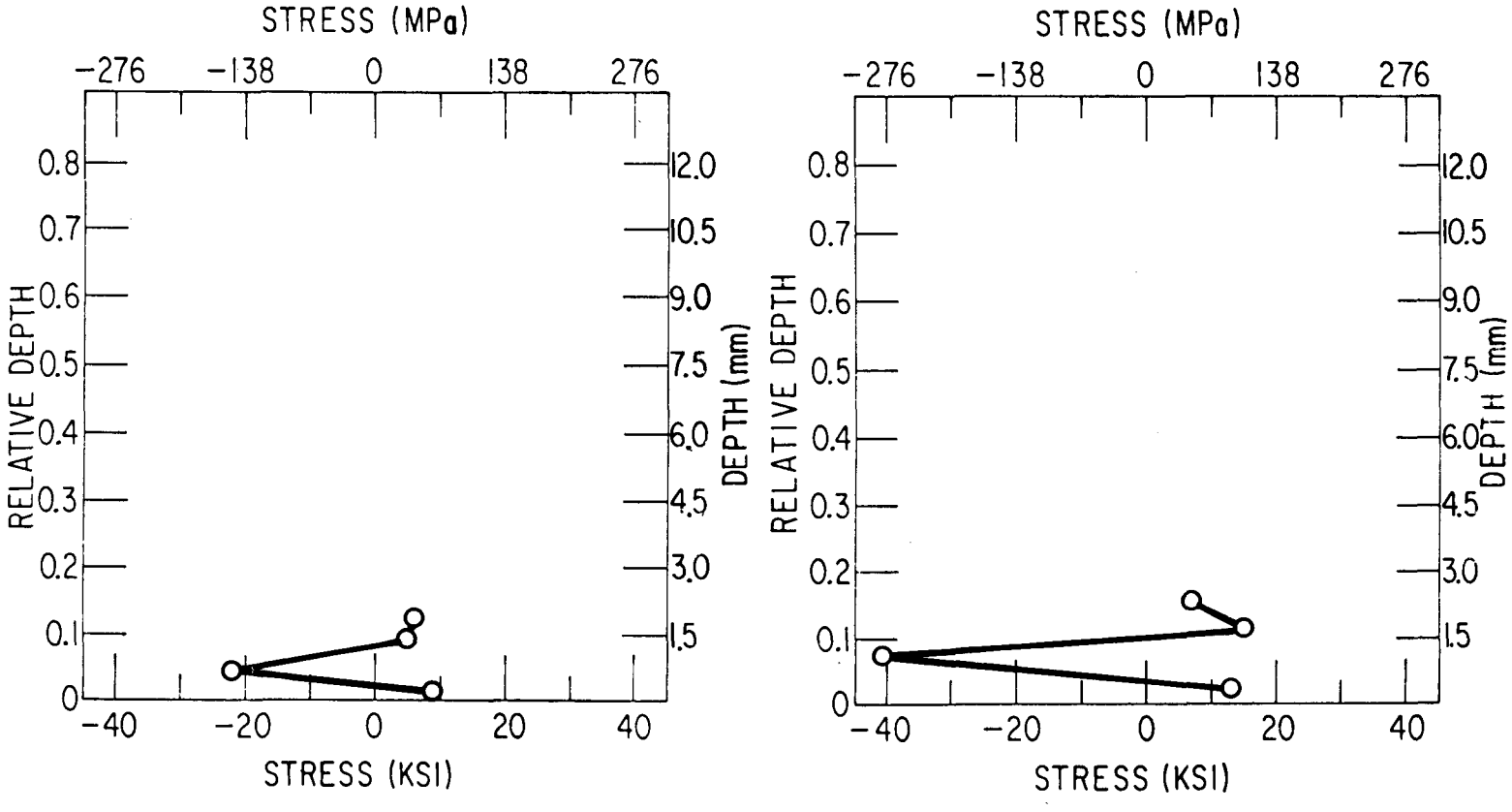

Fig. 4.5.19. Throughwall Distribution of Self-equilibrated Residual Stresses in the 10-in. Dresden 2 Weldment (θ = 112°) ~17 mm on Either Side of the Weld Center Line.

The throughwall distributions of residual stress in the specimen from the 26-in. weldment are shown in Figs. 4.5.20-23. There are a number of significant differences between the throughwall distributions of stress in the specimens from the 4- and 10-in. weldments and the specimen from the 26-in. weldment. The magnitude of the nonlinear residual stresses appears to increase with increasing pipe diameter. The residual stresses also appear to decay much more rapidly with axial distance in the 26-in. weldment. This is especially striking if the axial distances from the weld-fusion line are scaled with the pipe thickness t or the elastic decay length $\sqrt{Rt}$, where R is the midwall pipe radius. Thus, at the gauge positions $\sim$22 mm (= $0.7t = 0.15\sqrt{Rt}$ for the 26-in. weldment) from the weld-fusion line, the nonlinear throughwall stresses have essentially vanished. However, for the 4-in. weldments, sizable residual stresses still exist at the gauge positions $\sim$9 mm (= $t = 0.3\sqrt{Rt}$).

The throughwall distribution of the total residual stress in the undisturbed weldment is shown in Figs. 4.5.24-27. Qualitatively, they are not too different from the self-equilibrating distributions shown in Figs. 4.5.20-23. The tensile stresses on the inner surface have been slightly reduced, and the stresses at a depth $\sim t/4$ from the inner surface have become even more compressive.

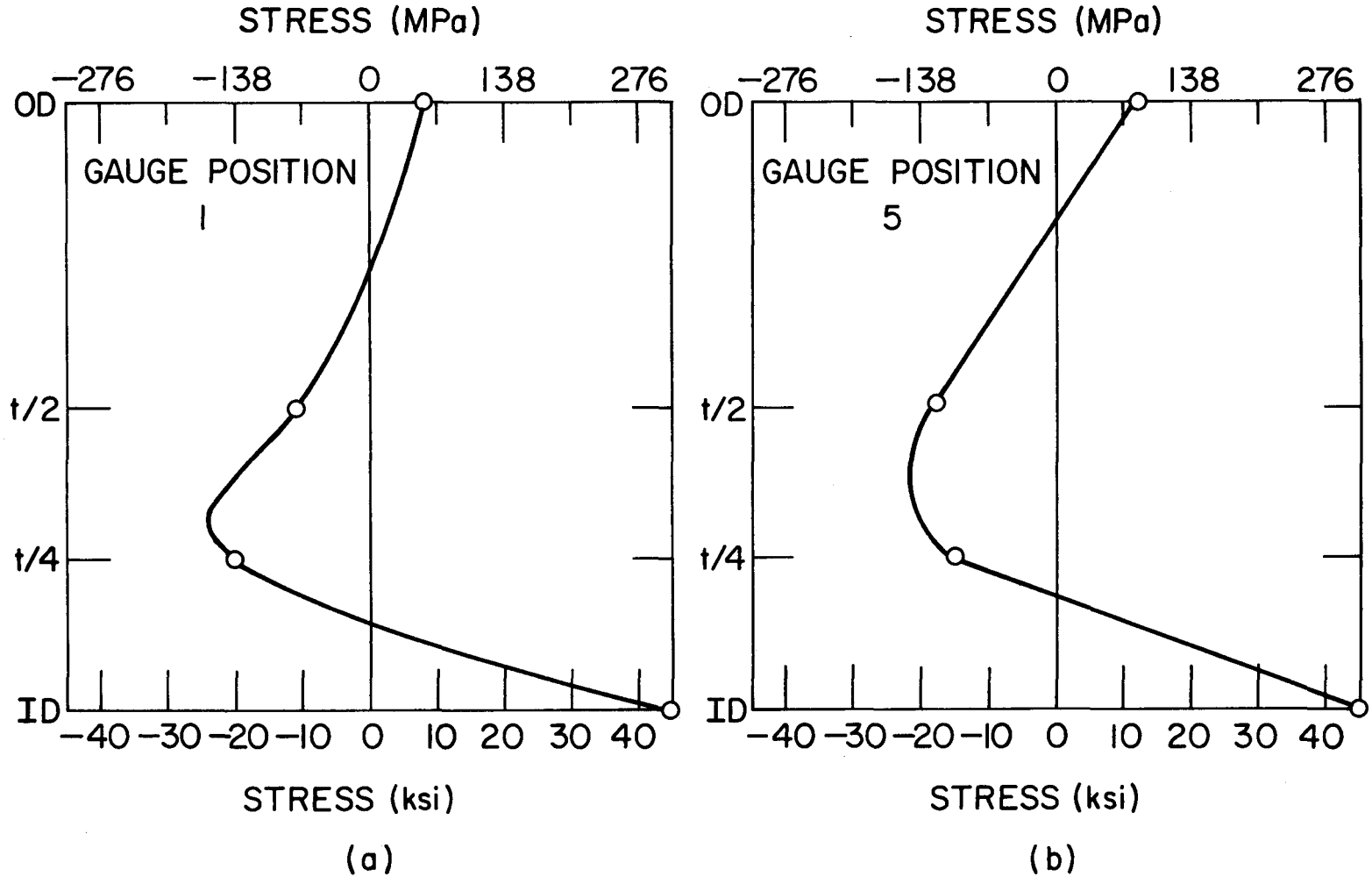

Fig. 4.5.20. Throughwall Distribution of Self-equilibrated Residual Stress in the 26-in. Weldment ∿8 mm on Either Side of the Weld Center Line.

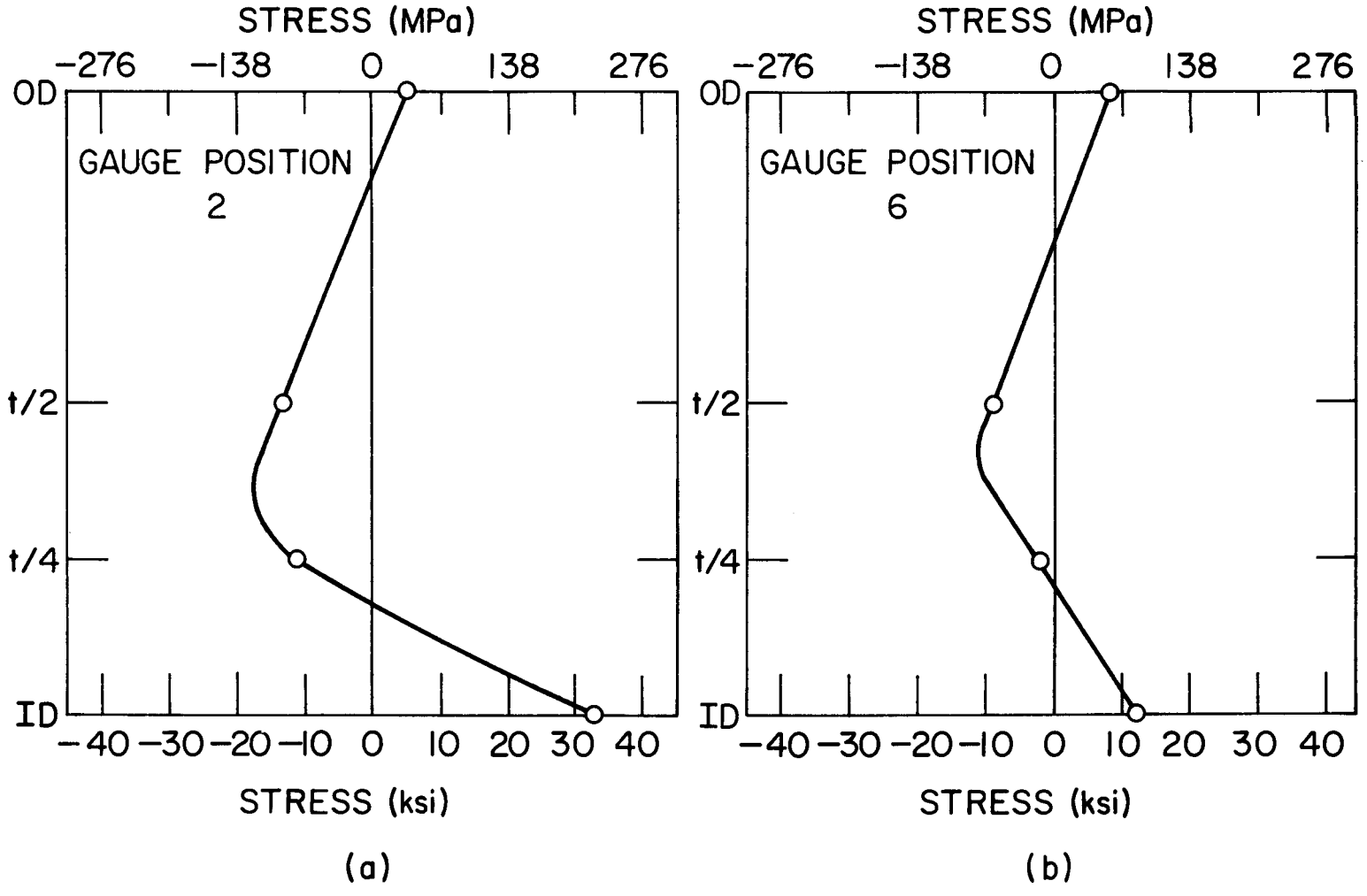

Fig. 4.5.21. Throughwall Distribution of Self-equilibrated Residual Stress in the 26-in. Weldment ∿13 mm on Either Side of the Weld Center Line.

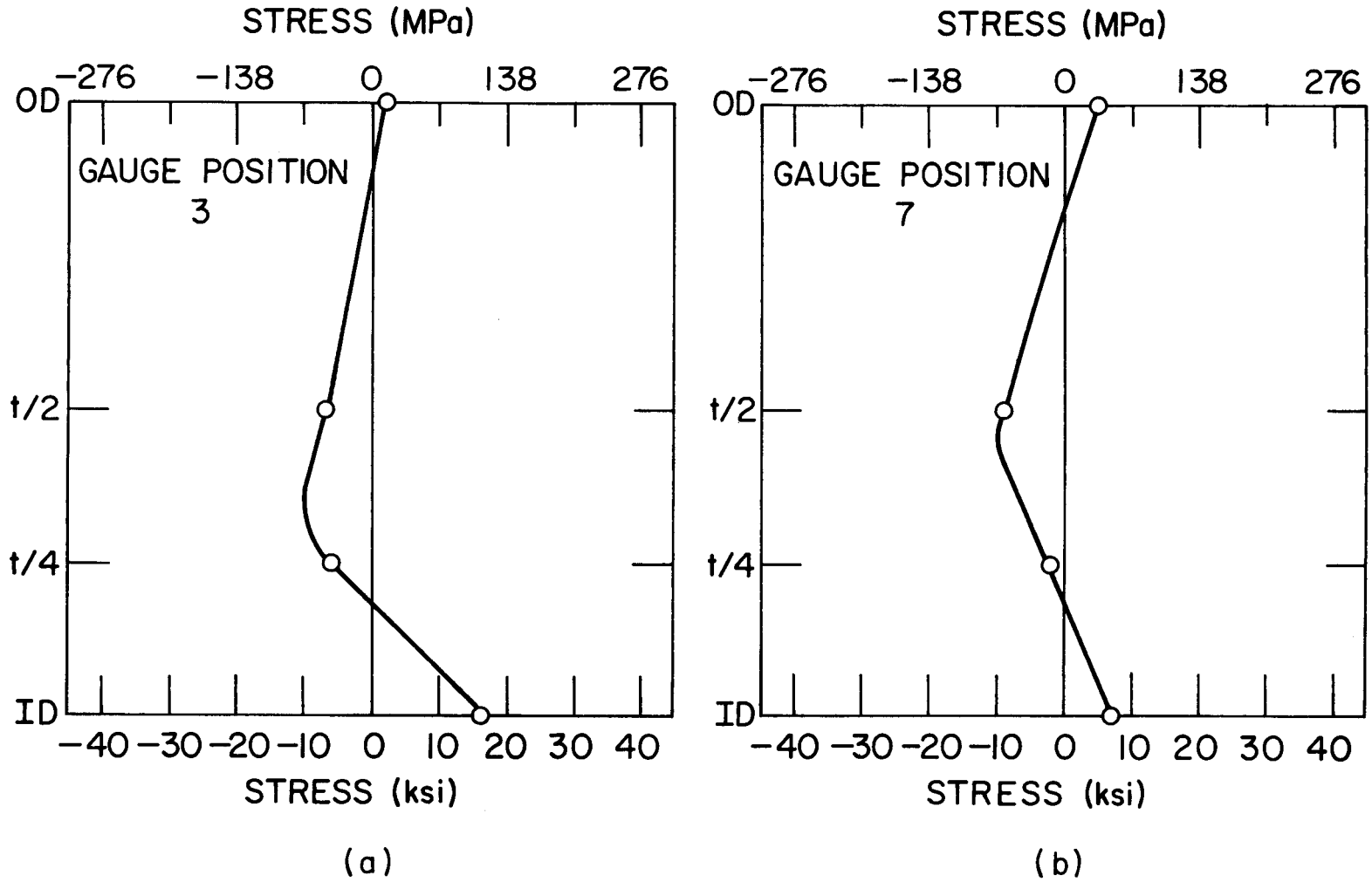

Fig. 4.5.22. Throughwall Distribution of Self-equilibrated Residual Stress in the 26-in. Weldment ∿17 mm on Either Side of the Weld Center Line.

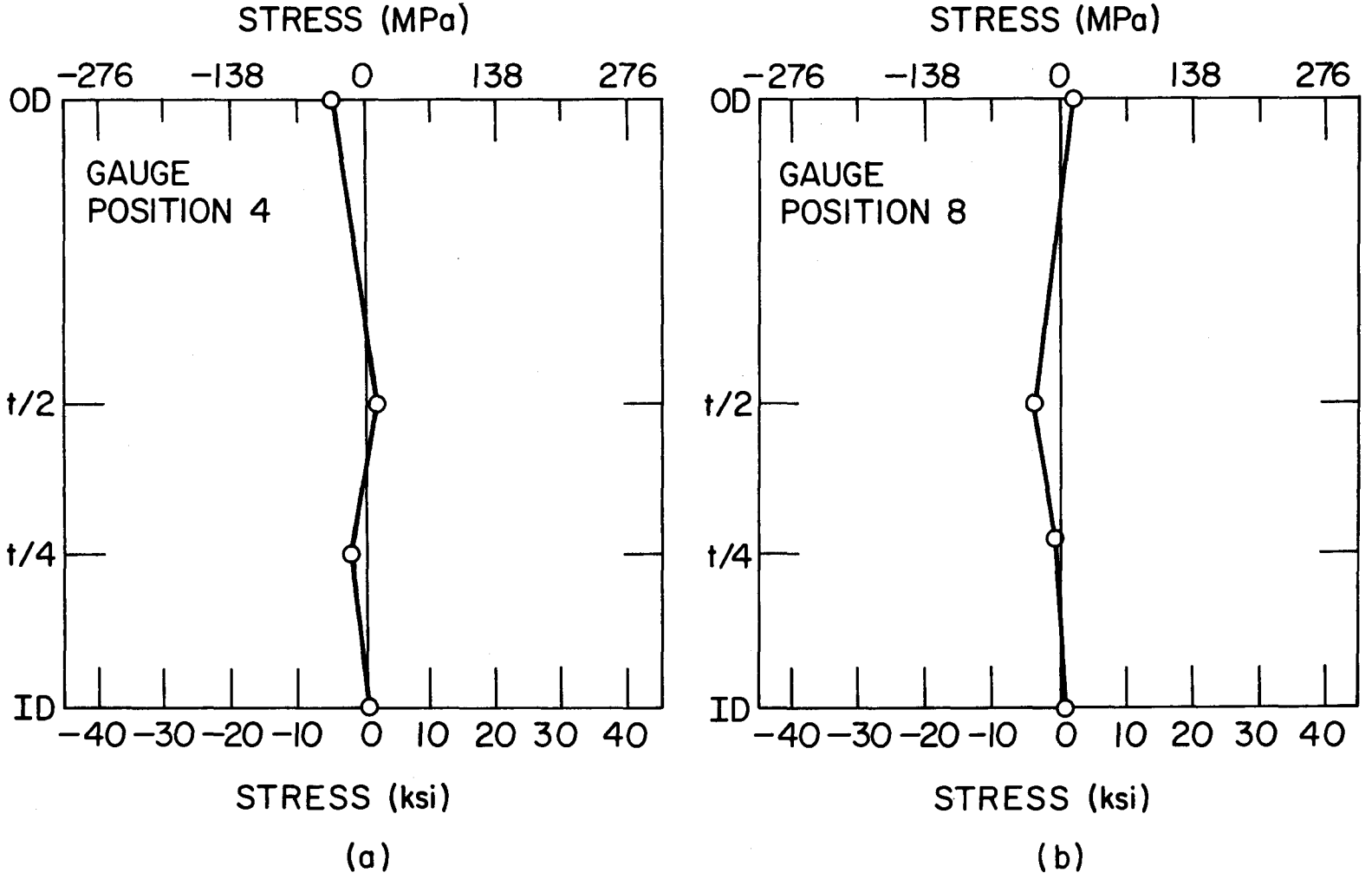

Fig. 4.5.23. Throughwall Distribution of Self-equilibrated Residual Stress in the 26-in. Weldment ∿27 mm on Either Side of the Weld Center Line.

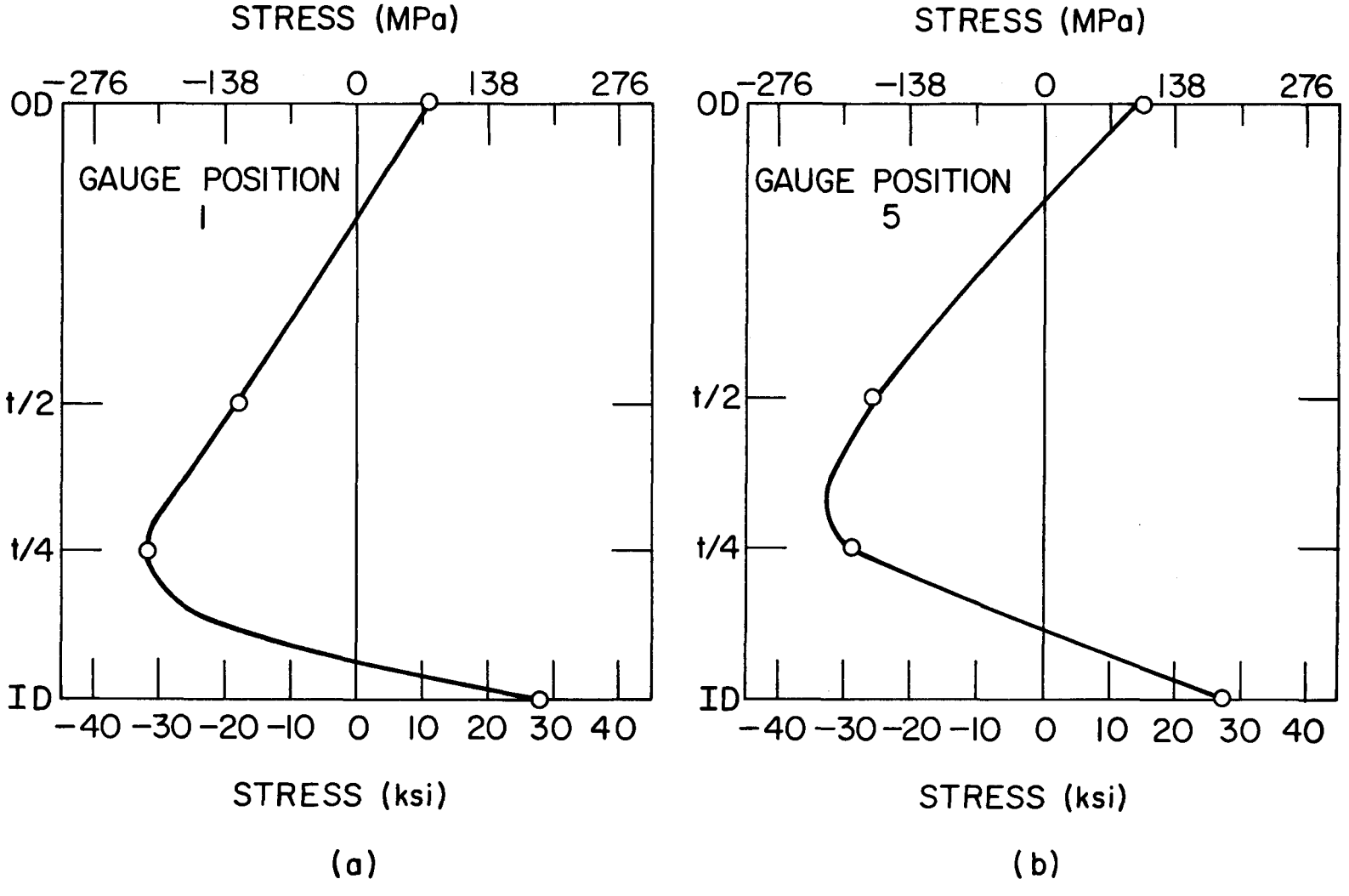

Fig. 4.5.24. Throughwall Distribution of Total Residual Stress ∿8 mm on Either Side of the Weld Center Line.

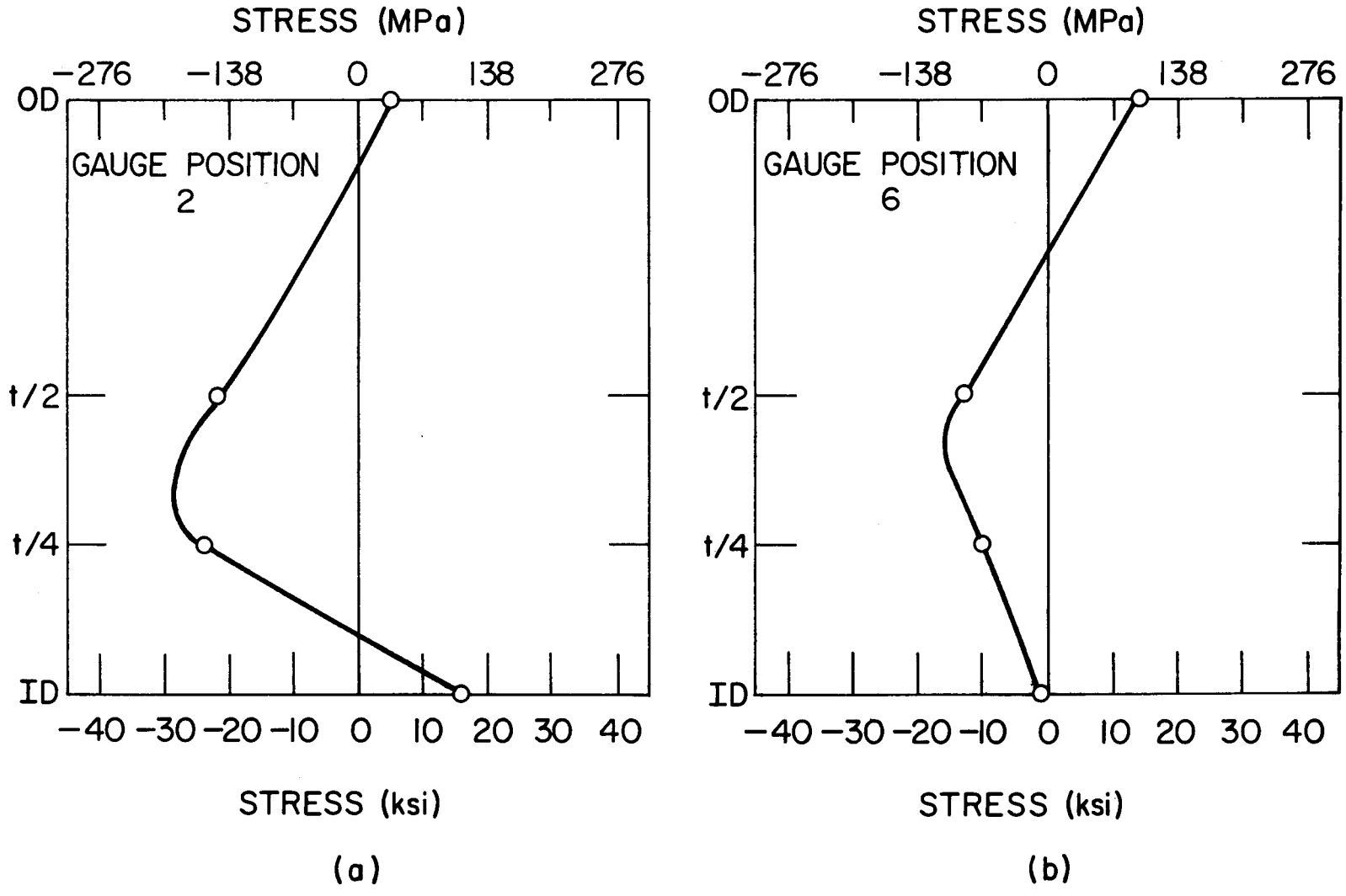

Fig. 4.5.25. Throughwall Distribution of Total Residual Stress ∿13 mm on Either Side of the Weld Center Line.

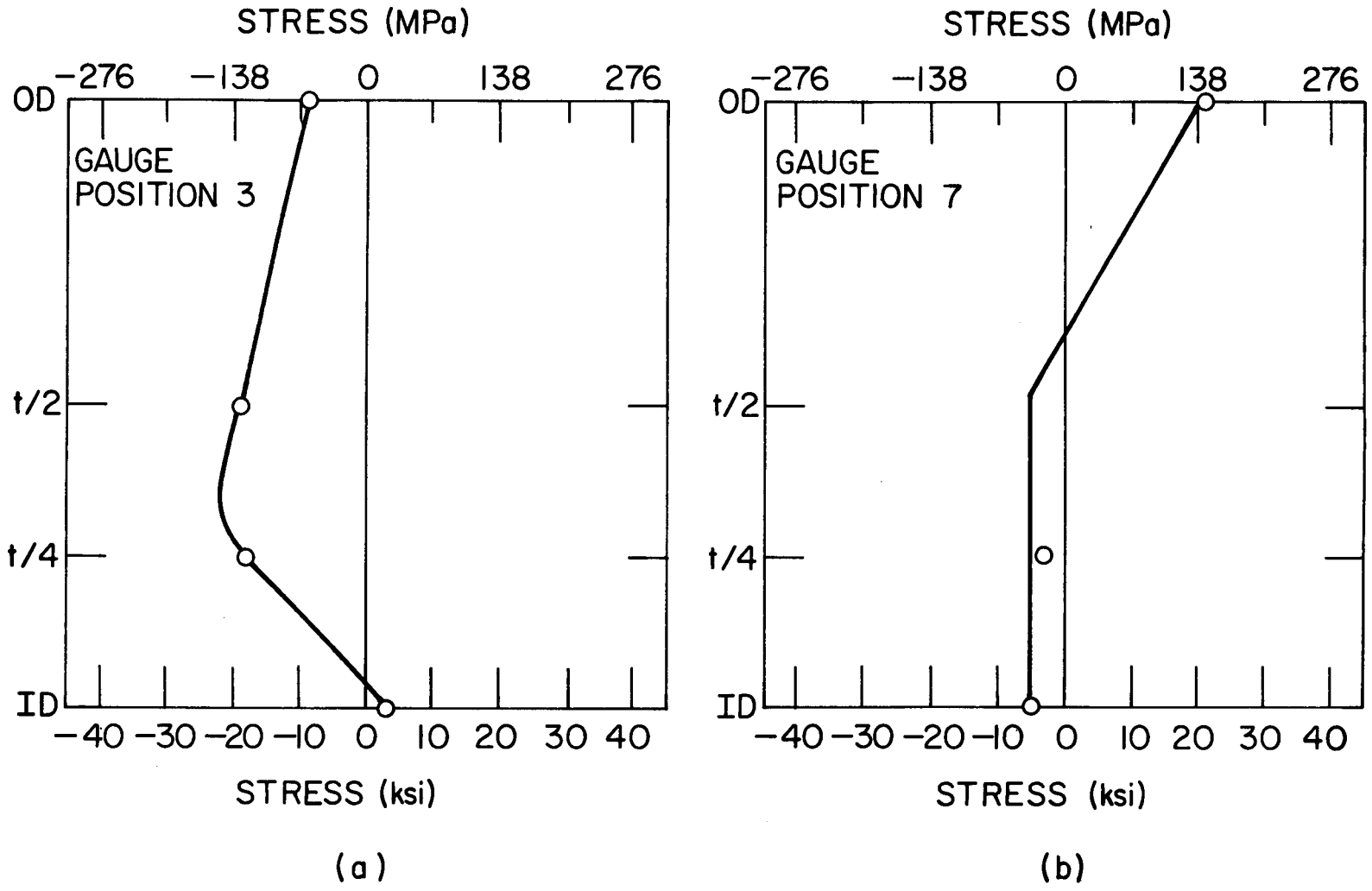

Fig. 4.5.26. Throughwall Distribution of Total Residual Stress ∿18 mm on Either Side of the Weld Center Line.

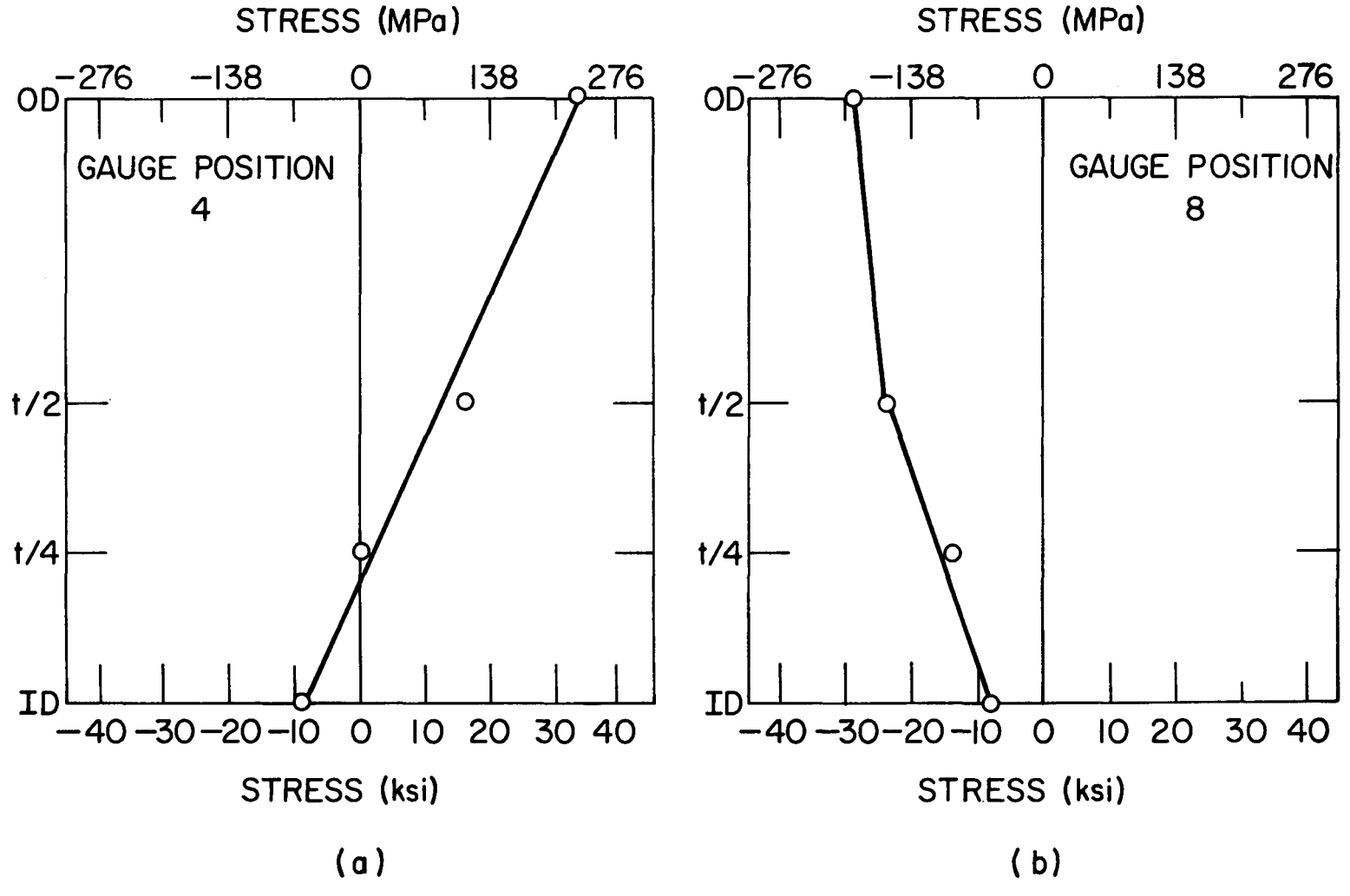

Fig. 4.5.27. Throughwall Distribution of Total Residual Stress ∿27 mm on Either Side of the Weld Center Line.

5. SUMMARY

Table 5.1 summarizes the results of bulk residual-stress measurements on the three 4-in. mockup weldments, the two 4-in. autopsy weldments, the 10-in. autopsy weldment, and the 26-in. mock-up weldment studied in this program. The data are taken from strain gauges placed in the weld land 2.5 mm (0.1 in.) from the weld-fusion line, which is the area of greatest concern and interest. To simplify the table, only axial stresses are reported here.

The peak axial stress at this position exceeds the yield stress [160 MPa (22 ksi) at the service temperature of 280°C (540°F)] on all the 4-in. weldments examined, except for the Dresden-3 autopsy weldment. Furthermore, in most cases, the average axial stress either exceeds or almost equals the yield stress at the service temperature. Note that the results reported here are all bulk residual stresses. Although these stresses are measured at the inner surface, they actually reflect the average stress relieved over a depth of $\sim$1.5 mm (0.060 in.). However, the data reported by General Electric,[10-12] based primarily on X-ray diffraction measurements, agree rather well with the measurements of the peak axial stresses reported here.

In no case was the form of the stress distribution axisymmetric, even allowing for the distortion introduced by variations in axial placement of the rosettes. However, the departure from axisymmetry varies widely from weldment to weldment. Weldment W27A is close to axisymmetric with a regular periodic "ripple" superimposed on a constant average value. The autopsy weldment from Monticello is also close to axisymmetric, except for the data point at the 90° azimuthal position. The other weldments, however, show a more irregular variation.

For the mock-up weldments, the weld-start positions are known; no correlation appears to exist between the weld-start positions and the peak-stress locations. Also, the piping used to fabricate the mock-up weldments in some cases exhibits significant variations in wall thickness ($\pm$15% from the mean thickness). However,

the azimuthal variation in wall thickness, as shown in Fig. 5.1, bears little resemblance to the azimuthal variation in residual stress. Although the form of the azimuthal variation for each weldment is almost independent of axial position, no consistent pattern to the variation is discernible between the various weldments. Incidentally, the consistency in the pattern between different axial positions is additional evidence that the variation is not simply due to variations in the axial position of the strain gauges.

It is difficult to draw any conclusions about the possibility that the high residual stresses "shake down" during service. The data from the Monticello and Dresden-3 weldments do show significantly lower stresses than the mock-up weldments. However, since the weldments are not exactly of the same geometric type as the straight-pipe mock-up weldments, it is not yet known whether these low values are typical of in-service weldments. Indeed the extremely low stresses in the Dresden-3 weldment seem unlikely to be produced by shakedown and appear to be more attributable to the change in geometry. The high residual stress levels in the 10-in. autopsy pipe certainly indicate that no shakedown or relaxation has occurred in this weldment.

Although no definite trend in the magnitudes of the residual stress on the inner surface with pipe size is observed, the distribution of throughwall residual stress in the 4-in. weldments does appear to differ significantly from that in the 26-in. weldment. At some, if not all, azimuthal positions, not only are there large tensile stresses on the inner surface of the 4-in. weldments, but also the throughwall residual stresses remain tensile through a large fraction ($\sim$50-75%) of the wall thickness. As the data reported here (and the data in Ref. 12) show, this is not the case for the 26-in. pipe.

If a crack initiates and grows, the residual stresses will redistribute. The nominal redistribution of stress in a 26-in. weldment caused by a growing crack has been calculated and is shown in Table 5.2. For crack lengths <10% of the wall thickness, very little redistribution occurs. Thus, a crack that

initiates on the inner surface would presumably be arrested by the compressive stress field after growing through only a relatively small (<10%) portion of the wall thickness. However, in addition to the residual stresses considered here, the stresses caused by service loads must be considered before any final conclusions about the crack-arrest behavior of throughwall cracks can be drawn.*

*Since the primary concern in this study has been on the role that welding residual stresses may have in the initiation and propagation of ISCC from the inner surface of pipe weldments, the measurements of the residual stresses obtained have not been reported directly (they have been used in obtaining throughwall profiles). A more complete listing of the raw data can be obtained by request to Dr. William J. Shack at Argonne National Laboratory.

TABLE 5.1

Bulk-Residual-Stress Summary for All Weldments

	Pipe Size	Average Axial Stress MPa (ksi)	Average Hoop Stress MPa (ksi)	Peak Axial Stress MPa (ksi)	Peak Hoop Stress MPa (ksi)	Gauge Position
W27A	4-in.	131 (19)	138 (20)	166 (24)	193 (28)	1
		186 (27)	242 (35)	242 (35)	283 (41)	5
W27B	4-in.	83 (12)	104 (15)	338 (49)	352 (51)	1
		138 (20)	207 (30)	352 (51)	400 (58)	4
W27C	4-in.	221 (32)	179 (26)	304 (44)	262 (38)	1
		214 (31)	242 (35)	248 (36)	386 (56)	3
Monticello Autopsy Weldment	4-in.	83 (12)	48 (7)	193 (28)	117 (17)	1
		97 (14)	83 (12)	152 (22)	117 (17)	4
Dresden 3 Autopsy Weldment	4-in.	0 (0)	-21 (-3)	41 (6)	83 (12)	1
		-28 (-4)	-124 (-18)	-7 (-1)	-55 (-8)	4
Average Value for All 4-in. Weldments (Excluding Dresden 3)		145 (21)	152 (22)	248 (36)	262 (38)	
10-in. Dresden-2 Autopsy Weldment	10-in.	283 (41)	55 (8)	352 (51)	117 (17)	1
		311 (45)	62 (9)	414 (60)	110 (16)	4

TABLE 5.2

Redistribution of Stress at Gauge Position 1, ∿3 mm from the Weld-fusion Line Caused by a Growing Crack

Crack Depth (mm)	Nominal Stress (MPa) at			
	Crack Tip	t/4	t/2	OD
0 (ID)	193	-221	-124	76
1	112	-218	-122	78
2	32	-216	-119	81
3	-47	-213	-116	83

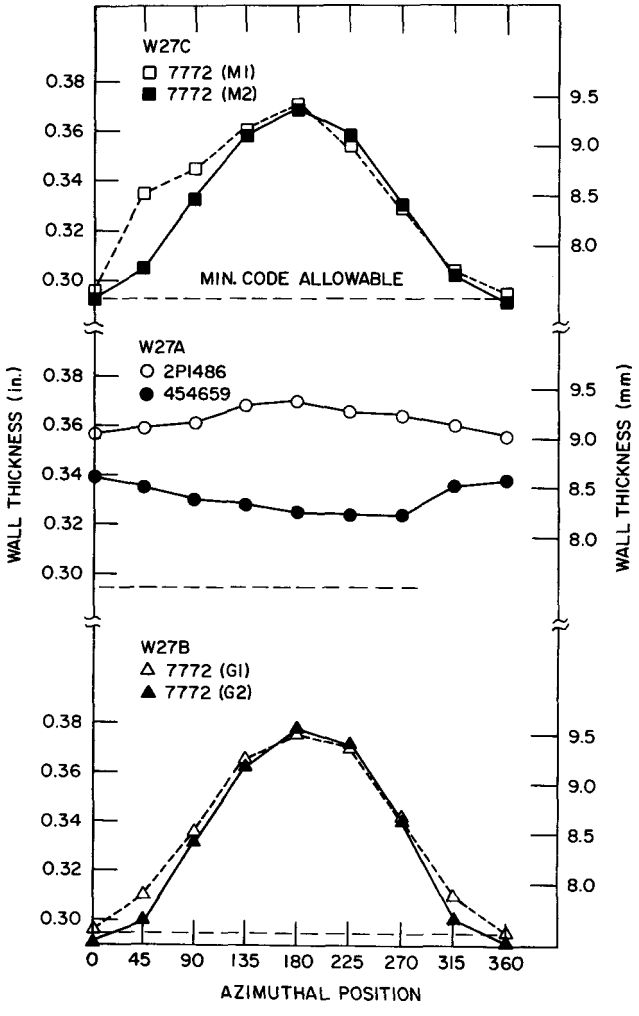

Fig. 5.1. Azimuthal Variation of Wall Thickness for 4-in. Seamless Stainless Steel Piping.

REFERENCES

1. Review of Chronology by M. Kennemui, Nuclear Regulatory Commission at a meeting on BWR Pipe Cracking, O'Hare Hilton Hotel, Chicago, March 4, 1975; sponsored by Electric Power Research Institute.

2. S. Timoshenko and S. Woinowsky-Krieger, Theory of Plates and Shells, McGraw-Hill, NY, 1959.

3. L. Tall "Residual Stresses in Welded Plates - A Theoretical Study," Welding J. Res. Supplement, 43, pp. 10-23, 1964.

4. S. Vaidyanathan, A. F. Todaro, and I. Finnie, "Residual Stresses Due to Circumferential Welds," J. Eng. Mats. and Tech., pp. 233-237, Oct. 1973.

5. N. Nagarasa and L. Tau, "Residual Stresses in Welded Plates," Welding J. Res. Supplement, pp. 468-480, Oct. 1961.

6. H. Hickel, H. Wohlfahrt, and E. Machelauch, Modellversuche zur Eigenspannungs-ausbildung Beim Schweissen, DVS-Belichte Bd. 26, Strahltechnik VI, DVS Düsseldorf 1973, pp. 49-52.

7. Personal Communication. Allen Parlane, Welding Research Institute, Cambridge, England, Sept. 1976.

8. E. Machelauch and H. Wohlfahrt, Die Ursachen des Schweisseigenspannungs-zustandes, IX, Schweisstechn, Hoshschulkolloquium, Essen, March 1975, Kurzfassungen der Vorträge, pp. 45-47.

9. H. H. Klepffer, et al., "Investigation of Cause of Cracking in Austenitic Stainless Steel Piping," NEDO-21000-1, General Electric Company, July 1975.

10. "Studies on AISI Type 304 Stainless Steel Piping Weldments for Use in BWR Application," Fifth Quarterly Report, EPRI Contract RP-449-2, NEDO-20985-5, General Electric Co., August, 1976.

11. "Studies on AISI Type 304 Stainless Steel Piping Weldments for Use in BWR Application," Fourth Quarterly Report, EPRI Contract RP-449-2, NEDO-20985-5, General Electric Co., March, 1976.

12. "Studies on AISI Type 304 Stainless Steel Piping Weldments for Use in BWR Application," Eighth Quarterly Report, EPRI Contract RP-449-2, NEDO-20985-5, General Electric Co., May, 1977.

APPENDIX A

Elastic Solution for the Reconstruction of Throughwall Stress Profiles

During the "layering" process for analyzing residual-stress distributions through the thickness, the removal of each layer alters the stress distribution through the remainder of the thickness. To deduce from the strain gauge data the original distribution of stress in the undisturbed piece, some assumptions must be made about the nature of the stress redistribution.

The simplest assumption is that the redistribution occurs elastically with no additional plastic deformation. The elastic redistribution is calculated by simple beam or plate theory. The analysis is easiest to follow in the beam case. Consider a free body as shown in Fig. A.1, where dF is the resultant force due to the residual stress σ in a layer of thickness $-dh$ ($dh < 0$), and dM is the moment about the neutral axis due to dF. The net resultant force and moment acting on the remainder of the cross section are equal in magnitude and opposite in direction to dF and dM.

When the layer is removed, net loads, dF and dM, must be applied to produce zero net load on the resultant cross section, as shown in Fig. A.2.

The change in curvature of the beam is then

$$d\left(\frac{1}{\rho}\right) = \frac{dM}{EI} = \frac{h}{2}\,\frac{\sigma b(-dh)}{EI}$$

$$= -\frac{d\sigma dh}{Eh^2} \qquad (1)$$

for a rectangular cross section. The change in strain is

$$d\varepsilon = y d\left(\frac{1}{\rho}\right) + \frac{1}{E}\frac{dF}{bh}$$

$$= y d\left(\frac{1}{\rho}\right) - \frac{\sigma}{E}\frac{dh}{h} , \qquad (2)$$

where $y = z - h/2$ is the distance from a material element to the neutral axis. Denoting by $d\varepsilon_L$ the change in strain on the lower side of the beam ($y = -h/2$), we have

$$d\varepsilon_L = -\frac{h}{2} d\left(\frac{1}{\rho}\right) - \frac{\sigma}{E}\frac{dh}{h} . \qquad (3)$$

Combining Eqs. 1 and 3 yields

$$d\varepsilon_L = -\frac{h}{3} d\left(\frac{1}{\rho}\right)$$

and

$$d\varepsilon_L = \frac{2\sigma}{Eh} dh . \qquad (4)$$

The change in stress in the remainder of the cross section due to the removal of the layer is

$$d\sigma(h,z) = E d\varepsilon , \qquad (5)$$

where $\sigma(h,z)$ is the stress at z when the beam is of thickness h. Note from Eqs. 2 and 4

$$d\varepsilon = \left(z - \frac{h}{z}\right)\left(-\frac{3}{h}\, d\varepsilon_L\right) - \frac{1}{2}\, d\varepsilon_L$$

$$= \left(1 - 3\,\frac{z}{h}\right) d\varepsilon_L \ . \tag{6}$$

From Eqs. 5 and 6,

$$d\sigma(h,z) = E\left(1 - 3\,\frac{z}{h}\right) d\varepsilon_L$$

or

$$\frac{d\sigma}{dh}\,(h,z) = E\left(1 - 3\,\frac{z}{h}\right)\frac{d\varepsilon_L}{dh} \ . \tag{7}$$

Integrating Eq. 7 from $h = z$ to $h = h_o$, the original thickness, we find

$$\int_z^{h_o} \frac{d\sigma}{dh}\,(h,z)\, dh = \sigma(h_o,z) - \sigma(z,z) \tag{8}$$

or

$$\sigma(h_o,z) = \sigma(z,z) + E \int_z^{h_o} \left(1 - 3\,\frac{z}{h}\right)\frac{d\varepsilon_L}{dh}\, dh \ . \tag{9}$$

From Eq. 4,

$$\sigma(z,z) = \frac{Ez}{2}\,\frac{d\varepsilon_L}{dh}\bigg|_{h=z} \tag{10}$$

Thus,

$$\sigma(h_o,z) = \frac{Ez}{2}\frac{d\varepsilon_L}{dh}\bigg|_{h=z} + E\int_z^{h_o}\left(1 - 3\frac{z}{h}\right)\frac{d\varepsilon_L}{dh}\,dh\ . \tag{11}$$

Equation 11 is the desired result. If $d\varepsilon_L/dh$ as a function of h is known from the experimental measurements, the original stress distribution can be computed from Eq. 11 by graphical or simple numerical techniques.

For a uniaxially loaded "plate," Eq. 11 is slightly modified

$$\sigma(h_o,z) = \frac{E}{1-\nu^2}\left\{\frac{h}{2}\frac{d\varepsilon_L}{dh}\bigg|_{h=z} + \int_z^{h_o}\left(1 - 3\frac{z}{h}\right)\frac{d\varepsilon_L}{dh}\,dh\right\}. \tag{12}$$

For a biaxial loaded "plate," the analysis is similar, but the algebra is somewhat more complex. Corresponding to the basic Eqs. 1, 3, and 5, we have the two-dimensional equivalents

$$d\left(\frac{1}{\rho_x}\right) = \frac{1}{D}\left(dM_x - \nu dM_y\right)$$

$$d\left(\frac{1}{\rho_y}\right) = \frac{1}{D}\left(dM_y - \nu dM_x\right) \qquad D = \frac{Eh^3}{12(1-\nu^2)} \tag{13}$$

$$d\varepsilon_x = y\,d\left(\frac{1}{\rho_x}\right) + \frac{1}{E}\left(\frac{dF_x}{h} - \nu\frac{dF_y}{h}\right)$$

$$d\varepsilon_y = y\,d\left(\frac{1}{\rho_y}\right) + \frac{1}{E}\left(\frac{dF_y}{h} - \nu\frac{dF_x}{h}\right) \tag{14}$$

$$d\sigma_x = \frac{E}{1-\nu^2}\left(\varepsilon_x + \nu\varepsilon_y\right)$$

$$d\sigma_y = \frac{E}{1-\nu^2}\left(\varepsilon_y + \nu\varepsilon_x\right)\ . \tag{15}$$

The moments and forces are related to the residual stresses in a layer of thickness (-dh) by

$$dM_x = \sigma_x(h,h)\left(-\frac{h}{2}\,dh\right)$$
$$dM_y = \sigma_y(h,h)\left(-\frac{h}{2}\,dh\right) \tag{16}$$

$$dF_x = \sigma_x(h,h)(-dh)$$
$$dF_y = \sigma_y(h,h)(-dh)\ . \tag{17}$$

The subsequent steps in the analysis are completely analogous to the beam case. The final equations for the original distribution of stress are

$$\sigma_x(h_o,z) = \frac{Ez}{2(1-\nu^2)}\left(\frac{d\varepsilon_{xL}}{dh} + \nu\frac{d\varepsilon_{yL}}{dh}\right)\Bigg|_{h=z} + \frac{E}{1-\nu^2}\int_z^{h_o}\left(1-3\frac{z}{h}\right)\left(\frac{d\varepsilon_{xL}}{dh} + \nu\frac{d\varepsilon_{yL}}{dh}\right)dh$$

and (18)

$$\sigma_y(h_o,z) = \frac{Ez}{2(1-\nu^2)}\left(\frac{d\varepsilon_{yL}}{dh} + \nu\frac{d\varepsilon_{xL}}{dh}\right)\Bigg|_{h=z} + \frac{E}{1-\nu^2}\int_z^{h_o}\left(1-3\frac{z}{h}\right)\left(\frac{d\varepsilon_{yL}}{dh} + \nu\frac{d\varepsilon_{xL}}{dh}\right)dh\ ,$$

where h_o is the original thickness, h the current thickness, z measures distances from the lower face, and ε_{xL} and ε_{yL} are the measured strains on the lower face of the plate.

To use Eq. 11 or 18 to analyze experimental data, very crude numerical approximations to the derivative $d\varepsilon_L/dh$ and the integral term should be adequate. Assume, for example, that the beam is layered sequentially $h_o > h_1 > h_2 > \ldots > h_n$. Then we can compute $\sigma(h_o,h_j)$ $j = 0, 1, 2, \ldots$ from

$$\sigma(h_o,h_o) = \frac{Eh_o}{2}\left(\frac{d\varepsilon}{dh}\right)_o$$

and (19)

$$\sigma(h_o,h_j) = \frac{Eh_j}{2}\left(\frac{d\varepsilon}{dh}\right)_j - E\sum_{k=1}^{j}\left(1 - \frac{3h_j}{h_k}\right)(h_k - h_{k-1})\left(\frac{d\varepsilon}{dh}\right)_k ,$$

where

$$\left(\frac{d\varepsilon}{dh}\right)_j = \frac{\Delta\varepsilon_j}{h_j - h_{j-1}} \tag{20}$$

and $\Delta\varepsilon_j$ is the change in strain measured in cutting from h_{j-1} to h_j.

To check on the numerical results, note that the net resultant force and moments acting on the section must vanish; i.e., for the beam case

$$\int_o^{h_o} \sigma(h_o,z)dz = 0$$

and (21)

$$\int_z^{h_o} z\sigma(h_o,z)dz = 0 .$$

Note that this is a check only on the numerical results and not the measured values of the strain, since Eq. 21 must hold for any choice of ε_L. To show this, note that from Eq. 11

$$\int_o^{h_o} \sigma dz = \int_o^{h_o} \frac{E_z}{2} \frac{d\varepsilon_L}{dh}\bigg|_{h=z} dz$$

$$+ E \int_o^{h_o} \int_z^{h_o} \left(1 - 3\frac{z}{h}\right) \frac{d\varepsilon_L}{dh} dhdz \ . \qquad (22)$$

Interchanging the order of integration in the second term gives

$$\int_o^{h_o} \int_z^{h_o} \left(1 - 3\frac{z}{h}\right) \frac{d\varepsilon_L}{dh} dhdz = \int_o^{h_o} \int_o^{h_o} \left(1 - 3\frac{z}{h}\right) \frac{d\varepsilon_L}{dh} dzdh$$

$$= \int_o^{h_o} \frac{d\varepsilon_L}{dh} \left(h - \frac{3}{2}\frac{h^2}{h}\right) dh$$

$$= \int_o^{h_o} -\frac{1}{2} \frac{d\varepsilon_L}{dh} hdh \ . \qquad (23)$$

Substituting back into Eq. 22 and noting that h and z are only dummy variables of integration yields

$$\int_o^{h_o} \sigma dz = \int_o^{h_o} \frac{Ez}{2} \frac{d\varepsilon_L}{dh}\bigg|_{h=z} dz - \int_o^{h_o} \frac{Eh}{2} \frac{d\varepsilon_L}{dh} dh = 0 \ . \qquad (24)$$

The analysis for the moment relation is similar, i.e.,

$$\int_o^{h_o} z\sigma dz = \int_o^{h_o} \frac{Ez^2}{2} \left.\frac{d\varepsilon_L}{dh}\right|_{h=z} dz$$

$$+ E \int_o^{h_o} \int_o^{h_o} z\left(1 - 3\frac{z}{h}\right) \frac{d\varepsilon_L}{dh} dhdz \ . \qquad (25)$$

Interchanging the order of integration in the second term gives

$$\int_o^{h_o} \int_o^{h_o} z\left(1 - 3\frac{z}{h}\right) \frac{d\varepsilon_L}{dh} dhdz = \int_o^{h_o} \int_o^{h_o} z\left(1 - 3\frac{z}{h}\right) \frac{d\varepsilon_L}{dh} dzdh$$

$$= \int_o^{h_o} \frac{d\varepsilon_L}{dh}\left(-\frac{h^2}{2}\right) dh \ . \qquad (26)$$

Substituting back into Eq. 25 and noting the h and z are only dummy variables of integration yields

$$\int_o^{h_o} z\sigma dz = \int_o^{h_o} \frac{Ez^2}{2} \left.\frac{d\varepsilon_L}{dh}\right|_{h=z} dz$$

$$+ \int_o^{h_o} -\frac{Eh^2}{2} \frac{d\varepsilon_L}{dh} dh = 0 \ . \qquad (27)$$

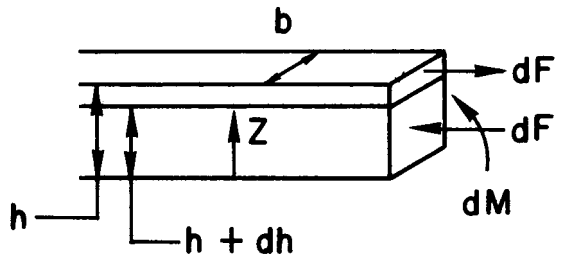

Fig. A.1. Geometry of the Layering Process.

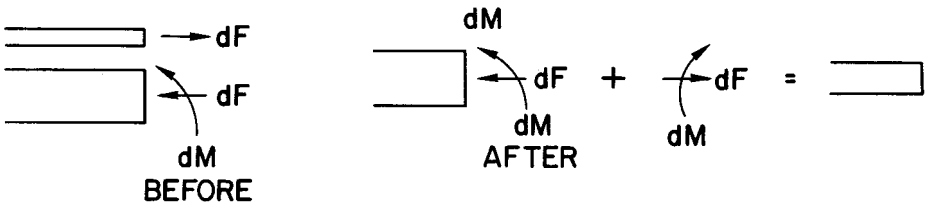

Fig. A.2. Load Changes During Layer Removal.

APPENDIX B

Weld Heat Input Data and Temperature Histories

ROOT PASS FUSION DATA

#7 Torch Cup
3/32" Ø Th. Tungsten electrode
Preset amps and volts to full pedal at 100 amps and 13 volts
15 CFH Argon - torch
5CFH purge
Position 2G
Travel: 2.2 - 3.2 IPM average using 4" Sch. 80 Grinnell insert
Weld 27A = 2P1486 and 454659
Weld 27B = 7772G1 & G2
Weld 27C = 7772M1 & M2

27A NOTE: Azimuth reading (orientation) taken from 454659
(2P1486 Azimuths running opposite from 0°)

First layer - start root at 80°
Second layer - bottom side of groove
Amps - 85
volts - 13
travel - 2.6 IPM
ER 308 - 3/32 Ø Ht. #S-0099
Start 90°
Third layer - top side of groove
Amps - 85
volts - 13
travel - 2.6 IPM
ER308 - 3/32 Ø
Heat #S-0099
Start 270°
Fourth layer - SMAW E308 1/8 Ø Ht. 1525090
Bottom of groove
95 Amps
23 volts
travel 7.1 to 7.3 IPM
Start 0° at bottom of groove
Fifth layer - SMAW E308 1/8 Ø Ht. 1525090
Top of groove
95 amps
23 volts
Travel 7.1 - 7.3 IPM
Start 270°
Sixth layer - SMAW E308 1/8 Ø Ht. 1525090
Bottom of groove
95 amps
23 volts
travel 7.1 - 7.3 IPM
Start 90°

Seventh layer - SMAW E308 1/8 Ø Ht. 1525090 - Bottom of groove
95 amps
23 volts
travel 7.1 - 7.3 IPM
Start 190°

27B

First layer - start root at 180°
#7 torch cup
3/32" Ø Th. tungsten electrode
preset amps and volts to full pedal at 100 amps and 13 volts
15 CFH argon torch
5 CFH Argon purge
Position - 2G
Travel 2.2 - 3.2 IPM average
4" Sch. 80 Grinnell insert
Second layer - bottom side of groove
amps - 85
volts - 13
travel - 2.6 IPM
ER308 - 3/32" Ø Ht. #S-0099
Start at 0°
Third layer - SMAW E308 1/8" Ø Ht. #1525090 - Bottom of groove
95 amps
23 volts
travel 7.1 - 7.3 IPM
Start 270°
Sixth layer - SMAW E308 1/8" Ø Ht. 1525090
Bottom of groove
95 amps
23 volts
travel 7.1 - 7.3 IPM
Start 0°
Seventh layer - SMAW E308 1/8" Ø Ht. 1525090
Top of groove
90 amps
23 volts
travel 7.1 - 7.3 IPM
Start 180°

27C

First layer - start root at 270° #7 torch cup
3/32" Ø Th. tungsten electrode
preset amps and volts to full pedal at 100 amps and 13 volts
15 CFH argon torch
5 CFH argon purge
Position 2G
travel 2.2 - 3.2 IPM average
4" Schedule 80 Grinnell insert
Second layer - Bottom side of groove
amps 85
volts 13
travel 2.6 IPM
ER308 - 3/32" Ø Ht. #S-0099
Start at 0°

Third layer - Top side of groove
amps 85
volts 13
travel 2.6 IPM
ER308 - 3/32" Ø Ht. S-0099
Start at 180°
Fourth layer - SMAW E308 1/8" Ø Ht. 1525090
95 amps
23 volts
travel 7.1 - 7.3 IPM
Start at 10°
Bottom of groove
Fifth layer - SMAW E308 1/8" Ø Ht. 1525090
Top of groove
95 amps
23 volts
travel 7.1 - 7.3 IPM
Start 180°
Sixth layer - SMAW E308 1/8" Ø Ht. 1525090
Bottom of groove
95 amps
23 volts
travel 7.1 - 7.3 IPM
Start 90°
Seventh layer - SMAW E308 1/8" Ø Ht. 1525090
Top of groove
95 amps
23 volts
travel 7.1 - 7.3 IPM
Start 9°

WELD PREP INFORMATION

Weld 27A - Hts. #2P1486 to 454659
Section - 2P1486 - ID surface machined to 125 RMS finish
Section 454659 - ID surface ground to 125 RMS finish

Weld 27B - Ht. #7772 pieces G1 and G2
Section G1 - ID surface ground to 63 finish
Section G2 - ID surface Ground to 125 finish

Weld 27C - Ht. #7772 pieces M1 & M2
Section M1 - ID surface machined to 63 finish
Section M2 - ID surface machined to 250 finish

NOTE: All finishes checked against surface roughness scale.

In connection with studies by GE on BWR pipe cracking,[1] they fabricated 4-in. weldments using weld-heat inputs nominally identical to those used in preparing the mockup weldments analyzed in the ANL residual-stress study. For their own study, GE also fabricated a 10-in. mock-up weldment. Although there is undoubtedly more variation in the welding parameters between this mockup and the 10-in.

autopsy weld from Dresden-2 than between the 4-in. weldments fabricated under nominally identical conditions, the GE measurements are also included here as typical of those occurring under field conditions.

To obtain the temperature measurements, 18 Chromel-Alumel thermocouples were spot-welded to the weldments. The location of the thermocouples on the weldment is shown schematically in Fig. B.1. The temperature histories for the 4-in. weldment are shown in Figs. B.2-4 in the form of cooling curves. The time t = 0 on the cooling curves is fixed at the time at which the maximum temperature is recorded for a given thermocouple. The maximum temperature at the inner surface for the 4-in. weldment is shown in Fig. B.5 as a function of axial position. The cooling curves for the 10-in. weldment are shown in Figs. B.6 and 7. Figure B.8 shows the distribution of maximum inside-surface temperature for the 10-in. weldment. Note that the 4-in. pipe is joined with seven weld passes, and the 10-in. pipe is joined with 14 weld passes.

REFERENCES

1. H. H. Klepffer, et al., Investigation of Cause of Cracking in Austenitic Stainless Steel Piping, NEDO-21000-1, General Electric Company, July, 1975.

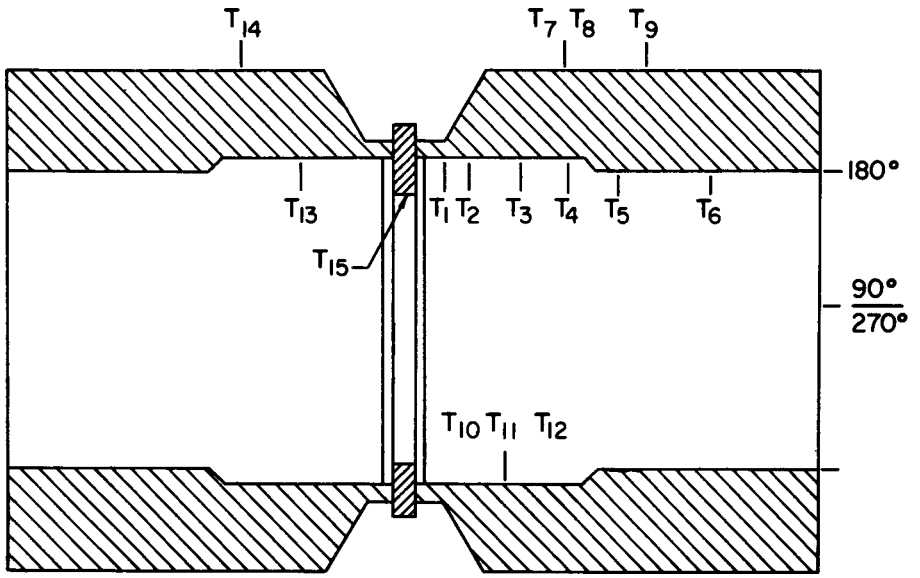

Fig. B.1. Placement of Thermocouples.

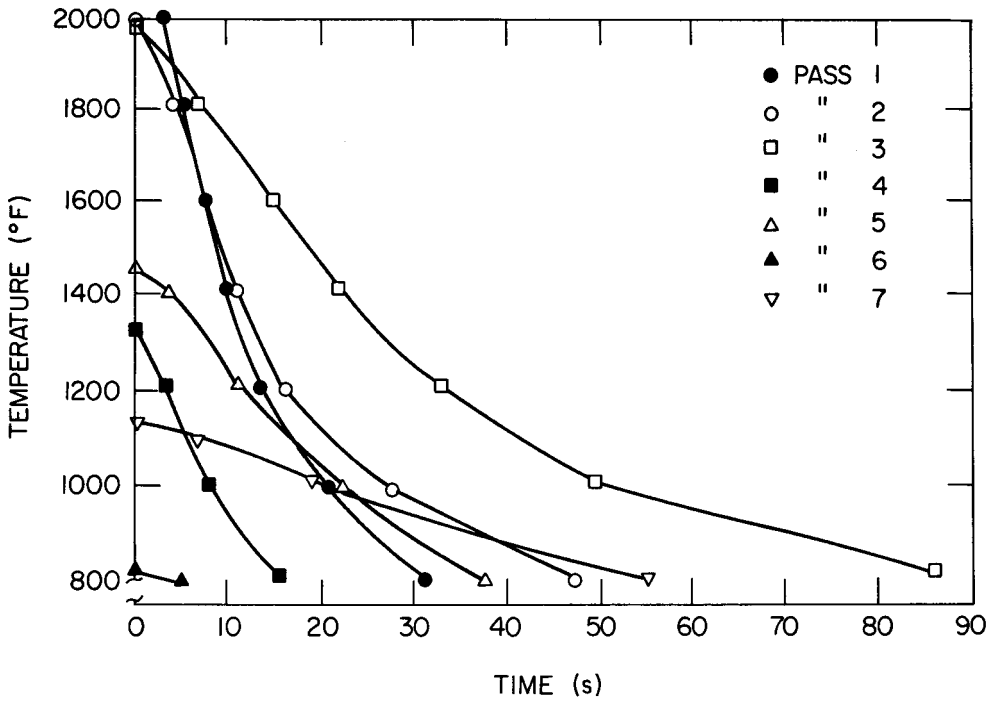

Fig. B.2. Cooling Curve for 4-in. Pipe (Thermocouple Located at Weld Fusion Line).

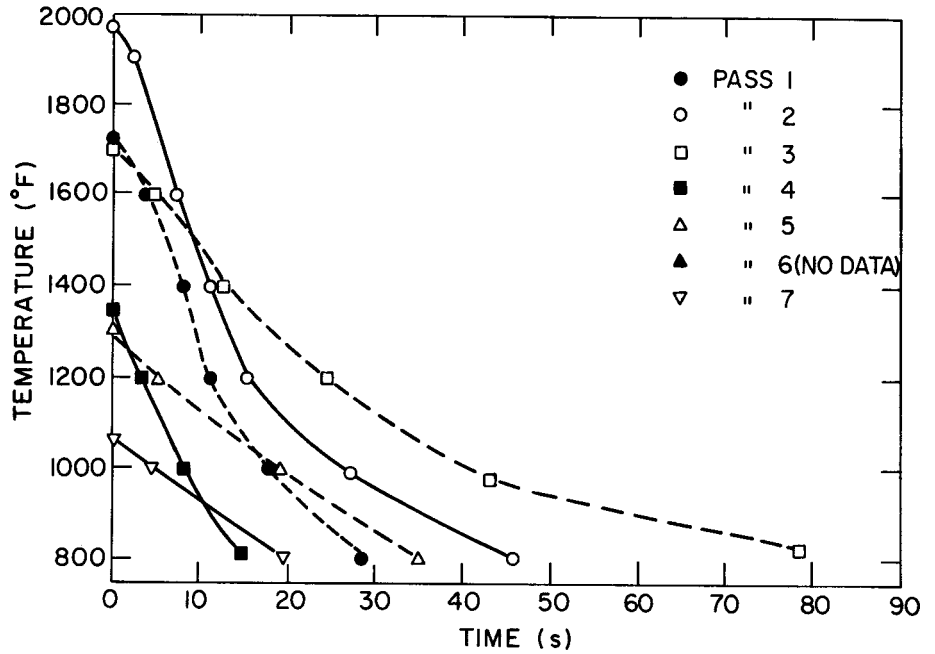

Fig. B.3. Cooling Curve for 4-in. Pipe (Thermocouple Located 3 mm from Weld Fusion Line).

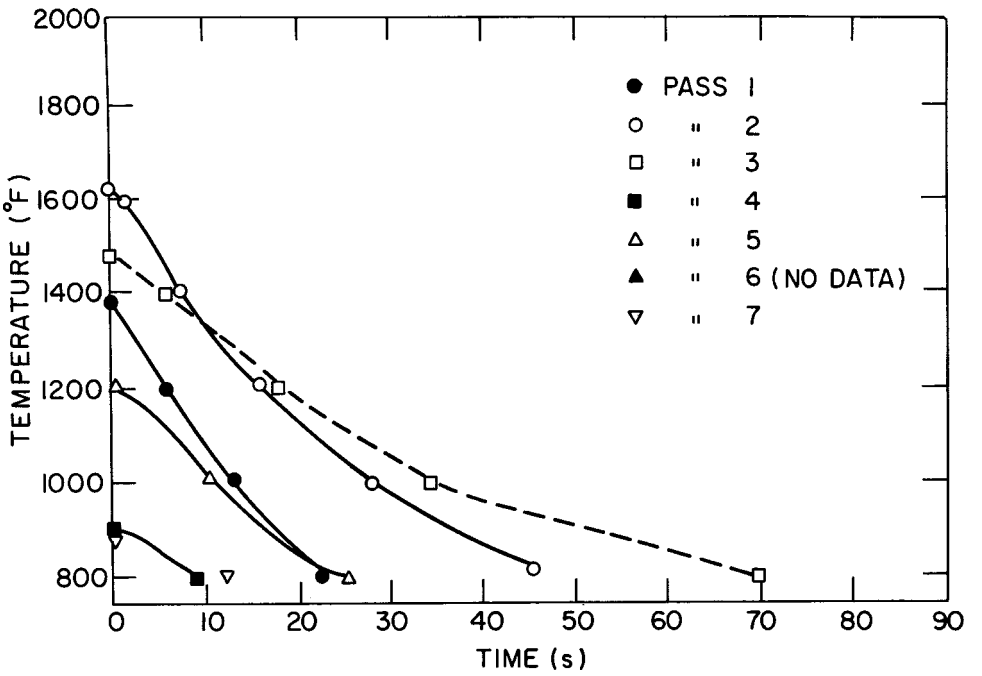

Fig. B.4. Cooling Curve for 4-in. Pipe (Thermocouple located 5 mm from Weld Fusion Line).

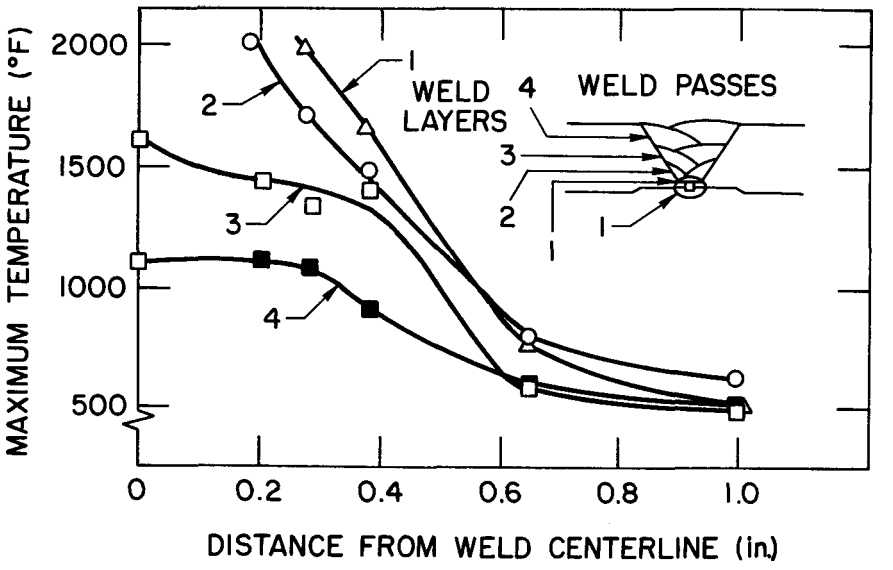

Fig. B.5. Distribution of Maximum Inside Surface Temperature for 4-in. Pipe.

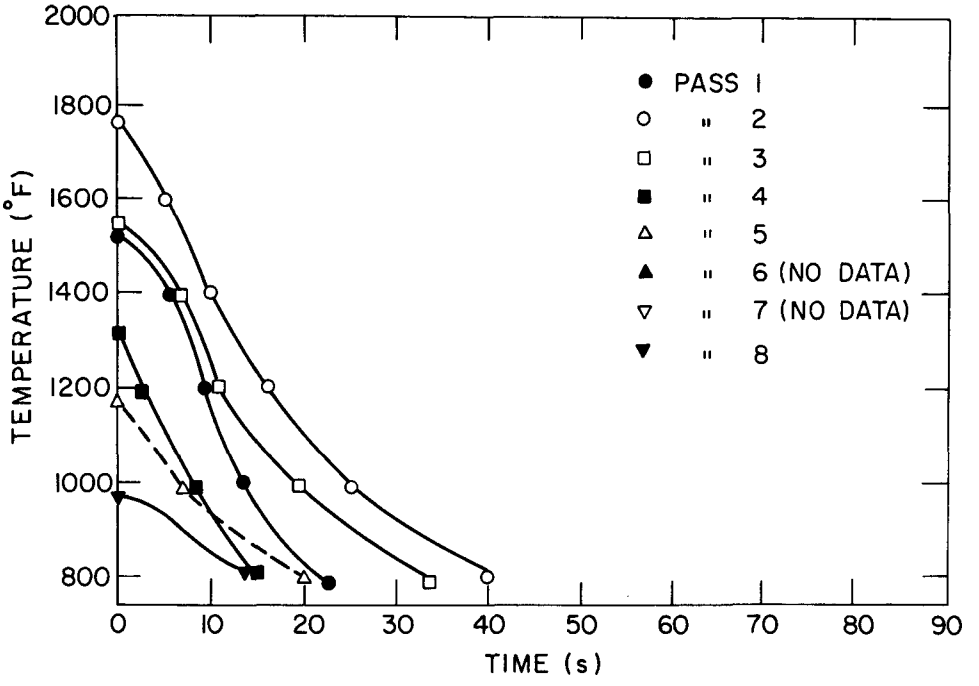

Fig. B.6. Cooling Curve for 10-in. Pipe (Thermocouple Located 3 mm from Weld Fusion Line).

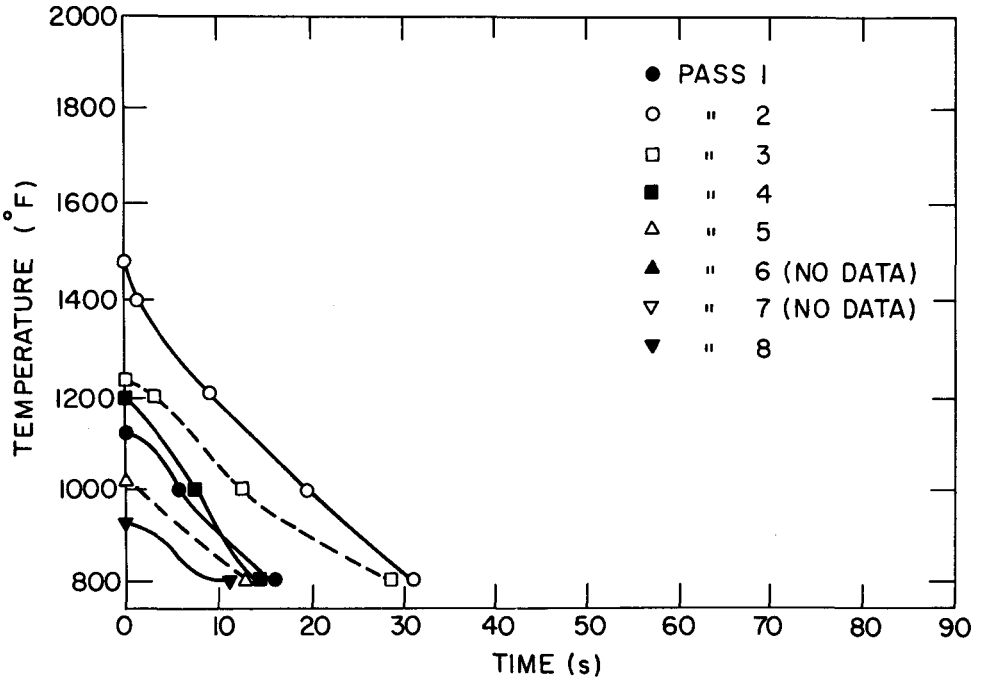

Fig. B.7. Cooling Curve for 10-in. Pipe (Thermocouple Located 5 mm from Weld Fusion Line).

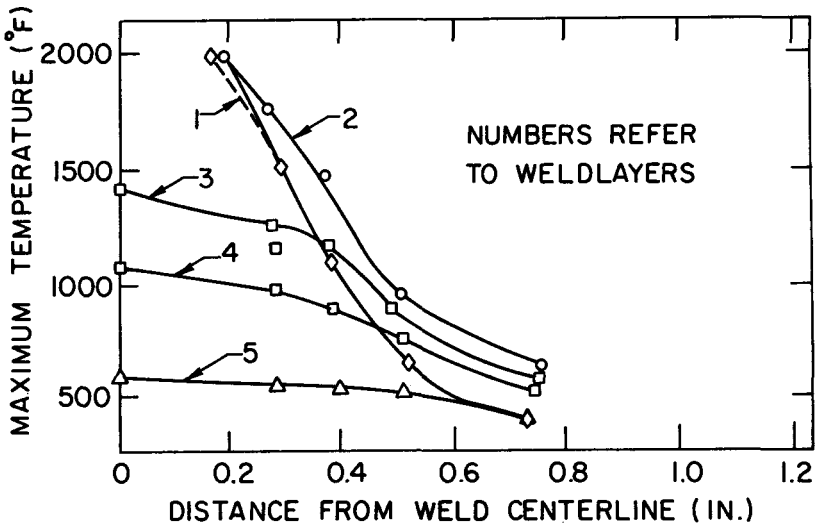

Fig. B.8. Distribution of Maximum Inside-surface Temperature for 10-in. Pipe.